BIOLOGICAL RESPONSES TO A SHAPE MEMORY POLYMER FOAM COATED COIL DESIGNED FOR ANEURYSM OCCLUSION

A Dissertation

by

SCOTT MICHAEL HERTING

Submitted to the Office of Graduate and Professional Studies of
Texas A&M University
in partial fulfillment of the requirements for the degree of

DOCTOR OF PHILOSOPHY

Chair of Committee,	Duncan J. Maitland
Committee Members,	Fred J. Clubb
	Richard H. Gomer
	Shreya Raghavan
Head of Department,	Michael J. McShane

December 2020

Major Subject: Biomedical Engineering

ABSTRACT

Embolic coils have become a valuable tool for occluding brain aneurysms to reduce the occurrence of hemorrhagic strokes and the associated high mortality and morbidity rates, but this strategy is still limited by high rates of recanalization and retreatment. Devices utilizing shape memory polymer foam for occlusion applications have demonstrated potential to enhance occlusion and improve healing associated with the treatment, which is expected to decrease recanalization rates. Extensive, rigorous testing is required to demonstrate that new devices, such as those utilizing the shape memory polymer foam, will be safe and effective in order to enable clinical translation. In this dissertation, we use established and novel methods to evaluate biological responses to a shape memory polymer foam-coated coil device designed for treating brain aneurysms.

Long-term implantation studies in the rabbit elastase aneurysm model demonstrated improved healing relative to standard bare platinum coil device controls. Additionally, the devices did not induce a chronic inflammatory response. *In vitro* cytocompatibility of the degradation products from this device was evaluated using novel methods, and it was observed that the degradation products are unlikely to cause a cytotoxic response. This is consistent with the aforementioned and other *in vivo* studies that have assessed the biocompatibility of this shape memory polymer foam. Finally, potential mechanisms for the improved healing associated with shape memory polymer foams were investigated using immunostaining and qPCR techniques with *in vivo* and *in*

vitro samples. The macrophage phenotypes associated with the inflammatory response to the devices were found to vary in *in vitro* and *in vivo* testing at early timepoints.

The findings from these studies support the continued evaluation of the shape memory polymer foam-coated coil devices as a valuable treatment option that may improve outcomes in endovascular occlusion procedures. Additionally, novel methods developed here may allow biocompatibility evaluation of polymer degradation products that could not have been directly evaluated previously.

DEDICATION

To my family, for their unconditional love and support.

ACKNOWLEDGEMENTS

I have so many people to thank for helping me get to this point. I would first like to thank my advisor, Dr. Duncan Maitland for giving me so many opportunities to grow and learn over the last 5 years. Dr. Maitland has been an incredible mentor, allowing me the freedom to pursue my own ideas and make my own mistakes while always keeping me on track and moving forward. I am incredibly grateful for his support, sincerity, and willingness to share his experiences to help us students. I also really appreciate the times Dr. Maitland brought us all together outside the lab for holidays, happy hours, or whatever the occasion was. He is a great leader, always pushing us to be better scientists and people.

I would also like to thank all of the members of my committee for their support. Dr. Fred Clubb taught one of my favorite classes and has taught me so much about pathology and the body's response to medical devices since the very beginning of my graduate school career. Dr. Richard Gomer has pushed me to cultivate my understanding of cell biology and helped me improve my experimental approaches with difficult questions and helpful advice. Dr. Shreya Raghavan helped me immensely to learn about and execute experimental methods I had only limited experience with when I devised my plan for my third aim, and she did so immediately when she arrived at Texas A&M while still setting up her own lab. Dr. Roland Kaunas served on my committee for my preliminary defense and sometime afterward, and I really appreciate his feedback and insightful questions that helped me improve my understanding of biomedical engineering research.

Dr. Mary Beth Browning Monroe joined the lab as a research scientist at the same time I started graduate school and became another great mentor of mine. I am very grateful for all of my meetings with her where she helped me design and troubleshoot experiments, navigate the stages of graduate school, and gave me advice on many things like managing our joint outreach effort and balancing responsibilities. She was an excellent professor in the classes I took with her and she remains an excellent mentor and friend.

Other professors were also very helpful to me in graduate school especially Dr. Bala Haridas as a professor in classes and as a mentor in our lab, as well as Dr. Daniel Alge as a professor in classes and as a mentor in the Society for Biomaterials.

I was lucky to have great collaborators at the Mayo Clinic who hosted me for an internship. Dr. David Kallmes and Dr. Ram Kadirvel were very welcoming and provided very helpful insight on my projects. Dr. Daying Dai and Dr. Yonghong Ding also became friends while they taught me a lot about aneurysms, interventional approaches, animal models, and pathology. I am also grateful to all of the other lab members who were great teammates and became friends while I was in Minnesota especially Kimberly Collins, Dr. Praveen Parameswaran, Dr. Jennifer Ayers-Ringler, Dr. Sean Fitzgerald, Dr. Zenith Khashim, Cody Fisher, Daniel Jakaitis, Dr. Solmaz Asnafi, Collin Johnson, and Gabe Tudor.

Dr. Bill Wustenberg is another collaborator who was very generous with his time to help me. His expertise in toxicology has been incredibly helpful for my project direction and educational for me as I move forward in my career.

I also appreciate the efforts of all the staff members in our department who are absolutely essential for the smooth function of our research programs and classes, particularly Barbara Slusher, Amanda Myatt, Ashlyn Montgomery, and Maria Lyons. There are so many other faculty and staff members in our department who help keep things running smoothly, and I am very grateful to all of them.

My friends within our lab have helped me learn new concepts, develop experimental approaches, troubleshoot at roadblocks, and keep things fun when they are inevitably frustrating and challenging. Dr. Todd Landsman was a fellow Cal Poly grad who introduced me to Dr. Maitland and Texas A&M. I am very grateful to Todd for helping me identify this opportunity and being a great mentor and friend to me as I got acclimated to graduate school. Grace Fletcher joined the lab as a graduate student at the same time I did, and we have been helping each other since day 1. Grace and I went through classes together, prepared for our preliminary defenses together, and have become great friends through this whole process. Dr. Landon Nash was a leader and role model in our lab who I still go to with questions. He is a great friend who has always kept everyone upbeat and smiling with surprise notes, memes, and our annual fantasy football league. Every single one of my Biomedical Device Lab friends have contributed to this research in some shape or form including Sam Briggs, Lance Graul, Lindy Jang, Achu Byju, Meghan Scott, Tyler Touchet, Dr. Tony Boyle, Dr. Mark Wierzbicki, Dr. Marziya Hasan, Dr. Brandis Keller, Dr. Nick Sears, Dr. John Horn, Dr. Staci Jessen, Dr. Andrew Weems, Adam Nathan, Rachael Muschalek, Adam Orendain, Annmarie Mullen, Taryn Barry, Kendal Ezell, Jane Frederick, Samuel Blair, Chris Hatch, and Anthony Powers.

I've also made some great friends in Texas outside my lab that have helped me enjoy the short breaks including Dr. Bryan Ngo, Natsuki Hara, Dr. Mike Frassica, Mallory Taylor, Dr. Jake Carrow, Dr. Faraz Jivan, Dr. Maddie Durkee, Stephanie Deveza, Zach Porter, Mia Anderson, and Connor Demott. I also really appreciate the support of my amazing group of friends in California that I've continued to text and call, visit at home, or that have come to visit me in Texas especially Ryan Veasy, Joe Jackson, Kyle Miller, Jake Hamilton, Zach Collins, Michael Bernardi, Wesley Goodson, Josh Johns, Russell Morra, Andy Wooldridge, Kevin Peters, Sean Peters, Henrik Ohrstrom, Mackey Hopen, Richard Squeri, Chris Wirfel, Curtis Lin, Steph Howard, and Christy Beymer.

Finally, I owe so much to my mom and dad, Jennifer and Doug Herting, who have always supported and encouraged me even when they wished they didn't have to do it from halfway across the country. They have been amazing role models my entire life and given me everything I could have asked for and more to help me live a happy, healthy, fulfilling life. My brother Steven has been my best friend making me laugh and bringing me out of my shell since he was born. I may be older, but I continue to learn so much from him all the time. My girlfriend Bianca Barth has been my partner for the past 7ish years, supporting me through every fun and difficult time. She gave feedback on many papers and presentations, she helped me flesh out plenty of experimental ideas and troubles with her own scientific expertise, and she did her best to pull me out of the lab every once in a while to have some fun with our dog Tucker and our human friends. I love you all and thank you so much!

CONTRIBUTORS AND FUNDING SOURCES

Contributors

This work was supervised by a dissertation committee consisting of Dr. Duncan J. Maitland, Dr. Fred J. Clubb, and Dr. Shreya Raghavan of the Biomedical Engineering Department, and Dr. Richard H. Gomer of the Biology Department at Texas A&M University. Dr. Roland R. Kaunas of the Biomedical Engineering Department also served on this committee from December 2017 until May 2020.

The work described in Chapter II was also supported by a team that included Dr. Anthony J. Boyle, Dr. Landon D. Nash, and Lance M. Graul from Texas A&M University; Dr. Yonghong Ding, Dr. Daying Dai, Dr. Solmaz Asnafi, Daniel R. Jakaitis, Collin R. Johnson, Dr. David F. Kallmes, and Dr. Ramanathan Kadirvel from the Mayo Clinic in Rochester, MN; and Chung Yeh from Shape Memory Medical. Parallel studies were also supported by a team that included Dr. Staci L. Jessen, Dr. Molly C. Friedemann, Annmarie E. Mullen, and Anne-Marie Ginn-Hedman from Texas A&M University. The work in Chapter III was supported by a team that included Dr. Mary Beth Browning Monroe, Dr. Andrew C. Weems, Samuel T. Briggs, Grace K. Fletcher, Samuel E. Blair, and Christopher J. Hatch from Texas A&M University. The work described in Chapter IV was supported by Taryn Barry, Anna Brokesh, and Dr. Akhilesh Gaharwar from Texas A&M University, and the Microscopy and Imaging Center at Texas A&M University.

Funding Sources

This project was supported in part by a fellowship award through the National Defense Science and Engineering Graduate (NDSEG) Fellowship Program, sponsored by the Air Force Research Laboratory (AFRL), the Office of Naval Research (ONR) and the Army Research Office (ARO). Support was also received from the National Institute of Health (NIH) National Institute of Neurological Disorders and Stroke (NINDS) grant U01-NS089692. This project was also supported in part by a Texas A&M Biomedical Engineering Graduate Trainee Fellowship. Its contents are solely the responsibility of the authors and do not necessarily represent the official views of the Department of Defense (DOD), the NIH, or Texas A&M University.

NOMENCLATURE

GDC	Guglielmi Detachable Coils
BPC	Bare Platinum Coils
SMP	Shape Memory Polymers
FCC	Foam-Coated Coils
FBGC	Foreign Body Giant Cells
IL-4	Interleukin 4
RCCA	Right Common Carotid Artery
DSA	Digital Subtraction Angiography
H_2O_2	Hydrogen Peroxide
TMHDI	Trimethyl Hexamethylene Diisocyanate
HPED	N,N,N',N'-tetrakis(2-hydroxypropyl) ethylenediamine
TEA	Triethanolamine
IPA	Isopropyl Alcohol
DMEM	Dulbecco's Modified Eagle Medium
NCS	Newborn Calf Serum
P/S	Penicillin/Streptomycin
DMSO	Dimethylsulfoxide
TM	TMHDI-based
Gly	Glycolic Acid
Lac	Lactic Acid

FTIR	Fourier Transform Infrared Spectroscopy
NMR	Nuclear Magnetic Resonance Spectroscopy
THF	Tetrahydrofuran
EA	Ethanolamine
Amino	1-Amino-2-Propanol
DEA	Diethanolamine
Bis	Bis(2-Hydroxypropyl) Amine
RO	Reverse Osmosis
3T3	BALB/3T3 Fibroblasts, Clone A31
IC_{30}	30% Inhibitory Concentration
PLGA	Poly(lactic-co-glycolic acid)
MCP-1	Monocyte Chemoattractant Protein-1
M1	Classical or Pro-Inflammatory Macrophage Phenotype
M2	Alternative or Anti-Inflammatory Macrophage Phenotype
DI	Deionized
TBS	Tris Buffered Saline
PMA	Phorbol 12-Myristate 13-Acetate
FBS	Fetal Bovine Serum
M0	Unpolarized Macrophages
qPCR	Quantitative Polymerase Chain Reaction
MNGC	Multinucleated Giant Cells
IL-10	Interleukin 10

ECM	Extracellular Matrix
SIS	Small Intestine Submucosa

TABLE OF CONTENTS

Page

LIST OF FIGURES

Page

LIST OF TABLES

CHAPTER I

INTRODUCTION

Aneurysms

An aneurysm is an abnormal ballooning of a blood vessel wall caused by breakdown of the internal elastic lamina[1]. Intracranial aneurysms occur in ~3% of the population and pose a risk of rupture that results in a 25-50% mortality rate, while leaving 2/3 of survivors requiring institutional care[2–5]. The probability of developing an aneurysm increases with certain genetic factors, hypertension, and smoking; and females are at higher risk as are people with family history of aneurysms or strokes[1].

The original method for treating brain aneurysms was the use of craniotomy and surgical clipping. A small metal clip was fitted to the neck of the aneurysm and tightened to close the ostium. This eliminated blood flow into the aneurysm, and the decreased hemodynamic pressure reduced the risk of rupture and hemorrhagic stroke. Dr. Guido Guglielmi was the first to introduce a minimally invasive approach to treating intracranial aneurysms. Dr. Guglielmi developed a detachable coil that could be delivered to an aneurysm by catheter. The coils were designed to occlude the aneurysm and block blood flow to the aneurysm dome. These “Guglielmi Detachable Coils” (GDCs) were approved by the FDA in 1995[6]. Since the release of these devices, many others have been developed to improve the ability of physicians to treat aneurysms with this minimally invasive technique.

Embolic coil treatment has provided a valuable tool for physicians, however aneurysm occlusion procedures have been reported to fail due to recanalization in 17-34% of cases, and up to 30% require retreatment[7–11]. Large to giant aneurysms can be especially difficult to treat, with 44% of aneurysms ≥ 10 mm recanalizing, requiring retreatment, or experiencing a bleeding episode after treatment with bare platinum coils[12]. This has led to the continued development of new devices and strategies for improving the stability of occluded aneurysms.

Clinically Used Devices

Bare Platinum Coils

GDCs were the first embolic coils cleared for use in humans by the FDA, but there are various types of embolic coils. GDCs are an example of "bare platinum coils" (BPCs), and BPCs remain the most widely available embolic coil in the clinic. These coils are typically made of a Platinum-Tungsten alloy, but the sizes and shapes of the devices vary significantly[13]. Devices are made at various lengths, and the shapes can be altered to allow different packing strategies. "Complex" and "framing" coils do not have the same simple helical shape as the original detachable coils, and this allows them to fill abnormal voids in the aneurysm or serve as baskets around the edges of an aneurysm to hold other coils inside. As mentioned above, these coils are designed to fill the aneurysm space as much as possible to halt bloodflow into the dome. Ideally, a clot forms around the devices that is later remodeled into connective tissue while endothelial cells cover the devices and clot at the neck of the aneurysm[14].

The healing response associated with bare platinum coils has recently been summarized by Brinjikji, et al[14]. Macrophages are expected to infiltrate the thrombus surrounding the coils from the periphery of the aneurysm dome in the first week. These macrophages enhance and remodel the provisional fibrin matrix on the surface of the coils. Between two and four weeks after implantation, fibroblasts are observed in the aneurysm dome with some differentiating to myofibroblasts. The macrophages and fibroblasts are expected to remodel the fibrin matrix to collagen in the aneurysm dome. After one to three months, the cells in the dome undergo apoptosis leaving hypocellular granulation tissue. Treatment with bare platinum coils typically yields loose, hypocellular connective tissue in the domes of aneurysms and thin, if any, endothelial layers at the necks of aneurysms[15,16]. It has been observed that increased packing of aneurysm domes has led to better healing with increased connective tissue deposition and decreased recanalization rates[17,18]. Because of these findings, physicians using BPCs for treating aneurysms typically target packing densities of 25-30% or greater[19].

Brinjikji, et al. proposed that a wound healing response that promotes collagen deposition in the dome and improved neoendothelialization at the neck could improve outcomes in coiled aneurysms. It is expected that dense, mature collagen deposition throughout the aneurysm dome can provide mechanical support to the coils to help reduce the risk of coil compaction. Similarly, complete endothelialization of the aneurysm neck is expected to provide a barrier to help reduce blood flow into the aneurysm dome.

Hydrocoils

Hydrocoils are similar to bare platinum coils, but they include a crosslinked acrylamide hydrogel component designed to expand upon implantation to increase volume filling within the aneurysm dome[20,21]. This increased filling is expected to reduce recanalization rates as was noted above in studies with BPCs. Multiple animal studies using bare platinum coil controls have demonstrated positive occlusion outcomes with Hydrocoil devices[21–24]. All of these studies show at least equivalence to bare platinum coils, and 3 of them show benefits in occlusion rates and thrombus organization rate over bare platinum coils. In these studies, the cellular response described after histologic examination is typically thinner layers of connective tissue and fewer foreign body giant cells between coils compared to bare platinum coils.

Clinical results with Hydrocoils are mixed. Some studies suggest superiority over bare platinum coils[20,25], while others suggest equivalence[12,26]. The variation may be due to differences in aneurysm size and treatment history. In large aneurysms and aneurysms needing retreatment after previous endovascular occlusion treatments, no benefits were observed with Hydrocoils [12,20]. Histology data obtained from 13 human explants suggest that thrombus organization begins after 10-40 days, and the necks of aneurysms are completely covered with neoendothelium by 74 days[27]. Hydrocephalus has also been observed as a complication potentially related to occlusion using Hydrocoil devices[8].

Matrix Coils

Matrix coils are another example of a polymer-coated platinum coil that has been used clinically. These coils included a PLGA fibered coating designed to degrade within three months and stimulate an immune response[28]. Early studies using Matrix coils showed excellent healing and good occlusion rates in multiple studies in the porcine sidewall aneurysm model[28–30]. One study found increased neointima thickness, slightly higher inflammatory scores, and earlier thrombus organization after treatment with Matrix coils[29].

Clinical results with matrix coils have been less favorable. Two studies completed single institution reviews of Matrix-treated aneurysms and found high rates of recanalization and retreatment[31,32]. Matrix coils showed higher recanalization and retreatment regardless of aneurysm size. Two mechanisms proposed for negative outcomes associated with Matrix coils included a) friction caused by the PLGA coating leading to decreased packing densities and b) resorption of the polymer leading to insufficient mass filling the aneurysm sac after degradation[32]. A more recent study followed a single physician's experience with GDC, Matrix, and Hydrocoil, and found aneurysms treated with Matrix coils were more likely to recanalize than aneurysms treated with either GDC or Hydrocoil[25]. A new prototype called the Matrix 2 has been developed with a thinner, smoother polymer coating, but clinical studies have failed to show the benefits of the Matrix 2 over GDCs[33].

Matrix coils were also studied in rabbit elastase aneurysms after 2, 6 and 10 weeks compared to bare platinum coils and Hydrocoils[22]. Matrix coils demonstrated increased

cellular reaction and neck healing compared to bare platinum coils, and neck healing was observed to be similar to Hydrocoils. Despite these results, Matrix exhibited significantly greater recanalization and compaction (33% for Matrix vs 22% for bare platinum and 0% for hydrocoil). The authors suggested that the different hemodynamic factors present in the rabbit elastase aneurysms compared to the porcine sidewall aneurysms may have been a cause of the differences observed.

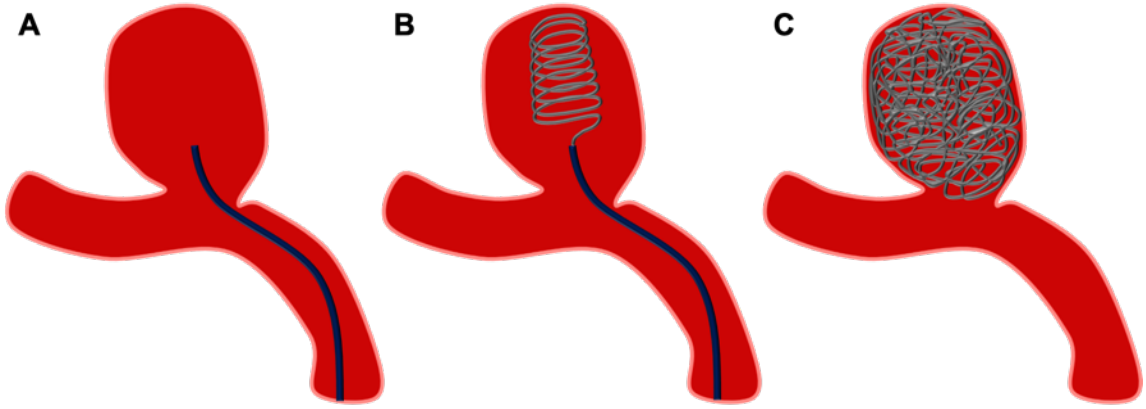

Figure I-1. Endovascular coiling of an aneurysm. A) The tip of the catheter is placed within the dome of the aneurysm. B) Coils are pushed out of the catheter into the aneurysm dome. C) The aneurysm dome is filled with coils and the catheter is removed.

Shape Memory Polymers

Shape memory polymers (SMPs) are a unique class of material that is capable of undergoing geometric programming and recovery cycles when exposed to appropriate stimuli[34]. Thermally actuated SMPs undergo these cycles around a characteristic transition temperature, such as the melting or glass transition temperature. When the material is heated above its transition temperature, it can be deformed then cooled to program its

secondary shape. This secondary shape will be maintained until the material is reheated above its transition temperature, and the primary shape of the material will be recovered. SMPs have many potential applications in various industries, but one promising area of research is in using SMPs for minimally invasive medical devices[35].

Our lab has designed a polyurethane SMP material system that can utilize chemical blowing processes to generate highly porous, ultra-low density SMP foams[36]. These highly tunable materials are capable of up to 70X volume recovery, and they can be synthesized with transition temperatures appropriate for passive or active actuation after implantation in the body[36,37]. These materials have also been demonstrated to elicit a beneficial healing response when implanted *in vivo* in cardiovascular occlusion applications[38–41]. The SMP foams induce rapid clotting, and the porous structure acts as a scaffold for connective tissue deposition and endothelial formation.

SMP foams have been observed to degrade slowly over long periods of time[42]. Minimal degradation of the SMPs was observed in previous animal studies up to 180 days, but *in vitro* evaluation of oxidative degradation suggests a faster rate. The effects of the degradation products from these materials on cells have not yet been thoroughly investigated, and the degradation of biomaterials is an important factor in assessing foreign body response and healing[43–45].

A novel SMP foam-coated coil (FCC) device was designed by Boyle, et al. to enable clinical translation of this SMP foam technology for the treatment of intracranial aneurysms[46]. This new device allows for the benefits of SMP foam technology to be harnessed in a form that is easily adoptable by clinicians. Feedback from collaborators has

indicated that this device is sufficiently soft and radiopaque to be clinically viable. The *in vivo* responses to implantation of the SMP FCC will be investigated in this work.

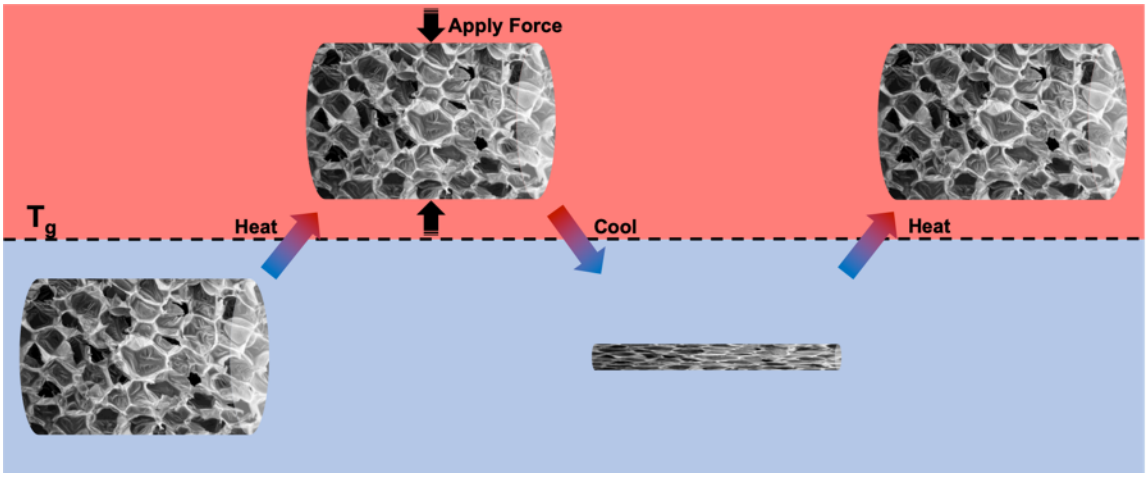

Figure I-2. One cycle of the shape memory effect for a shape memory polymer foam.

Foreign Body Response

The implantation of any biomaterial in the body elicits a foreign body response. This reaction differs based on the composition, structure, mechanical properties and location of the implant as well as the species and disease state of the implant recipient[47,48]. The implantation process inherently causes an injury, which initiates an inflammatory response based on the extent of injury, damage to basement membranes, blood-material interactions, and amount of necrosis[48]. After the injury, hemostasis processes begin then lead to the formation of a provisional protein matrix on the surface of the implant[49]. The formation of this protein matrix is driven by the Vroman effect, which describes the process that allows serum proteins to be replaced over time by proteins with a higher

affinity for the biomaterial surface[43]. The conformation of the adsorbed proteins is also critically important to the cell and tissue responses, and the conformations will be determined by interactions with the surface of the biomaterial[50]. Complement adhesion and activation can also affect the amount and types of cell adhesion to a biomaterial[51]. Inflammatory cells infiltrate the site of injury and begin clearing debris and any pathogens present by phagocytosis and release of proteolytic enzymes or reactive oxygen and nitrogen species[47]. These cells will include mostly neutrophils early on, and eventually there will be a shift toward macrophages and then fibroblasts[48]. Lymphocytes, mast cells, and eosinophils can also be present at various stages of the foreign body response to the implant[43]. Macrophages may also fuse to form foreign body giant cells (FBGCs) in an attempt to phagocytose the foreign material depending on the material surface chemistry and the presence of relevant T helper 2 type stimuli, such as interleukin 4 (IL-4)[52]. Another important role of the macrophage is the release of cytokines and chemokines that recruit fibroblasts and other cells to initiate healing, the final stage of the foreign body response[53,54]. Formation of granulation tissue composed of macrophages, fibroblasts, and neovascularization is a strong indication of the initial healing response after inflammation[43]. Continuous remodeling of the provisional matrix to form new tissue may also lead to integration or encapsulation and exclusion of the implant from the host tissue. The final stages of the healing response typically consist of fibrous encapsulation and/or fibrosis[43].

Macrophage Polarization

Recent studies investigating the biological response to implanted materials and devices have introduced the importance and the variability of macrophage phenotypes[44]. Macrophages have been observed to exist in a spectrum of phenotypes that can range from the "classical" macrophage that fights infection and clears debris to another "alternative" activation state that engages in wound healing and immunoregulation[44,45,55,56]. The former has been deemed the "M1" macrophage and the latter has been deemed the "M2" macrophage. M1-like macrophages are expected to generate more pro-inflammatory cytokines, while also producing more reactive oxygen and nitrogen species; and M2-like macrophages are expected to generate more anti-inflammatory cytokines, while producing more growth factors and remodeling the extracellular matrix.

In reality, M1 and M2 are the extremes of a spectrum, and various terminology has been created to help explain what type of activity is expected from a population of macrophages[57,58]. Recent nomenclature uses the activator molecules to describe a macrophage phenotype, for instance a M[IL-4] macrophage might be expected to express CD206 as a subset of the M2-like phenotype.

The activity of macrophages has been hypothesized to determine the outcome of an implant[59,60]. The presence of M1-like macrophage responses and M2-like macrophage responses have both been demonstrated to be necessary for appropriate healing and integration of biomaterial implants[45,59–61]. However, prolonged M1-like responses and/or early overexpression of M2-like responses are believed to be associated with necrosis, chronic inflammation, and pathologic fibrosis[62,63].

Purpose of this Research

In this dissertation, the biologic responses to implantable SMP FCCs have been evaluated using a combination of *in vitro* and *in vivo* techniques. The rabbit elastase aneurysm model was utilized to evaluate long term healing after implantation of SMP FCCs compared to BPC controls. *In vitro* cell culture was used to test relative cytotoxicity thresholds of degradation products from the SMP foams. Immunostaining was used on tissues from the rabbit elastase aneurysm study to evaluate macrophage phenotypes at these long term timepoints in relation to the healing observed. Finally, *in vitro* cell culture experiments were used to assess the polarization of macrophages seeded on SMP FCCs and BPC controls with qPCR analysis.

CHAPTER II

IN VIVO COMPARISON OF SHAPE MEMORY POLYMER FOAM-COATED AND BARE METAL COILS FOR ANEURYSM OCCLUSION IN THE RABBIT ELASTASE MODEL[*]

Introduction

Bare platinum coils (BPCs) have been used extensively for occlusion of intracranial aneurysms since the first versions, Guglielmi Detachable Coils, were cleared for clinical use by the FDA in 1995. These platinum microcoils promote the formation of a stable thrombus within the aneurysm, which is meant to be remodeled into connective tissue and covered by a neoendothelial layer across the ostium. The minimally-invasive nature of BPC treatment has been beneficial for many patients; however, BPC-treated aneurysm recanalization rates have been reported from 17-34% in studies using 6-18 month follow up schedules[7–9]. Recanalization can lead to aneurysm rupture, and up to 30% of treated aneurysms require retreatment to prevent such adverse outcomes[10,11]. Other endovascular

---

[*] Reprinted with permission from "In Vivo Comparison of Shape Memory Polymer Foam-Coated and Bare Metal Coils for Aneurysm Occlusion in the Rabbit Elastase Model" by **Herting, S.,** Ding, Y., Boyle, A.J., Dai, D., Nash, L.D., Asnafi, S., Jakaitis, D.R., Johnson, C.R., Kallmes, D.F., Kadirvel, R., Maitland, D.J., 2019. *Journal of Biomedical Materials Research, Part B.* Vol 107, pp 2466-2475, Copyright 2019 John Wiley and Sons.[71]

devices and strategies have been developed to reduce these recanalization rates, including coated coils, stent-assisted coils, flow diverters, and liquid embolics[21,28,64–66]. However, some additional issues remain to be resolved such as hydrocephalus induced by HydroCoils and coil compaction after deployment of Matrix coils[8,67]. The introduction of flow diverters has been beneficial in some cases, but coil embolization of intracranial aneurysms remains widely used. There is no need to use anticoagulation drugs after coiling, and occurrence of thromboembolic events in the parent artery is much lower than with flow diverter implantation.

One main concern with aneurysm coiling is incomplete occlusion, especially in large and wide-necked aneurysms[8]. Shape memory polymer (SMP) foam-coated coils (FCCs) are a new type of coated coil that utilizes ultra-low density SMP foam to increase packing density, promote rapid thrombus formation, and encourage remodeling and connective tissue deposition within the aneurysm[46]. The polyurethane SMP foam coating on these devices enables ~2.5x volume expansion upon thermal actuation at the glass transition temperature[36]. This large volume expansion allows for increased packing densities, and increasing packing density has been reported to decrease recanalization rates[18,19,68,69]. The porous foam also acts as a scaffold to support tissue healing, and previous studies in porcine sidewall aneurysms demonstrated increased connective tissue deposition within the domes and thicker neointimal formation at the necks of SMP foam-treated aneurysms[39,41]. Previous studies utilized “foam only” devices, which were not deemed clinically viable due to limitations to device delivery through a 5-6F guide catheter. SMP

FCCs are a new prototype device that utilizes the foam material in a more clinically relevant design that is deliverable through an 0.021" ID (2.7F) microcatheter.

It has been hypothesized that dense collagen deposition and thick neointima formation, as has been observed after implantation of similar SMP foams, will lead to improved outcomes for endovascular aneurysm occlusion procedures by increasing the stability of the occlusion and preventing recanalization[14]. This type of foreign body response is not often observed in aneurysms treated with BPCs. The goal of the research described here is to evaluate chronic aneurysm healing in the rabbit elastase aneurysm model after treatment with SMP FCC devices.

Materials and Methods

Test Devices

The SMP FCC devices consist of SMP foam cylinders adhered to the outside of platinum-tungsten coils as seen in Figure 2.1. A more detailed manufacturing process has been presented by Boyle, et al[46]. Briefly, platinum-tungsten wire wrapped in a tight, spring shape is formed into a helical secondary shape. Then, the SMP foam is synthesized using a three-step process that combines diisocyanates with polyols and water to form a highly crosslinked poly(urethane urea) foam as described previously[70]. SMP foams are cut into cylinders using biopsy punches, then helical platinum-tungsten coils are pulled straight and threaded through the center axis of the foam cylinders. A mixture of the same diisocyanates and polyols used to synthesize the foam is applied to the assemblies, then heat-cured to act as a glue adhering the foam to the coil. The FCCs are attached to a

delivery pushwire designed for electrolytic detachment of the coils when used with a separate detachment controller system. The devices are packaged in foil pouches and sterilized by electron beam irradiation at a minimum of 25 kGy before use.

SMP FCC sizes available for this study included 2 x 2, 2 x 4, 4 x 6, 4 x 10, and 6 x 10 (helical diameter in mm x coil length in cm). The Barricade Coil System (Blockade Medical) was used as the BPC control device in this study. Available Barricade sizes included 1 x 2, 1.5 x 2, 1.5 x 3, 1.5 x 4, 2 x 1, 2 x 2, 2 x 3, 2 x 4, 2 x 6, 2 x 8, 2.5 x 3, 2.5 x 4, 3 x 4, 3 x 6, 3 x 8, 3 x 10, 4 x 6, 4 x 8, 4 x 10, 4 x 13, 5 x 8, 5 x 9, 5 x 10, 5 x 15, 5 x 17, 6 x 10, 6 x 11, 6 x 15, 6 x 16, 6 x 20, 7 x 13, 7 x 15, 7 x 20, 7 x 30 (helical diameter in mm x coil length in cm).

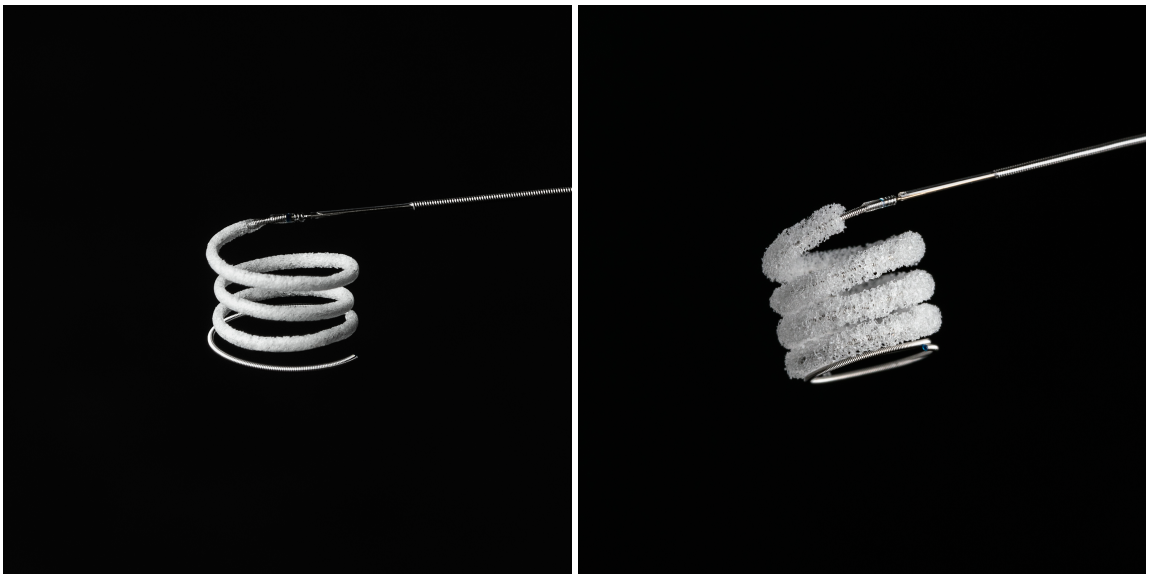

Figure II-1. Shape memory polymer foam-coated coil device used in this study. The 0.750 mm diameter shape memory polymer foam coating is compressed to a 0.381 mm diameter (left) before implantation, then expands (right) when exposed to blood after implantation. Reprinted with permission from (Herting, 2019).[71]

Aneurysm Creation Procedure

All the animal procedures were conducted according to Mayo Clinic AUP# A68514-15-R17. New Zealand White rabbits were anesthetized through intramuscular injection of ketamine/xylazine, intubated, and then anesthesia was maintained with 2.5-3% isoflurane carried by 100% oxygen. Aneurysms were created in rabbits with elastase incubation as described by Altes, et al[72]. Briefly, using sterile technique, the right common carotid artery (RCCA) was exposed and ligated distally, a 5 French sheath was advanced retrograde in the RCCA to a point approximately 3 cm cephalad to the CCA origin. Through this indwelling sheath, a 3 French Fogarty balloon was advanced to the origin of the right CCA at its junction with the right subclavian artery. The balloon was inflated with iodinated contrast just enough to achieve flow arrest in the RCCA. Porcine elastase (approximately 100 U/ml) mixed at a 1:1 ratio with iodinated contrast was incubated for 20 minutes in the dead space of the RCCA, above the inflated balloon. Following incubation of the elastase solution, the balloon was deflated and the sheath was removed and the RCCA was ligated below the sheath entry site. The skin was closed with running 4-0 Vicryl suture, and the rabbits were sent to recovery.

Embolization Procedure

Aneurysms were embolized with BPC controls or SMP FCCs at least 3 weeks after aneurysm creation[73]. The anesthesia procedure was the same as at the time of aneurysm creation. Using sterile technique, surgical exposure of the right common femoral artery was performed, and a 5 French sheath was placed in the right common femoral artery

followed by 500 units heparin injection through the sheath. Using coaxial technique, with continuous heparinized saline flush, a Rebar-18 (SMP FCC Delivery) or Echelon-14 (BPC Delivery) microcatheter was advanced into the aneurysm cavity. The size of the aneurysm was assessed using direct comparison to radiopaque sizing devices during digital subtraction angiography (DSA) assuming the aneurysms were ellipsoids. Aneurysms were packed with multiple BPCs or multiple SMP FCCs and the packing density was calculated as the total volume of coils implanted divided by the aneurysm volume. The test device to be used for each aneurysm was chosen before initial DSA and measurement of the aneurysm. Two packing densities were calculated for SMP FCCs: 1) before and 2) after SMP foam expansion. The crimped and expanded foam volume values used in the calculations were measured in previous benchtop expansion experiments. Following coil placement and embolization, a final control DSA was performed. Aneurysm occlusion was evaluated using a 3-point scale as follows: Grade 1, complete occlusion; Grade 2, near complete occlusion; and Grade 3, incomplete occlusion. The catheters and sheath were removed, the femoral artery was ligated, and the incision was closed with 4-0 Vicryl suture.

Sacrifice/Tissue Harvest

Angiographic follow-up was performed 30, 90, or 180 days after coil embolization followed by sacrifice and tissue harvest. The same types of sheaths and catheters were used for the follow-up angiograms as were used for the treatment procedures. At the designated timepoint, animals were deeply anesthetized. DSA of the brachiocephalic

artery was performed, and aneurysm occlusion was evaluated using the same 3-point scale: Grade 1, complete occlusion; Grade 2, near complete occlusion; and Grade 3, incomplete occlusion. After the follow up, a comparative scale was used to compare occlusion scores at the time of sacrifice to occlusion scores immediately after treatment. The potential comparative scores included stable aneurysm occlusion, which indicates that the same grade was assigned at both timepoints; progressive aneurysm occlusion, which indicates that a better grade was assigned at follow up; or aneurysm recanalization, which indicates that a worse grade was assigned at follow up. The animals were then euthanized with a lethal injection of pentobarbital, and the aneurysms and parent arteries were harvested. Harvested tissue samples were immediately fixed in 10% neutral buffered formalin.

Gross Evaluation

Gross images of each explanted tissue sample were acquired, and then each aneurysm's neck orifice was exposed to acquire gross images of the tissue coverage at the neck. Tissue coverage was evaluated to assign the corresponding neck healing score for the ordinal scoring system.

Histologic Evaluation

Formalin fixed tissues were processed as has been previously described[15]. Briefly, samples were placed in alcoholic formalin followed by ascending alcohol concentrations from 70 to 100%. Next, specimens were placed in two changes of Xylene followed by

three changes of liquid paraffin. Finally, specimens were embedded in paraffin blocks. The aneurysm was sectioned with an Isomet Low Speed saw at 1000-micron intervals in a coronal orientation, permitting long-axis sectioning of the aneurysm neck. Metal coil fragments were carefully removed with forceps under a dissection microscope. Following removal of all fragments, the slices were re-embedded in paraffin blocks. A microtome with disposable blades was used to section the blocks at 4-micron intervals. Sections were floated in a water-bath (42 ºC) then mounted on Superfrost Plus slides and dried overnight in an oven (37 ºC).

Slides were de-paraffinized and hydrated in water, followed by Hematoxylin & Eosin staining for histologic scoring or Masson's Trichrome staining for collagen deposition evaluation. An ordinal grading system was used to evaluate histological healing[74]. Briefly, neck healing score was calculated based on tissue coverage, coil micro-compaction at the neck was based on the shape of the coil mass across the neck, and the healing characteristics in the dome were categorized based on the density of cellular infiltration and area of organized tissue. The neck average, micro-compaction and healing scores were added together to obtain a total score representative of the aneurysm's healing.

The degree of inflammation was scored for areas near the wall of the aneurysm and within the bulk of the dome of the aneurysm. These scores were defined as: 0 – no inflammatory cell infiltration; 1 – mild, scant, scattered inflammatory cell infiltration; 2 – moderate, patchy inflammatory cell infiltration; 3 – marked, attenuated, diffuse inflammatory cell infiltration.

Image Pro Plus 7.0 was used to view and measure neointima thickness with a calibrated measurement tool. The measurement method was adapted from Schwartz, et al[75]. The distance from the surface of the metal coils to the surface of the neointimal tissue was measured for each coil loop located at the necks of the aneurysms. Coil loops in the parent arteries were excluded because the tissue growth on coil loops extending into the parent artery is typically greater than coil loops within the aneurysm, and therefore would not be representative of the response to the devices at the neck interface. Tissue that extended from multiple adjacent coil loops was also excluded because it would not be representative of the response to individual devices.

The fibrosis ratio (collagen deposition) was calculated for each aneurysm as the total area of fibrosis within the aneurysmal cavity and neck divided by the total area of the aneurysmal cavity and neck. Photoshop was used to determine the number of pixels stained blue by Masson's Trichrome, and this measurement was used as the total area of fibrosis. The aneurysmal cavity and neck were traced in Photoshop to obtain the total area.

In Vivo Degradation Measurement

One H&E stained slide was selected from each animal near the midpoint of the aneurysm and scanned with an OLYMPUS Digital Microscope at a magnification of 100x. The scanned images were then evaluated using the OlyVIA Virtual Microscope. Using the virtual histology slides, the cross sectional area of the remaining polymer was measured at each timepoint to calculate the surface area loss of the polymer over time.

Statistical Analysis

Data analysis was conducted using t-tests to compare parametric data and Mann-Whitney tests to compare nonparametric data. Two-tailed tests were used with a significance level < 0.05. Occurrence of recanalization and progressive occlusion between BPCs and FCCs were compared using Fisher's exact test.

Results

A total of 60 aneurysms were created and embolized using BPCs (n = 29) or SMP FCCs (n = 31). There were four unexpected fatalities. Two cases treated with FCCs for the 90 day group were sacrificed one day after treatment due to complications determined to be related to introducer sheath sizing. Two cases treated with BPCs for the 180 day group were sacrificed early: one at 11 days due to tracheal occlusion and one at 150 days due to an unknown cause. The number of animals that survived to the planned follow-up timepoint, mean aneurysm size, coil packing density, and the coil length used per aneurysm volume for each group are shown in Table 2.1. The aneurysms in groups treated with SMP FCCs for 30 and 180 days were significantly larger than the aneurysms in groups treated with BPCs for the corresponding timepoints. Two values of packing density are listed for SMP FCC-treated aneurysms to indicate the packing densities pre- and post-polymer expansion. Packing densities after foam expansion for all three SMP FCC-treated aneurysm groups were significantly higher than packing densities in BPC-treated aneurysm groups. Packing densities before foam expansion in 30 and 180 day groups

treated with SMP FCCs were significantly lower than corresponding BPC-treated aneurysm groups.

Table II-1. Aneurysm Treatment Summary. Reprinted with permission from (Herting, 2019).[71]

Device Type	Number of Animals	Aneurysm Size Before Treatment (mm^3)	Packing Density (%)	Coil Length per Aneurysm Volume (cm/mm^3)
Bare Platinum Coil				
30 Day	10	51.2 ± 26.1	23.7 ± 7.8	0.438 ± 0.16
90 Day	5	119.3 ± 114.9	24.3 ± 7.8	0.417 ± 0.18
180 Day	12	39.8 ± 20.1	29.4 ± 9.7	0.515 ± 0.17
Foam Coated Coil				
30 Day	10	144.9 ± 106.2	Pre: 17.1 ± 4.2 Post: 43.7 ± 10.8	0.173 ± 0.04
90 Day	5	85.9 ± 63.1	Pre: 22.4 ± 10.5 Post: 56.5 ± 28.1	0.229 ± 0.11
180 Day	14	71.7 ± 31.9	Pre: 17.2 ± 3.6 Post: 41.4 ± 8.7	0.175 ± 0.06

Angiographic Evaluation

Angiographic follow-up was performed at explant for all groups. Representative images are presented in Figures 2.2-2.4. Detailed outcomes for each timepoint and device type are listed in Table 2.2. The observed differences were not statistically significant in any of the three timepoint groups.

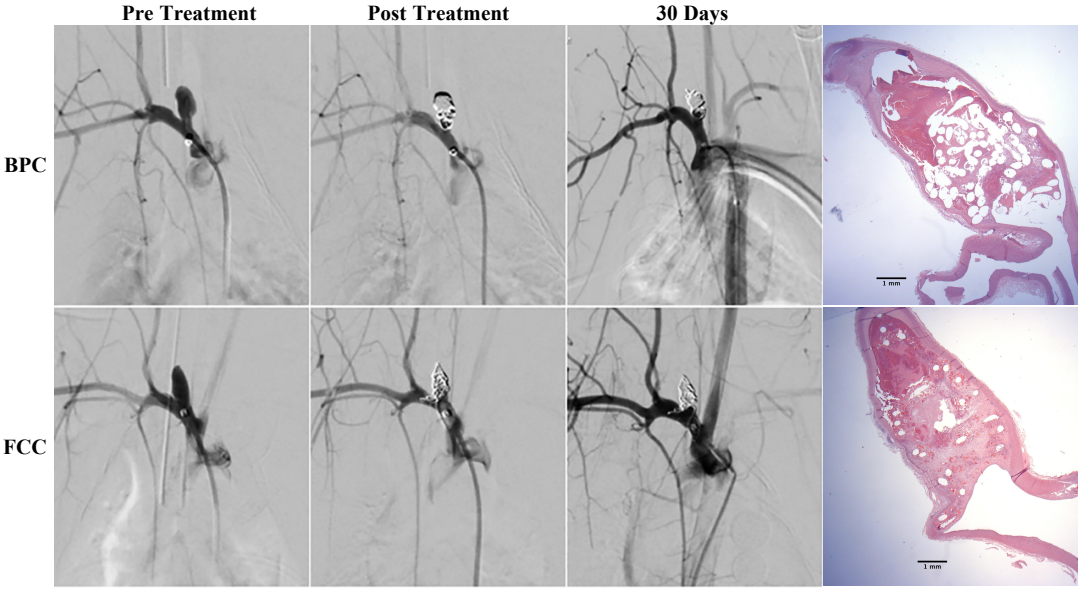

Figure II-2. Angiographic and histologic follow-up at 30 day time point. From left to right, aneurysm before treatment, immediately after treatment, at sacrifice and histologic features (top row was treated with bare platinum coils; bottom row was treated with foam-coated coils). The black arrow identifies a SMP foam strut, which is staining bright red with H&E. The yellow star indicates one location where a metal coil was removed during processing for histology. BPC: bare platinum coil. FCC: foam-coated coil. SMP: shape memory polymer. Reprinted with permission from (Herting, 2019).[71]

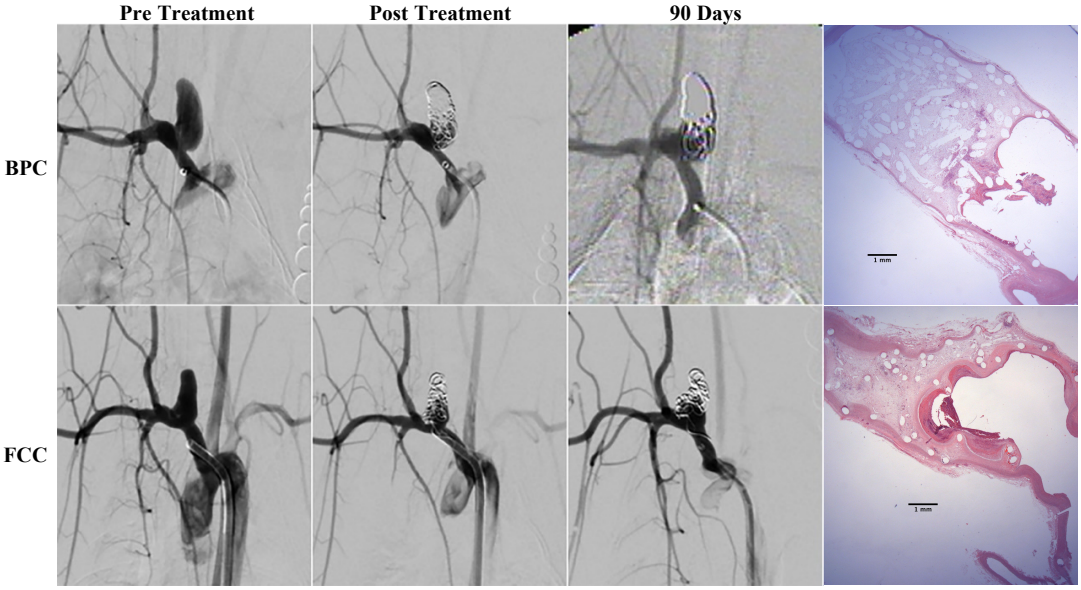

Figure II-3. Angiographic and histologic follow-up at 90 day time point. From left to right, aneurysm before treatment, immediately after treatment, at sacrifice and histologic features (top row was treated with bare platinum coils; bottom row was treated with foam-coated coils). BPC: bare platinum coil. FCC: foam-coated coil. Reprinted with permission from (Herting, 2019).[71]

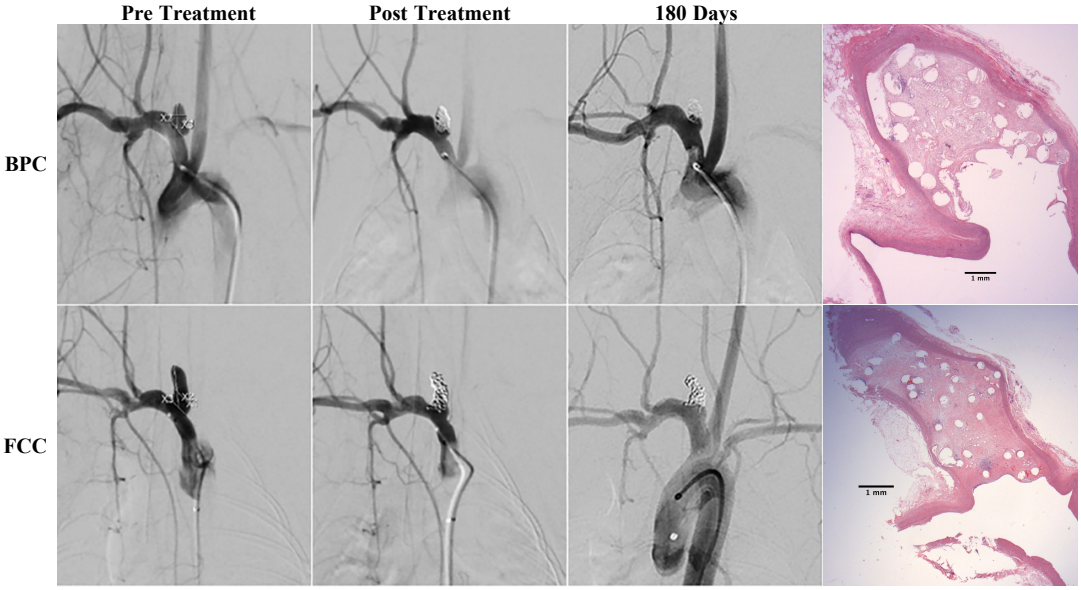

Figure II-4. Angiographic and histologic follow-up at 180 day time point. From left to right, aneurysm before treatment, immediately after treatment, at sacrifice and histologic features (top row was treated with bare platinum coils; bottom row was treated with foam-coated coils). BPC: bare platinum coil. FCC: foam coated coil. Reprinted with permission from (Herting, 2019).[71]

Table II-2. Angiographic Outcomes at Follow-up. Reprinted with permission from (Herting, 2019).[71]

Device Type	Stable Occlusion	Progressive Occlusion	Recanalization
Bare Platinum Coil			
30 Day	3	1	6
90 Day	3	0	2
180 Day	8	2	2
Foam Coated Coil			
30 Day	1	3	6
90 Day	1	0	4
180 Day	3	3	8

Histological Evaluation

Evaluation by an experienced pathologist indicated that there was no evidence of undesirable events related to thrombogenicity of the coils. In some cases, coil loops were present in the parent artery as a result of implantation, but the parent vessels remained

patent at explant in all cases. This occurred in 11 cases treated with SMP FCCs and 4 cases treated with BPCs.

Histological evaluation of the aneurysm sacs showed a combination of loose connective tissue, thrombus, and inflammatory cells. Quantitative scoring using the method published by Dai, et al resulted in total histologic score means and standard deviations for BPC-treated aneurysms at 30, 90, and 180 days of 5.9 ± 2.2, 4.5 ± 2.4, and 7.2 ± 1.1, respectively.[74] Total histologic scores for FCC-treated aneurysms were 5.5 ± 2.3, 7.8 ± 2.1, and 7.4 ± 1.2, respectively (Figure 2.5).

Chronic inflammatory foci were observed to be associated with devices in both groups. These foci were primarily composed of macrophages and multinucleated giant cells. Inflammation scores among the two groups at the three follow-up time points are listed in Table 2.3. The scores at the aneurysm wall were significantly higher in FCC-treated aneurysms at 30 days, but there were no statistically significant differences at later timepoints.

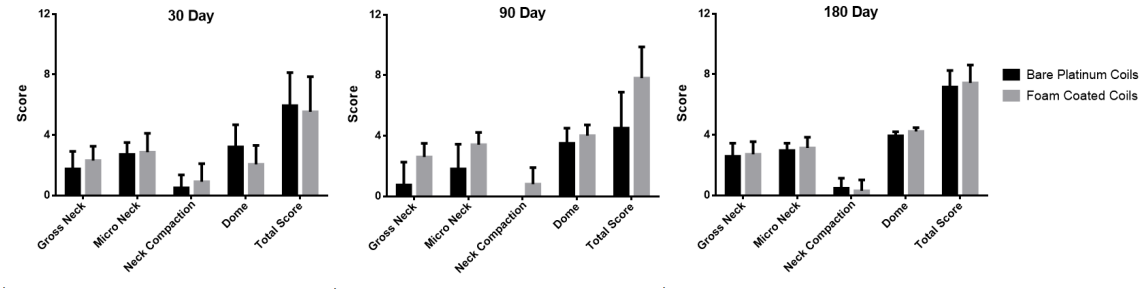

Figure II-5. Histologic healing score comparison between the two groups at each time point. Error bars represent standard deviation. Reprinted with permission from (Herting, 2019).[71]

Table II-3. Inflammation at Follow-up. Reprinted with permission from (Herting, 2019).[71]

Device Type	Dome	Wall
Bare Platinum Coil		
30 Day	0.90 ± 0.74	0.40 ± 0.84
90 Day	2.0 ± 0.0	0
180 Day	2.0 ± 0.58	0
Foam Coated Coil		
30 Day	1.7 ± 0.95	2.5 ± 0.97
90 Day	2.2 ± 0.45	0.80 ± 1.1
180 Day	2.0 ± 0.39	0

Neointima Thickness

As shown in Figure 2.6, mean neointimal tissue thickness at the necks of aneurysms was significantly higher in FCC-treated aneurysms at all three follow up time points (0.16 ± 0.06 vs 0.05 ± 0.04 mm at 30 days; 0.13 ± 0.02 vs 0.03 ± .01 mm at 90 days, 0.11 ± 0.05 vs 0.02 ± 0.01 mm at 180 days). The largest p value calculated was 0.000096 for the 30 day group. Representative *en face* images of the neointimal tissue coverage are provided in Figure 2.7.

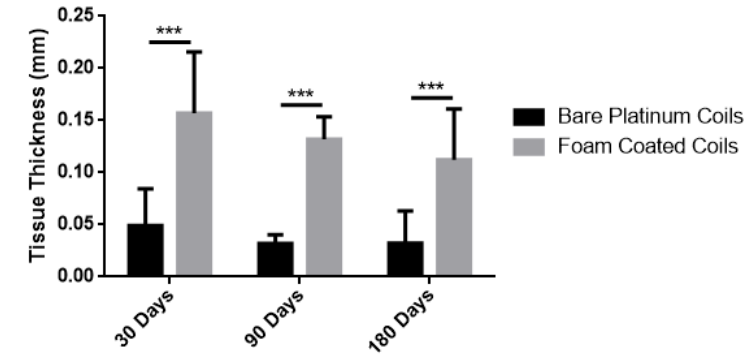

Figure II-6. Neointimal tissue thickness comparison between the two groups. Error bars represent standard deviation. ***: $p < 0.001$. Largest p value = 0.000096 in the 30 day group. Reprinted with permission from (Herting, 2019).[71]

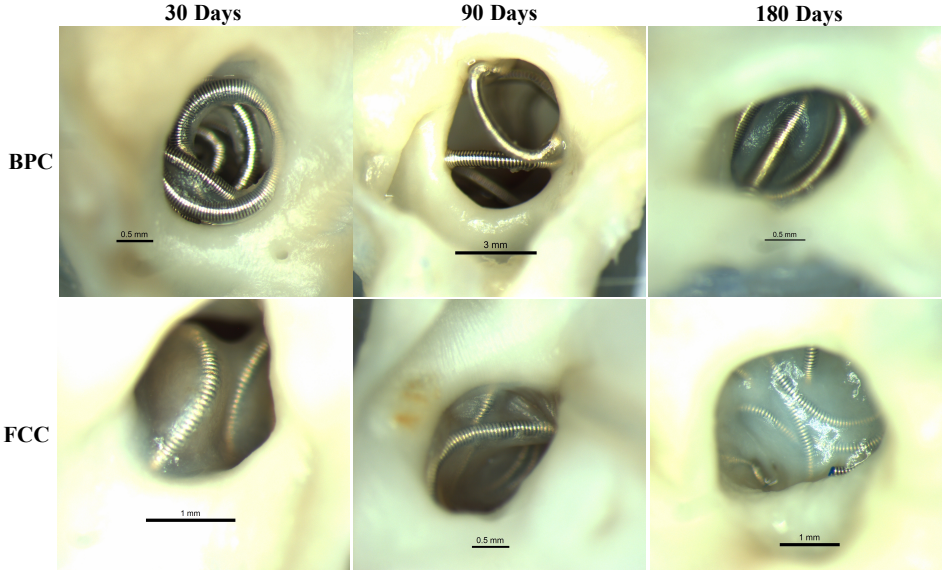

Figure II-7. Gross images of BPC-treated aneurysms (top row) and FCC-treated aneurysms (bottom row) at 30 (left), 90 (middle), and 180 day (right) time points. BPC: bare platinum coil. FCC: foam-coated coil. Reprinted with permission from (Herting, 2019).[71]

Collagen Deposition

Collagen deposition was measured as the percent area positive for Masson's Trichrome staining at 30, 90, and 180 days. Aneurysms treated with BPCs were observed to be filled with 0.77 ± 0.67% collagen at 30 days, 2.33 ± 3.04% collagen at 90 days, and 8.78 ± 2.98% collagen at 180 days. FCCs were observed to be filled with 1.68 ± 2.52% collagen at 30 days, 6.06 ± 2.77% collagen at 90 days, and 10.43 ± 2.28% collagen at 180 days. Representative sections stained with Masson's Trichrome are shown in Figure 2.8 and a chart with these values is presented in Figure 2.9.

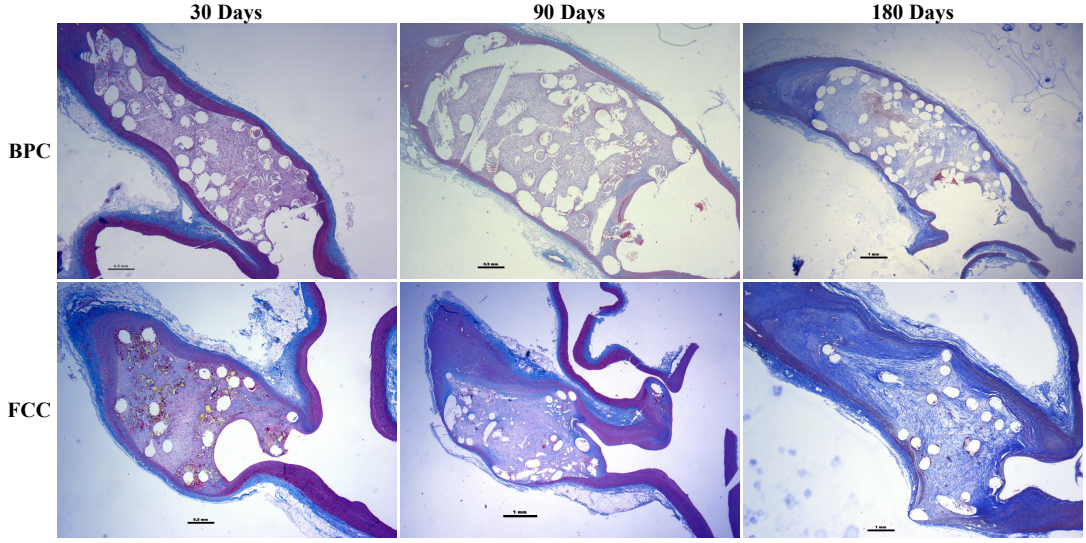

Figure II-8. Collagen deposition comparison between BPC-treated aneurysms (top row) and FCC-treated aneurysms (bottom row) at 30 (left), 90 (middle), and 180 day (right) time points. The black arrow identifies a SMP foam strut, which is staining yellow with Masson's Trichrome. BPC: bare platinum coil. FCC: foam-coated coil. SMP: shape memory polymer. Reprinted with permission from (Herting, 2019).[71]

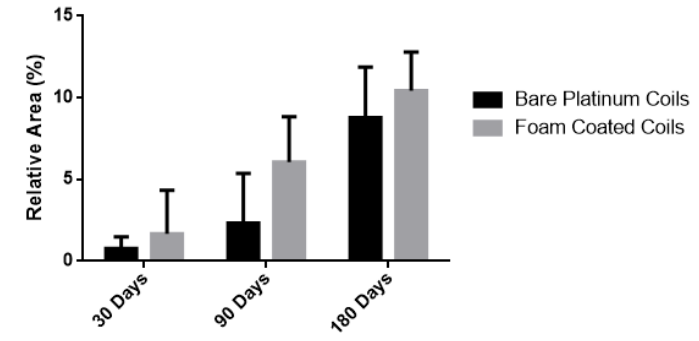

Figure II-9. Collagen deposition comparison between the two groups. Error bars represent standard deviation. Reprinted with permission from (Herting, 2019).[71]

In Vivo Degradation Measurement

In the 30 day group (n=10), polymer mass loss was estimated to be 13.57 ± 2.75% based on surface area analysis. In the 90 day group (n=5), approximate mass loss was 98.61 ± 0.22%, and in the 180 day group approximate mass loss was 97.50 ± 2.81%.

Discussion and Conclusions

Although BPCs have been widely used for intracranial aneurysm occlusion, limited tissue healing and high rates of incomplete occlusion persist as drawbacks, especially in large and giant aneurysms. Researchers have attempted to improve interventional outcomes by using either biostable or biodegradable polymers, less invasive procedures, higher volume filling of the aneurysm, and implant materials with mechanical properties that more closely match the native vessel properties[76]. Hydrocoils, for example, are covered in a hydrogel designed to expand within the aneurysm to displace blood from the aneurysm lumen, resulting in better packing attenuation. However, researchers have reported that treatment success rates were not improved in a multicenter, clinical trial,

which indicated less than 50% of aneurysms were completely occluded during follow-up[8]. While PGA/PLA fiber coated Matrix coils are reported to promote tissue reaction after deployment, they were reported to be susceptible to coil compaction and have not decreased recanalization rates from those reported previously for BPCs[67]. In this study, we tested a new generation of coils coated with porous SMP that physically changes shape to expand and more than double its volume after deployment. Similar to Hydrocoils, this expanding coating improves volume packing within aneurysms, but differs from hydrogels by providing a porous scaffold for full volume clot integration and guided tissue healing. The goal of this study was to evaluate the long term tissue healing in the domes of aneurysms treated using these new SMP FCC devices.

Greater packing densities were achieved in aneurysms treated with SMP FCCs for all groups after foam expansion. The SMP foam coating passively expands upon implantation and exposure to body fluid and temperature. This allows the foam coating to fill the interstitial space between the implanted coils that cannot be filled with standard bare platinum coil devices. Additionally, this higher volume filling can potentially allow for treatment of aneurysms using less coils, as indicated by the use of significantly less coil length per aneurysm volume treated.

Both increased packing density and porous materials are expected to lead to tissue remodeling in the aneurysm dome and at the aneurysm neck[17,41,77,78]. Our results indicated thicker neointima covering the aneurysm neck was achieved using FCCs by comparison with BPCs, and there was a trend toward earlier collagen deposition after treatment with FCCs. The average neointimal tissue thickness was 2-3 times higher in groups treated with

SMP FCCs than in groups treated with BPCs. This is likely related to the scaffold provided by the highly porous SMP foam at the aneurysm necks. Both thicker neointima and increased collagen deposition have been hypothesized to improve the stability of aneurysm embolization[14]. The increased thickness of the neointimal tissue may provide a barrier to prevent residual blood flow into aneurysms, while additional collagen or denser collagen within the aneurysm dome is believed to support the bulk tissue to resist compaction.

Ordinal scoring by an experienced pathologist indicated that healing in aneurysms treated with FCCs was not significantly different from healing in aneurysms treated with BPCs for any timepoint. The scores for BPC-treated aneurysms were similar to those previously reported in literature using this scoring system[74]. There was a trend toward accelerated healing with FCCs. The 90 day scores were higher than the BPC group at that timepoint, but the difference was not statistically significant due to a small sample size.

In the 90 day group, it was noted that a large portion of the shape memory polymer foam material from FCC devices had degraded. Previous work using this material system has described the susceptibility of the foam to oxidative degradation[42]. Analysis of foam explanted from a porcine sidewall aneurysm model has indicated that this SMP foam degrades slowly with exposure to reactive species produced by cells during the foreign body response[39,42]. Using image processing techniques on images from a previous study, SMP foam mass loss in the porcine venous pouch sidewall aneurysm model was estimated to be 12.91 ± 3.10 % at 90 days and 13.66 ± 2.70% at 180 days. The rate of degradation observed in this study using the rabbit elastase model was faster than expected based on

the images analyzed from the porcine venous pouch sidewall aneurysm models[41]. At 30 days (n=10), we determined an approximate mass loss of 13.57 ± 2.75% for the FCC devices used in this study. However, at 90 days (n=5) we observed mass loss of 98.61 ± 0.22%. 180 day explants showed a similar level of degradation, with approximate mass loss values of 97.50 ± 2.81%. Other embolic devices, such as Matrix coils, have utilized a polymer coating that degrades by hydrolysis[22,28]. The polymer used in the Matrix devices was observed to degrade at similar rates in different animal models and humans because the mechanism of degradation primarily depended on the presence of water in the environment. The inflammatory responses that produce reactive species, which are the primary cause for degradation of the proposed shape memory polymer foam, appear to differ depending on the animal model used. Recent research has described a spectrum of phenotypes for inflammatory cells that can range from pro-inflammatory to pro-healing, with pro-inflammatory phenotypes producing more reactive species[44]. We hypothesize that cells in the rabbit elastase model produce more reactive species than in the porcine sidewall model due to differences in the transition between inflammatory phenotypes during the healing process, and therefore lead to accelerated degradation of oxidatively degradable polymers. Currently, it is not known which animal model most accurately depicts the reactive species production in human aneurysms.

In this study, qualitative scoring of inflammation indicated that FCCs elicited more inflammatory cell infiltration at the walls of aneurysms at 30 days than BPCs. This inflammation could be related to the high surface area of the porous shape memory polymer used in the implant. Anderson, et al. state that implantation of materials with a

high surface area to volume ratio such as the shape memory polymer foams used in SMP FCC implants is expected to result in higher numbers of macrophages and foreign body giants cells at the implant site[58]. It is also reported that the specific cell types present at the implant site are important in determining the outcome of the foreign body response, and inflammatory cell presence is desired in a normal healing process[79]. The inflammatory response also may be higher at the wall at this earlier timepoint because cell infiltration of coiled aneurysms typically initiates from the walls and progresses toward the center of the dome[14]. The similar inflammatory responses observed between the two groups at the 90 and 180 day timepoints suggest that the degradation products from the SMP foam do not initiate a prolonged toxic local response.

In evaluating the treatment stability angiographically, we observed higher rates of recanalization in FCC-treated aneurysms for the 90 and 180 day groups relative to the BPC-treated aneurysms at the corresponding timepoints, but these differences were not statistically significant. The exact reason for recanalization remains unknown. It was noted that aneurysms treated with SMP FCCs were significantly larger for the 30 and 180 day groups, and it is known that larger aneurysms are more difficult to treat and more likely to recanalize[8]. Additionally, the FCC devices used were prototypes with limited device sizes available. In some cases, this led to the use of device sizes that were not optimal for the treatment of the rabbit elastase aneurysms. While the final packing densities were higher in the FCC-treated groups after foam expansion, the device volume before foam expansion was lower than desired. Additional device designs and sizes could lead to the ability to consistently achieve packing densities greater than 24% before foam expansion,

as is desired to reduce the likelihood of recanalization with other clinically-used coils[19]. Another potential factor is the accelerated degradation of the SMP foam material used in FCC devices. The material degraded at a rate faster than expected based on previous studies, which allows less time for tissue healing to provide a stable tissue matrix[39,42]. Finally, some inflammatory responses may also be related to tissue contraction and coil compaction.

Limitations for this study include the small sample size in the 90 day treatment group (5 per time point) which limits the statistical comparisons that can be made. Additional limitations include non-ideal SMP FCC packing densities in some cases. Packing was stopped after the experienced interventional radiologist performing the implantations felt that the aneurysm was packed sufficiently for a clinical case or once they felt that the implantation of more devices would risk leaving coil loops in the parent artery. Limited device size availability of SMP FCCs also resulted in suboptimal packing. Finally, the method chosen to randomize the cases in this study was imperfect, and aneurysm sizes differed between groups. This is an inherent limitation to all studies using this animal model, as there is limited control of the size of aneurysms created using elastase.

The devices investigated in this study, SMP FCCs, were found to increase neointima thickness at the aneurysm neck in the rabbit elastase aneurysm model. Treatment with these devices was associated with higher packing densities after expansion of the foam coating, and additional device sizes and shaping procedures are being developed to further improve device packing. Additionally, oxidative degradation of

polymeric materials likely differs between aneurysm animal models and should continue to be investigated to understand potential clinical impact. Overall, this study demonstrates that the SMP FCC device tested shows potential to enhance the healing response after endovascular treatment of aneurysms.

CHAPTER III

IN VITRO CYTOCOMPATIBILITY TESTING OF OXIDATIVE DEGRADATION PRODUCTS

Introduction

Medical devices must meet several rigorous standards of biocompatibility to demonstrate that they will be safe and effective for use in humans. ISO 10993-5 is an important standard that outlines cytocompatibility testing of medical devices, which is a screening method that allows for early detection of devices or materials that may cause harm when implanted in the body[80]. There are various methods that have been deemed acceptable by ISO 10993-5 for determining cytotoxicity, including direct and indirect contact tests using various cell types[81]. However, there is little guidance for assessing the cytotoxicity of long-term degradation byproducts.

Multiple groups have assessed the toxicity of degradation products from biomaterials[82–84]. However, these studies have all focused on materials that degrade by hydrolysis. Hydrolytically-degradable materials can be broken down using aqueous solutions, which yields a solution that can be added to cell culture media at the desired concentrations. While hydrolysis is the most prevalent degradation mechanism of commonly used biomaterials, oxidatively-degradable biomaterials allow for cell-mediated degradation of implants, which can be favorable in a number of applications[36,42]. Cell-mediated degradation allows for spatial guidance of the biological response, and it can potentially enable new tissue formation as the material is degrading to provide graded load

transfer[85–87]. One challenge with oxidatively-degradable systems is that the degradation products are difficult to characterize and may not be naturally occurring metabolites, such as those that are released from some frequently used hydrolytically degradable materials (e.g., polylactic acid or polyglycolic acid)[88]. For this reason, it is very important to investigate the potential effects that degradation products will have on adjacent cells and tissues as the materials degrade to enable clinical translation of these materials. In comparison with aqueous degradation media used for hydrolytically-degradable materials, oxidative degradation is assessed using hydrogen peroxide (H_2O_2), which is toxic to cells at concentrations used in degradation assays[89]. Therefore, cytotoxicity testing of oxidative degradation products must isolate the effects of the byproducts from the toxic effects of the H_2O_2.

To address this issue, we used oxidatively-degradable shape memory polymer (SMP) foams as a model system for characterization of degradation byproduct cytocompatibility. SMPs are a class of smart materials that can be programmed into a secondary shape, then actuated to return to their primary shape upon exposure to a designated stimulus. The properties of these materials enable designs that can be beneficial in a variety of biomedical applications[35]. Polyurethane foams are one example of SMPs that is being investigated for use in medical devices, including potential applications such as embolic devices and tissue scaffolds[71,90–94]. SMP foams can be designed to be compressed in a low-profile secondary shape that enables minimally invasive delivery and actuation at body temperature. After serving their purpose in the specific application and

allowing for the desired new tissue growth, these foams can be designed to degrade in the body[94–96].

Here, we employ a new approach to assess compatibility of degradation products from oxidatively-degradable SMPs designed for use in medical devices and tissue scaffolds. We use H_2O_2 solutions to degrade the foam materials and then add liver catalase, an enzyme that converts H_2O_2 to water and oxygen, to yield an aqueous solution of degradation products that is suitable for standard cytocompatibility testing[97]. To our knowledge, no one else has approached degradation toxicity characterization of oxidatively-degradable materials in this manner. This approach provides information on overall cytocompatibility of byproducts; however, if the fully degraded materials are not cytocompatible, it does not allow for rational redesign of the polymer system to improve degradation toxicity. In a complimentary approach, we synthesize previously identified possible SMP foam oxidative degradation products to validate the results from our new method and understand the potential effects of each byproduct that could contribute to the host response during degradation[42]. Combined, these two methods, which could be applied to a number of oxidatively-degradable polymers, provide a more complete picture of the potential effects of degradation byproducts on surrounding cells.

Materials and Methods

Shape Memory Polymer Foam Synthesis

The SMP foam synthetic protocol was originally developed by Singhal et al. and modified for specific applications[36]. Briefly, the reaction scheme used in SMP foam synthesis was a classic 2-sided polyurethane reaction where Side A contains all isocyanate components, surfactants, and a cell opener while Side B contains all hydroxyl components and catalysts.

The isocyanate monomer used was trimethyl hexamethylene diisocyanate (TMHDI, TCI America). The hydroxyl monomers used were N,N,N',N'-tetrakis(2-hydroxypropyl) ethylenediamine (HPED, 99%) and triethanolamine (TEA), and these were used as received from MilliporeSigma. The SMP foam composition used in these studies contained 60 mol% HPED and 40 mol% TEA of the hydroxyl components. The catalysts BL-22 and T-131 (Air Products) were added at 1.3 wt%, and the surfactants DC1990 and DC5943 (Air Products) were added at 7.7 wt%. The cell opener Ortegol (Evonik) was added at 0.5 wt%. The physical blowing agent Enovate 245fa (Honeywell) was added by volume to the mixture.

An isocyanate pre-polymer containing TMHDI and a portion of the hydroxyl monomers, HPED and TEA, was prepared in a glovebox and mixed by hand before placing in the oven to cure. The curing cycle was programmed into the oven (CascadeTek) to ramp up to 50°C and then return to room temperature over 48 hours. Once the pre-polymer cure cycle was complete, the isocyanate pre-polymer, surfactants, and cell opener were added by weight to a FlackTek mixing cup (FlackTek Inc.) and mixed for 60 seconds

at 2540 rpm. The remaining hydroxyl monomers and DI water were added to another FlackTek cup and mixed at 2540 rpm for two 30 second intervals, manually mixing with a spatula in between before adding the catalysts and mixing for another 30 seconds. The FlackTek cup containing the hydroxyl mixture was added to the isocyanate mixture and mixed for 15 seconds, 2 mL of Enovate was added, and the cup was mixed for another 15 seconds. The mixture was immediately poured onto a pan and placed in the oven at 90°C for 30 minutes.

Degraded Foam Solution Sample Preparation

SMP foams were cut into small pieces and then pulverized into a powder using a blender. SMP foam powder was then cleaned to remove any unreacted monomers, surfactants, and catalysts using alternating washes of isopropyl alcohol (IPA) and 0.22 µm filtered DI water under sonication. The foam powder was then dried under vacuum at 50°C overnight.

All handling of the foam after cleaning was conducted using aseptic technique. Samples of approximately 250 mg of foam powder were immersed in 10 mL of a 20% H_2O_2 solution at 70°C. The exact weights for each sample varied slightly but were recorded. Lines were drawn on the vials at the starting liquid level, and 20% H_2O_2 was added to the vials periodically to replace evaporating solution. After the foams had degraded, the H_2O_2 concentration of the degradation solutions was checked using test strips (Indigo Instruments).

Subsets of foam samples were used to test the cytocompatibility of degradation products at different endpoints throughout the process of degradation. Endpoint targets included 20%, 50%, and 90% mass loss in addition to one month after 90% mass loss, and the day on which to stop sample degradation was determined using sacrificial samples. Before weighing, each material sample was rinsed with 0.22 μm filtered DI water which was collected and used for the dilution of the H_2O_2 in later steps, and then the material was rinsed with ethanol. Samples were dried overnight at 50°C under vacuum and weighed.

Catalase Neutralization of H_2O_2

1%, 2%, and 5% H_2O_2 solutions were made from 50% H_2O_2 (MilliporeSigma) and DI water then treated with 75, 150, 300, 600, or 1500 U/mL catalase for 7 days. The concentration of H_2O_2 remaining in the solutions was measured using a ferric thiocyanate kit (Chemetrics), the concentration of catalase remaining in the solutions was measured using a Pierce Coomassie Plus Protein Assay (ThermoFisher Scientific), and the cytocompatibility of the solutions was tested using methods described below. The results were used to inform the methods for testing solutions with degraded SMP foam material.

Degraded Foam Solution Cytocompatibility Sample Preparation

Degraded foam solutions were diluted to ~2% H_2O_2 with 0.22 μm filtered DI water, then incubated with 1500 U/mL catalase at 37°C for 7 days with agitation. At this point a sample was taken to test the remaining concentration of H_2O_2 using the ferric

thiocyanate kit. If the H_2O_2 concentration was greater than 0.1 ppm, precipitated catalase was filtered out of the solution, and then 1500 U/mL were reintroduced for an additional 7 days. This process was repeated until all samples were confirmed to contain <0.1 ppm H_2O_2 after neutralization using the ferric thiocyanate test kit before cytotoxicity testing. A fresh sample of 2% H_2O_2 and a sample of sterile DI water were also treated with catalase to serve as controls for the cytotoxicity assay.

Media samples for cell exposure were made using 10X Dulbecco's Modified Eagle Medium (DMEM, MilliporeSigma) diluted to 1X with each sample solution, including controls. These media samples were also supplemented with 10% newborn calf serum (NCS, MilliporeSigma), 1% penicillin/streptomycin (P/S, VWR), 0.1% fungizone (VWR), 3.5 mg/mL glucose, 3.7 mg/mL sodium bicarbonate, 4 µg/mL folic acid, and 0.584 mg/mL L-glutamine. The maximum concentration tested was the concentration achieved after addition to cell culture media, and serial dilutions were performed from this concentration to test a range that produced a dose-response curve.

Degradation Byproduct Analog Synthesis

TM-Gly and TM-Lac: TMHDI (TM) was dissolved in dimethylsulfoxide (DMSO) at ~1 g/ml under anhydrous conditions. The TMHDI solution was added dropwise to glycolic acid (Gly) or lactic acid (Lac) at a 1:2.1 molar ratio while stirring on a magnetic stir plate under nitrogen. The reaction was carried out for 24 hours at room temperature and then an additional 24 hours at 50°C. The final product was dried under

vacuum for ~72 hours to remove DMSO. Fourier transform infrared (FTIR) and nuclear magnetic resonance (NMR) spectroscopy were utilized to confirm synthesis. Samples were solution cast directly onto KBr pellets for acquisition of transmission FTIR spectra using a Bruker TENSOR 27 spectrometer. Proton NMR spectra of control and functionalized polymers were recorded on Mercury 300 MHz spectrometer using a TMS/solvent signal as an internal reference.

TM-Gly: ^{1}H NMR ($(CD_3)_2SO$ with 0.05% v/v TMS, 300 MHz): 0.85 ppm (m, -C*H*$_2$C*H*(C*H*$_3$)C*H*$_2$C(C*H*$_3$)$_2$-, 14H), 2.71-3.19 ppm (m, -NHC*H*$_2$-, 4H), 3.76-3.92 ppm (m, -OC*H*$_2$C=O, 4H), 4.94-7.85 ppm (m, -N*H*-, 2H).

TM-Lac: ^{1}H NMR ($(CD_3)_2SO$ with 0.05% v/v TMS, 300 MHz): 0.85 ppm (m, -C*H*$_2$C*H*(C*H*$_3$)C*H*$_2$C(C*H*$_3$)$_2$-, 14H), 1.06-1.38 ppm (m, -OCH(C*H*$_3$)C=O, 6H), 2.63-3.15 ppm (m, -NHC*H*$_2$-, 4H), 3.97-4.17 ppm (m, -OC*H*(CH_3)C=O, 2H), 4.72-7.78 ppm (m, -N*H*-, 2H).

Boc Protection of Amine Groups: Di-tert-butyl carbonate was dissolved in tetrahydrofuran (THF) at ~2-4 g/ml and added dropwise to the amine component (ethanolamine (EA), 1-amino-2-propanol (Amino), diethanolamine (DEA), or bis(2-hydroxypropyl) amine (Bis)) at a 1.1:1 molar ratio. The reaction was vented to allow for CO_2 escape and allowed to proceed at room temperature for 1 hour. The reaction was dried under vacuum at 65°C for ~24 hours to remove THF and tert-butanol. The final product was analyzed using FTIR and NMR spectroscopy as described in the previous section. FTIR confirmed introduction of the carbonyl of the urethane at ~1650-1700 cm^{-1} and methyl groups at ~2800-3000 cm^{-1}, **Figure S1 (Supplemental)**.

Boc-EA: ^{1}H NMR ($(CD_3)_2SO$ with 0.05% v/v TMS, 300 MHz): 1.35 ppm (m, -C*H*$_3$, 9H), 2.98 and 3.45 ppm (m, -NHC*H*$_2$-, 2H), 4.55 ppm (m, -C*H*$_2$OH, 2H), 6.60 ppm (s, O*H*-, 1H).

Boc-Amino: ^{1}H NMR ($(CD_3)_2SO$ with 0.05% v/v TMS, 300 MHz): 0.97 and 1.35 ppm (m, -C*H*$_3$, 12H), 2.85 and 3.58 ppm (m, -NHC*H*$_2$-, 2H), 4.55 ppm (m, >C*H*OH, 1H), 6.55 ppm (s, O*H*-, 1H).

Boc-DEA: ^{1}H NMR ($(CD_3)_2SO$ with 0.05% v/v TMS, 300 MHz): 1.35 ppm (m, -C*H*$_3$, 9H), 3.22 ppm (m, >NC*H*$_2$-, 4H), 3.50 ppm (m, -C*H*$_2$OH, 4H), 4.71 ppm (s, O*H*-, 2H).

Boc-Bis: ^{1}H NMR ($(CD_3)_2SO$ with 0.05% v/v TMS, 300 MHz): 0.97 and 1.35 ppm (m, -C*H*$_3$, 15H), 3.00 and 3.24 ppm (m, >NC*H*$_2$-, 4H), 3.80 ppm (m, >C*H*OH, 2H), 4.73 and 4.91 ppm (s, O*H*-, 2H).

All amine-containing molecules were functionalized with Boc groups at ~90-95%, according to the NMR spectra, **Figure S1**.

TM-EA and TM-Amino: TM-EA and TM-Amino were synthesized using the same method as TM-Gly and TM-Lac, using the Boc-protected EA and Amino products. At the completion of the reaction, 4M HCl in dioxane was added to the reaction vessel at a 1:1 ratio (HCl:Boc). The resulting solution was stirred under nitrogen at 60°C overnight. Then, 4M NaOH in water was added at a 1:1 ratio (NaOH:HCl) to neutralize the reaction. The solution was stirred and vented, and the solvent was filtered off. The product was washed with reverse osmosis (RO) water 5 times to remove residual solvent and byproducts and then dried under vacuum at 65°C for 48 hours. FTIR and NMR spectroscopy confirmed synthesis of TM-EA and TM-Amino.

TM-EA: ^{1}H NMR ($(CD_3)_2SO$ with 0.05% v/v TMS, 300 MHz): 0.85 ppm (m, -C*H*$_2$C*H*(C*H*$_3$)C*H*$_2$C(C*H*$_3$)$_2$-, 14H), 2.62-3.12 ppm (m, -NHC*H*$_2$- and –OCH$_2$C*H*$_2$NH$_2$, 8H), 4.13 ppm (s, -OC*H*$_2$CH$_2$NH$_2$, 4H), 5.16-7.79 ppm (m, -N*H*-, 2H).

TM-Amino: ^{1}H NMR ($(CD_3)_2SO$ with 0.05% v/v TMS, 300 MHz): 0.85 ppm (m, -C*H*$_2$C*H*(C*H*$_3$)C*H*$_2$C(C*H*$_3$)$_2$-, 14H), 1.05-1.71 ppm (m, -OCH(C*H*$_3$)CH$_2$NH$_2$, 6H), 2.67-3.15 ppm (m, -NHC*H*$_2$- and OCH(CH$_3$)C*H*$_2$NH$_2$, 8H), 3.85 ppm (s, -OC*H*(CH$_3$)CH$_2$NH$_2$, 2H), 4.64-7.75 ppm (m, -N*H*-, 2H).

TM-DEA-Gly, TM-DEA-Lac, TM-Bis-Gly, TM-Bis-Lac, TM-DEA-EA, TM-DEA-Amino, TM-Bis-EA, and TM-Bis-Amino: Under anhydrous conditions, TMHDI was dissolved in DMSO (~1 g/ml) and added to Boc-protected DEA or Bis dropwise at a 2.1:1 ratio while stirring under nitrogen. Gly, Lac, Boc-EA, or Boc-Amino was dissolved in DMSO (~1 g/ml) and added dropwise to the other components while stirring under nitrogen. The reaction was carried out at room temperature for 24 hours and then at 50°C for an additional 24 hours. Then, 4M HCl in dioxane was added to the reaction vessel at a 1:1 ratio (HCl:Boc), and the reaction was carried out overnight under nitrogen at 60°C. After cooling to room temperature, 4M NaOH was added (1 NaOH:1 HCl), and the solution was stirred and vented before filtering off the solvent. The final product was washed 5 times with RO water and dried under vacuum at 65°C for 48 hours. Synthesis was confirmed using FTIR and NMR spectroscopy. Synthetic schemes and product structures are available in the electronic supplementary information.

TM-DEA-Gly: ^{1}H NMR ($(CD_3)_2SO$ with 0.05% v/v TMS, 300 MHz): 0.85 ppm (m, -C*H*$_2$C*H*(C*H*$_3$)C*H*$_2$C(C*H*$_3$)$_2$-, 28H), 2.65-3.15 ppm (m, -NHC*H*$_2$-, 12H), 3.71 and 3.86 ppm (d, -OC*H*$_2$-, 8H), 4.75-7.90 ppm (m, -N*H*-, 5H).

TM-DEA-Lac: ^{1}H NMR ($(CD_3)_2SO$ with 0.05% v/v TMS, 300 MHz): 0.85 ppm (m, -C*H*$_2$C*H*(C*H*$_3$)C*H*$_2$C(C*H*$_3$)$_2$-, 28H), 1.07-1.45 ppm (m, -OCH(C*H*$_3$)C=O, 6H), 2.65-3.15 ppm (m, -NHC*H*$_2$-, 12H), 3.61 and 3.92 ppm (m, -OC*H*(CH_3)C=O and –OC*H*$_2$-, 6H), 4.75-7.90 ppm (m, -N*H*-, 5H).

TM-Bis-Gly: ^{1}H NMR ($(CD_3)_2SO$ with 0.05% v/v TMS, 300 MHz): 0.85 ppm (m, -C*H*$_2$C*H*(C*H*$_3$)C*H*$_2$C(C*H*$_3$)$_2$-, 28H), 1.41 ppm (m, -OCH(C*H*$_3$)-, 6H), 2.65-3.15 ppm (m, -NHC*H*$_2$-, 12H), 3.59 and 3.78 ppm (d, -OC*H*$_2$- and -OC*H*(CH_3)-, 6H), 4.75-7.90 ppm (m, -N*H*-, 5H).

TM-Bis-Lac: ^{1}H NMR ($(CD_3)_2SO$ with 0.05% v/v TMS, 300 MHz): 0.85 ppm (m, -C*H*$_2$C*H*(C*H*$_3$)C*H*$_2$C(C*H*$_3$)$_2$-, 28H), 1.07-1.45 ppm (m, -OCH(C*H*$_3$)C=O and -OCH(C*H*$_3$)-, 12H), 2.65-3.15 ppm (m, -NHC*H*$_2$-, 12H), 3.85 and 3.92 ppm (d, -OC*H*(CH_3)-, 4H), 4.75-7.90 ppm (m, -N*H*-, 5H).

TM-DEA-EA: ^{1}H NMR ($(CD_3)_2SO$ with 0.05% v/v TMS, 300 MHz): 0.85 ppm (m, -C*H*$_2$C*H*(C*H*$_3$)C*H*$_2$C(C*H*$_3$)$_2$-, 28H), 2.65-3.15 ppm (m, -NHC*H*$_2$- and –OCH$_2$C*H*$_2$NH$_2$, 16H), 4.12 and 4.22 ppm (d, -OC*H*$_2$, 8H), 4.75-7.90 ppm (m, -N*H*-, 5H).

TM-DEA-Amino: ^{1}H NMR ($(CD_3)_2SO$ with 0.05% v/v TMS, 300 MHz): 0.85 ppm (m, -C*H*$_2$C*H*(C*H*$_3$)C*H*$_2$C(C*H*$_3$)$_2$-, 28H), 1.07-1.45 ppm (m, -OCH(C*H*$_3$)CH$_2$NH$_2$, 6H), 2.65-3.15 ppm (m, -NHC*H*$_2$- and -OCH(CH_3)C*H*$_2$NH$_2$, 16H), 4.23 ppm (s, -OC*H*(CH_3)CH$_2$NH$_2$ and –OC*H*$_2$-, 6H), 4.75-7.90 ppm (m, -N*H*-, 5H).

TM-Bis-EA: ^{1}H NMR ($(CD_3)_2SO$ with 0.05% v/v TMS, 300 MHz): 0.85 ppm (m, -C*H*$_2$C*H*(C*H*$_3$)C*H*$_2$C(C*H*$_3$)$_2$-, 28H), 1.07-1.45 ppm (m, -OCH(C*H*$_3$)-, 6H), 2.65-3.15 ppm (m, -NHC*H*$_2$- and –OCH$_2$C*H*$_2$NH$_2$, 16H), 4.01 ppm (s, -OC*H*$_2$ and -OC*H*(CH$_3$)-, 6H), 4.75-7.90 ppm (m, -N*H*-, 5H).

TM-Bis-Amino: ^{1}H NMR ($(CD_3)_2SO$ with 0.05% v/v TMS, 300 MHz): 0.85 ppm (m, -C*H*$_2$C*H*(C*H*$_3$)C*H*$_2$C(C*H*$_3$)$_2$-, 28H), 1.07-1.45 ppm (m, -OCH(C*H*$_3$)CH$_2$NH$_2$ and -OCH(C*H*$_3$)-, 12H), 2.65-3.15 ppm (m, -NHC*H*$_2$- and -OCH(CH$_3$)C*H*$_2$NH$_2$, 16H), 3.84 and 4.05 ppm (d, -OC*H*(CH$_3$)CH$_2$, 4H), 4.75-7.90 ppm (m, -N*H*-, 5H).

Byproduct Analog Cytocompatibility Sample Preparation

Synthesized degradation byproduct analogs were dissolved in DMSO at 200 mg/mL. These product/DMSO solutions were added to cell culture media composed of 1X DMEM, 10% NCS, 1% P/S, and 0.1% fungizone to afford final concentrations of 0.5% DMSO and 1 mg/mL of the specified degradation product. DMSO was used to enhance the solubility of the degradation products in media. Glyoxal and oxalic acid are expected degradation products that are commercially available. These chemicals were purchased from MilliporeSigma and dissolved using the same methods.

Four of the six byproduct analogs with lactic acid and glycolic acid end groups (TM-DEA Lac, TM-Bis Lac, TM-DEA Gly, and TM-Bis Gly) still precipitated when added to cell culture media in DMSO. To obtain testable solutions, these products were extracted in sterile DI water with 5% DMSO at a concentration of 10 mg/mL for 72 hours at 37°C under agitation. The extract was then filtered through a 0.45 μm centrifuge tube

filter top to remove particulates. The tube used for extraction and the filter used were dried and weighed before initiating the extraction so that the degradation product mass remaining after extraction could be measured and used to determine the concentration of the degradation product in the extraction solution. The extraction solution was added to cell culture media to afford a 10% solution, resulting in a DI water concentration of 10%, a DMSO concentration of 0.5%, and a degradation product concentration of 10% of the calculated extract concentration.

Cytocompatibility Assays

For each assay, BALB/3T3 Fibroblasts, Clone A31 (3T3s, ATCC) were seeded in 96-well tissue culture plates at a concentration of 7,500 cells/well and incubated in a humidified incubator at 37°C with 5% CO_2 for 24 hours. Cell morphology was observed in all wells using an inverted microscope and even cell distribution was confirmed before treatment. Cell culture media was aspirated, and cells were incubated with degraded foam solutions or byproduct analog samples in cell media to determine cytocompatibility. An untreated control was included in each assay to provide a reference for 100% cell viability. These untreated controls were made from the media used to dissolve the degradation products tested in the same assay. For degraded foam samples, untreated controls were made from 10X DMEM, using sterile DI water as the diluent instead of a degraded foam solution. For synthesized samples, untreated controls were made from cell culture media with 0.5% DMSO, and for samples that required extraction, untreated controls included

0.5% DMSO and 10% DI water. Cells were incubated with treatments for 48 hours at 37°C with 5% CO_2.

Following incubation, cell morphology was observed using an inverted microscope to evaluate changes induced by addition of the treatments. The cells were washed with DPBS, then 200 µL of a solution of 5% resazurin (MilliporeSigma) in cell culture media were added to each well for 3 hours. Resazurin is a blue dye that is converted to a fluorescent pink form, resorufin, by metabolically active cells. After 3 hours, the fluorescence intensity of the solution in each well relative to blanks with no cells was quantified with a Tecan Infinite M200 Pro plate reader using an excitation wavelength of 560 nm and an emission wavelength of 590 nm. Cell viability was calculated using the following equation:

$$Cell\ Viability\ (X) = \frac{RFU_{560/590}(X) - RFU_{560/590}(blanks)}{RFU_{560/590}(Untreated\ Control) - RFU_{560/590}(blanks)}$$

where X is any treatment group and RFU is relative fluorescent units (i.e. fluorescence intensity).

The cytocompatibility of H_2O_2 and catalase were tested first by adding them to cell culture media alone. Testing for each byproduct analog was done in two steps. The first step tested a broad range of concentrations to determine an appropriate subset of concentrations to evaluate. The second step was used to calculate the concentrations at which a 30% reduction in cell viability would be observed (IC_{30}) for each sample. In ISO 10993-5, it is recommended that a treatment be considered cytotoxic if it reduces cell viability by 30% or more as measured by a metabolic assay. The IC_{30} values were

considered the cytotoxic thresholds for this study based on the guidelines in ISO 10993-5. IC_{30} values were calculated for all products by fitting to the Graphpad Prism [Inhibitor] vs Response – Variable Slope model then interpolating the x value (concentration) for a y value (cell viability) of 70%.

Statistical Analysis

All IC_{30} determination assays were repeated at least 3 times. One-way ANOVA was used to test for differences between the mean IC_{30} values from the degraded foam solutions at different endpoints (i.e. 20% degraded vs 50% degraded vs 90% degraded vs 1 month after 90% degraded).

Results

Neutralization of H_2O_2 with Catalase

The cytocompatibility of H_2O_2 and catalase were tested as shown in Figure 3.1. To isolate the potentially toxic effects of the degradation product samples from the effects of the vehicle solution, the H_2O_2 must be sufficiently neutralized without introducing toxic levels of the catalase enzyme. However, it was observed that the catalase enzyme precipitates out of solution over time so filtration of the catalase enzyme with a sterile 0.22 μm syringe filter was implemented after these assays.

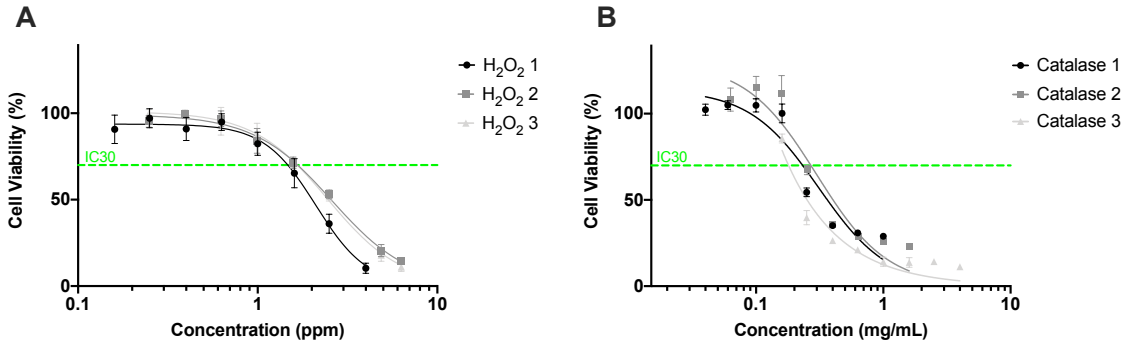

Figure III-1. Cytocompatibility of (A) H_2O_2 and (B) catalase enzyme when added to cell culture media. The average IC_{30} for H_2O_2 was 1.60 ± 0.11 ppm and the average IC_{30} for catalase was 227 ± 45 µg/mL. The numbers 1, 2, and 3 in the legends indicate replicate runs of the assays. Error bars represent standard deviation (n=6 wells per concentration).

Neutralization of H_2O_2 solutions without polymer degradation products required ~7 days incubation at 37°C with agitation. Cytocompatibility was observed for 1% solutions neutralized with 300 U/mL of catalase or greater, for all 2% solutions, and for 5% solutions neutralized with 1500 U/mL as seen in Figure 3.2. In all cases, the catalase remaining in solution after filtration was below its IC_{30}, which was measured to be 227 µg/mL (785 U/mL). The H_2O_2 remaining in solution was below the measured IC_{30} of 1.60 ppm for 1% and 2% H_2O_2 samples treated with 600 or 1500 U/mL.

In some cases, the H_2O_2 remaining exceeded the IC_{30} of H_2O_2 by as much as 1 ppm, but the solutions were still observed to be cytocompatible in testing. The residual catalase may have a small protective effect on the cells, but this needs to be tested further. In subsequent experiments, the catalase was denatured after neutralization by submersion in a water bath at 65°C for >15 minutes.

When degraded foam solutions were tested, <0.1 ppm H_2O_2 was not always achieved within 7 days. In these cases, the solutions were filtered with a 0.22 µm syringe filter and re-treated with catalase until sufficient neutralization was achieved. The degradation products in solution may have some inhibitory effect on H_2O_2 neutralization.

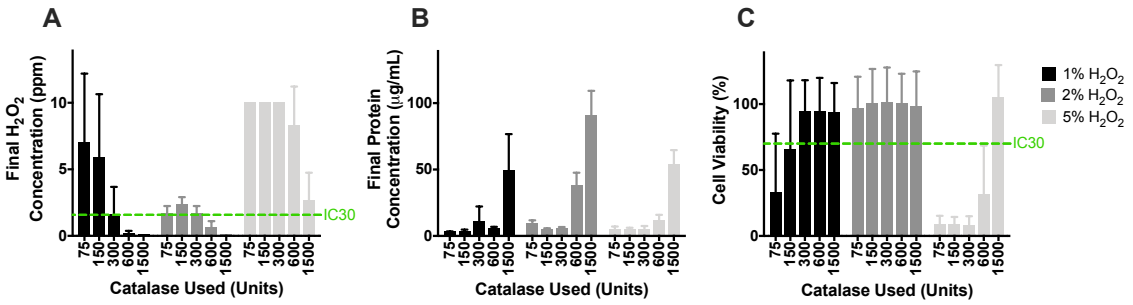

Figure III-2. Concentrations of A) H2O2 and B) catalase remaining in 0.22 µm filtered solutions, and C) cytocompatibility of resulting solutions after neutralization of varied H2O2 concentrations with varied catalase concentrations. The experimentally obtained IC30 of H2O2 is shown on chart A for reference. The maximum concentration reading possible for the kit used is 10 ppm H2O2. The experimentally obtained IC30 of catalase is above the range shown by chart B. Error bars represent standard deviation (n=3).

Cytocompatibility of Degraded Foam Solutions

The H_2O_2 concentration remaining after degradation was ~20% for all samples. Average measured mass losses were 15.5 ± 4.4% for the 20% target samples, 46.0 ± 4.2% for the 50% target samples, and 91.1 ± 2.1% for the 90% target samples. Samples degrading for 1 month more than the 90% target samples did not have any measurable mass remaining. Dose-response curves were obtained for the samples from each endpoint and are presented in Figure 3.3. Average IC_{30} values were determined to be 0.381 ± 0.176 mg/mL for 20% degraded samples, 1.295 ± 0.946 mg/mL for 50% degraded samples,

1.103 ± 0.354 mg/mL for 90% degraded samples, and 0.567 ± 0.198 mg/mL for samples degraded for 1 month more than the 90% degraded samples. One-way ANOVA indicated that there were no statistically significant differences between these mean IC_{30} values ($p=0.12$). The 50% group had the greatest range of IC_{30} values from 0.366 mg/mL at the lowest to 2.257 mg/mL at the highest. Two of the samples from the 50% group did not result in 30% cell death at the highest concentrations tested, and therefore the IC_{30} values had to be extrapolated from the curves obtained.

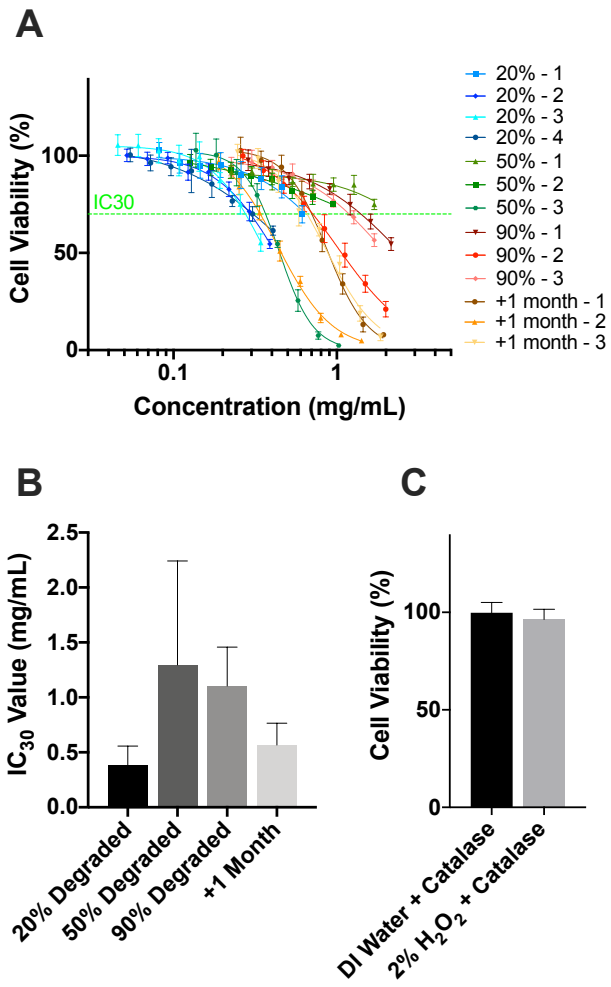

Figure III-3. Cytocompatibility of degraded foam solutions after neutralizing the H_2O_2. A) Dose-response curves for the replicates at each target endpoint tested. The numbers 20%, 50%, 90%, and +1 month indicate the target degradation endpoint for that group of samples. The numbers 1, 2, 3, and 4 in the legend indicate replicate runs of the assays, and 6 wells were tested for each concentration. B) The average IC_{30} values for each endpoint determined using the curves in A. C) Cell viability results for cytocompatible control solutions, which included DI water and 2% H_2O_2 that underwent the same neutralization process as the degraded foam solutions in parallel. Error bars represent standard deviation.

Synthesis of Degradation Byproduct Analogs

Byproduct synthesis was confirmed using FTIR and NMR spectroscopy. All final products showed an increased methylation at ~2900 cm^{-1} with the addition of TMHDI and a lack of isocyanate at ~2250 cm^{-1}, indicating that all TMHDI was reacted. The introduction of a secondary amine peak at ~3300 cm^{-1} and the introduction/shifting of the carbonyl peak to ~1640 and 1540 cm^{-1} can be viewed in the spectra of byproducts with carboxylic acid end groups, Figure 3.4A. Loss of the primary amine peak at ~3350 cm^{-1} and introduction of a carbonyl peak at ~1700 cm^{-1} is observed in the amine-terminated byproduct spectra, Figure 3.4B. NMR spectroscopy was utilized to quantify functionalization of byproducts with desired end and middle groups. Carboxylic acid-terminated byproducts were all 83-90% functionalized with the desired end and/or middle groups in comparison to TMHDI, Figure 5.2 (Appendix), and amine-terminated byproducts were functionalized with desired end/middle groups at 77-91%, Figure 5.3 (Appendix).

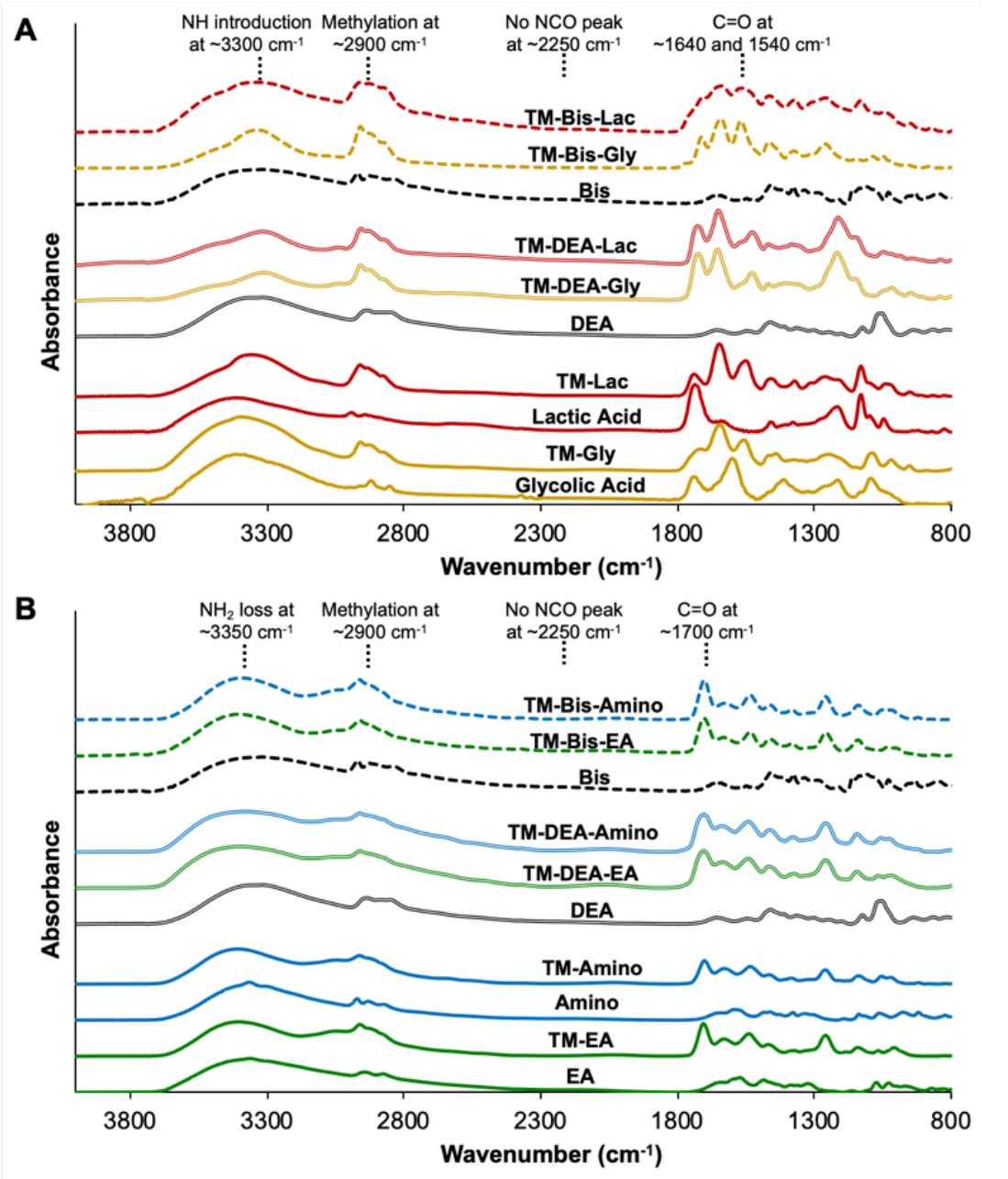

Figure III-4. Fourier transform infrared spectra of (A) carboxylic acid-terminated and (B) amine-terminated degradation byproducts with peaks of interest labeled above. The abbreviations for the components used to synthesize each degradation product are as follows: TM – trimethyl hexamethylene diisocyanate, Bis – bis(2-hydroxypropyl) amine, DEA – diethanolamine, Lac – lactic acid, Gly – glycolic acid, Amino – 1-amino-2-propanol, EA – ethanolamine.

Cytocompatibility of Degradation Byproduct Analogs

Dose-response curves were obtained for degradation byproduct analogs within a concentration range of 0.001 to 3.160 mg/mL. The IC_{30} values obtained range from 0.009 mg/mL to 1.384 mg/mL. In general, analogs with amine end groups tended to have lower IC_{30} values than analogs with carboxylic acid end groups. Representative dose-response curves are presented in Figure 3.5 and average IC_{30} values for each product are listed in Table 3.1.

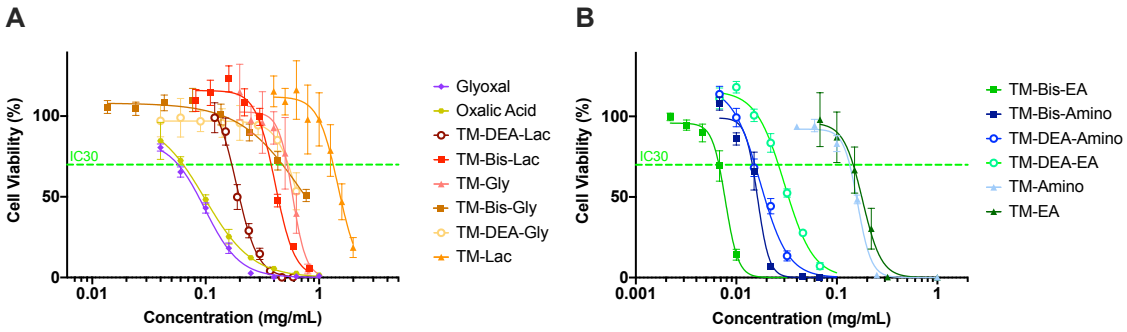

Figure III-5. Cytocompatibility of degradation byproduct analogs with (A) carboxylic acid and aldehyde end groups or (B) amine end groups. Each degradation byproduct analog was tested in 3 separate assays with 6 wells used per concentration tested, and 1 representative curve was selected for each to reduce clutter in this figure. Error bars represent standard deviation. The abbreviations for the components used to synthesize each degradation product are as follows: TM – trimethyl hexamethylene diisocyanate, DEA – diethanolamine, Bis – bis(2-hydroxypropyl) amine, Lac – lactic acid, Gly – glycolic acid, EA – ethanolamine, Amino – 1-amino-2-propanol.

Table III-1. Average IC_{30} values for synthesized degradation byproduct analogs with standard deviations.

End Groups	IC_{30} (mg/mL)
Glyoxal	0.044 ± 0.015
Oxalic Acid	0.092 ± 0.052
TM-DEA-Lac	0.297 ± 0.120
TM-Bis-Lac	0.320 ± 0.059
TM-Gly	0.390 ± 0.119
TM-Bis-Gly	0.544 ± 0.221
TM-DEA-Gly	0.800 ± 0.241
TM-Lac	1.384 ± 0.056
TM-Bis-EA	0.009 ± 0.004
TM-Bis-Amino	0.021 ± 0.006
TM-DEA-Amino	0.024 ± 0.009
TM-DEA-EA	0.041 ± 0.015
TM-Amino	0.167 ± 0.061
TM-EA	0.169 ± 0.129

Discussion and Conclusions

Biodegradable polymers are an essential tool for many strategies aimed at improving drug delivery, medical devices, and tissue regeneration. Biodegradation can be used as a method of delivering a payload at a desired rate or allowing a material to evolve with the biological environment in which it is implanted. In some applications, it can be beneficial to develop a material that degrades in response to specific cell activity such as enzyme or reactive oxygen species release[85–87]. Polymers have been designed to degrade upon exposure to reactive oxygen species for use in drug delivery, biosensing, and tissue engineering applications[85,98–102]. The methods described here could be used to evaluate degradation products from these systems for toxicity or for their impact on the desired

outcomes after implantation. These methods may also be useful in evaluating other polymers that may degrade by oxidation as one of multiple mechanisms as is proposed of some other polyurethane scaffolds and poly (ethylene glycol) hydrogels[103–108].

While the definition of biocompatibility varies depending on the intended application of the material and the final form of the device, determining if the material will be toxic to adjacent cells and tissues is one of the early testing priorities. In this work, we describe methods of assessing the cytocompatibility of polymers designed to degrade oxidatively. This type of testing traditionally presents a challenge, because the common method of simulating oxidative degradation *in vitro* utilizes exposure to H_2O_2 solutions. H_2O_2 solutions are toxic to cells and tissues at concentrations that are substantially lower than the ISO 10993 recommended concentration for degradation studies (1.6 ppm vs 3%). Therefore, it is necessary to isolate the toxic effects of the degradation products from the toxic effects of the H_2O_2 solution used to obtain them.

The method established here utilize a catalase enzyme to convert H_2O_2 in solution to water and oxygen, and polymer synthesis techniques were used to create analogs of the expected degradation products to validate the results. In our experiments, these degraded material solutions and synthesized byproduct analogs were used in standard cytocompatibility assays to assess cell viability after exposure to the test articles. The degraded foam solution experiments provide a better representation of the likely distributions of byproducts, but testing each individual product analog can identify those with stronger contributions to toxicity. If one product is found to be excessively toxic or mutagenic, new monomers can potentially be selected to redesign a material without these

negative effects. Conversely, if one product is found to enhance cell proliferation or modulate the inflammatory response, a material can be redesigned to boost these positive effects. These methods could be utilized to test cell proliferation, gene or protein expression changes, and/or genotoxicity in response to *in vitro* exposure to degradation products from oxidatively-degradable polymers. Additionally, an injectable degradation product solution could be used to test systemic toxicity, reproductive toxicity, and/or carcinogenicity *in vivo.*

Based on these studies, we expect that the degradation of the SMP foam tested is unlikely to cause a cytotoxic response *in vivo*. Interestingly, the toxicity thresholds appeared to vary depending on the extent to which the materials had degraded, but these differences were not found to be statistically significant. The toxicity threshold was lowest at the earliest timepoint tested then increased at the next timepoint and appeared to decrease until the last timepoint tested. This may suggest a changing distribution of the degradation products in solution over time.

Weems et al. evaluated the degradation mechanism for these materials in both model compounds and bulk material studies; tertiary amine oxidation was quantified with regards to the formation of amine oxides, secondary amines, primary amines, and carboxylic acids[42]. In this study, we observed that the degradation products with amine end groups tended to have lower IC_{30} values than the products with carboxylic acid end groups. In the degraded foam solutions generated *in vitro,* the amine end group products are likely more abundant at early timepoints until the amines are further oxidized. At the latest timepoints, the smallest degradation products, glyoxal and oxalic acid, are likely

increasing in abundance, and these were products that also had some of the lower IC_{30} values. Synergistic effects of products may also play a role in determining toxicity.

Based on previous studies using 3% H_2O_2, which is the ISO 10993 standard for real-time *in vitro* degradation media, this foam composition degrades at ~0.78% mass loss per day [unpublished data]. As the IC_{30} values from our studies are concentration values, a comparison to degradation rates requires consideration of the tissue volume where the degradation products will be produced. One proposed application for this material is as a coating for an embolic coil that can be used in the occlusion of aneurysms[46,71,92]. In order to make a rough comparison of degradation product mass to tissue volume, we assumed an aneurysm diameter of 11 mm to represent an aneurysm larger than 92% of aneurysms in a clinical study[109]. To determine the amount of foam that would be present in this aneurysm, we assumed a packing density of 23% with foam-coated coil devices before the devices had expanded, which correlates with a packing density of ~58% after foam expansion, based on our previous work[8,110]. Using the 0.78% mass loss per day observed in previous studies, a daily degradation product exposure of 0.224 mg/mL would be observed in the aneurysm. This concentration is lower than all of the IC_{30} values obtained for degraded foam solutions in this study, which suggests that the rate of product release would not be expected to cause a cytotoxic response in the aneurysm based on the recommendations presented in ISO 10993-5[81]. This calculation assumes no product accumulation at the implant site based on our previous study in the rabbit elastase aneurysm model. In that study, we observed 13.6% mass loss after 30 days and 98.6% mass loss after 90 days, but we did not observe necrosis or toxic effects at any timepoint[71].

While cytotoxicity testing gives an initial idea of material or degradation product toxicity, toxicologists typically rely on systemic toxicity and other *in vivo* experiments to further evaluate potential risks found in cytotoxicity experiments. *In vitro* cytotoxicity has been studied relative to *in vivo* methods for identifying toxicity, and the predictive ability of cytotoxicity alone is generally not sufficient[111,112]. A combination of these methods is necessary to provide a more complete profile of the safety and efficacy of devices that utilize oxidatively-degradable polymers. However, cytotoxicity may play an important role in elucidating mechanisms of toxicity, relative impact of isolated degradation products, or effects on different cell types, and initial cytotoxicity screening is important for minimizing animal numbers.

In previously published *in vivo* studies, no toxic effects have been observed from similar SMP foam formulations, which were observed to degrade to various extents during the life of the implants[38–41,71,92,93]. By contrast, all of these studies found that SMP foam implants resulted in similar or enhanced healing compared to control devices. These studies have included implants in both pig and rabbit models, and implants in aneurysm models and peripheral vasculature. Time points have been as long as 180 days in both pigs and rabbits. These data, taken with the measurements in the current study, indicate that the rate of release of SMP foam degradation byproducts is unlikely to cause cytotoxic effects after implantation.

It is important to note that the progression of the degradation mechanism is complex, and the relative abundance observed for these byproduct species could differ *in vivo* compared to *in vitro.* In the *in vitro* case, there is no removal or metabolism of the

byproducts as they are solubilized which may allow them to be further oxidized. Another limitation of this *in vitro* approach is the possibility of differences between submersion in H_2O_2 as a homogeneous degradation catalyst versus the heterogeneous, cell-mediated, oxidative degradation that occurs *in vivo.* Similar degradation was confirmed in previous studies with *ex vivo* samples, but the molecular weight of solubilized degradation products and the distribution of chemical species may be slightly variable[42]. The catalyst for degradation may further complicate these factors over time. Additionally, the clearance rate of these varying degradation products should be further evaluated with consideration of the implant site and systemic circulation.

Other limitations of this study include the use of accelerated degradation. Preferably, toxicity testing would use a solution that yields the best approximation of real time *in vivo* degradation that is available at 37°C. Accelerated degradation was used in this study because of long degradation timeframes expected for real time use. Additionally, the method of neutralizing H_2O_2 with catalase can vary based on the activity of the enzyme, potential inhibition of the enzyme by degradation products in solution, and pH of the degradation product solution.

Future studies will attempt to utilize these methods to evaluate other cell types and cell responses, such as cell proliferation and gene and protein expression. The specific cell types used for an assay would ideally match the most relevant cells in the response to the device for the desired application. Additional toxicity studies should also be undertaken to acquire a complete toxicological profile of these biomaterials *in vitro* and *in vivo*. These

studies may include systemic toxicity, genotoxicity, carcinogenicity, and reproductive toxicity tests depending on the intended application of the medical device.

In conclusion, new methods were established to enable cytotoxicity testing of degradation byproducts from oxidatively-degradable polymers. These methods were used to test degradation products from a SMP foam that has been investigated for use in occlusion devices, and it was found that the degradation of this material is unlikely to cause a cytotoxic response *in vivo*. The methods described here may also be useful for other types of toxicological testing and may be used with other oxidatively-degradable polymeric materials.

CHAPTER IV

MACROPHAGE PHENOTYPES ASSOCIATED WITH SMP FOAM-COATED OR BARE PLATINUM COILS FOR ANEURYSM OCCLUSION

Introduction

Embolic coils enabled minimally invasive treatment of brain aneurysms, but high rates of recanalization and retreatment persist as weaknesses of this approach[7–9,11,113]. One hypothesis for addressing this recanalization is that the biological response can be enhanced to resist coil compaction and reduce recanalization risk[14,114,115]. The suggested response includes robust collagen deposition between the coils in the aneurysm dome and a complete reendothelialization at the aneurysm neck[14]. The robust collagen deposition is expected to provide mechanical support that resists coil compaction, and the complete reendothelialization is expected to provide a barrier to decrease hemodynamic pressure on the coil mass.

A variety of modifications have been tested to enhance the biological response to platinum coils deployed in aneurysms. These modifications have included the addition of cells, proteins, and polymers[21,28,114–118]. Some coils, such as those coated with poly(lactic-co-glycolic acid) (PLGA) and/or monocyte chemoattractant protein-1 (MCP-1), were observed to induce inflammation that stimulated a fibrotic response and led to more tissue deposition than control coils[28,114].

The macrophage is one of the primary cell types that respond after endovascular coil implantation, and the macrophage reaction has been hypothesized to determine the

outcome of many different types of implants[14,59,60,63]. Recent research also shows that there is a spectrum of macrophage activation states, ranging from a pro-inflammatory phenotype ("M1-like") to a pro-regenerative phenotype ("M2-like"), and the regulation of these phenotypes can have important implications in various pathological conditions, including wound healing[44,45,55,56,119]. It has also been demonstrated that different biomaterial properties, such as material modulus, surface roughness, degradability and porosity can drive macrophages toward different phenotypes[60,63]. These phenotypes then can have different effects on the bioresponse surrounding the implant. Early M1 responses have been demonstrated to play a role in angiogenesis, and M2 responses have been associated with increased tissue deposition and remodeling[59,120]. Stimulating the appropriate balance of macrophage activity may lead to the enhanced collagen deposition and reendothelialization desired in the response to embolic coils for aneurysms, and it's possible that this could be accomplished using modifications of existing devices. The information about macrophage phenotypes present in healing aneurysms is very limited, but Khashim et al. suggest that M2-like polarization correlates positively with histologic healing scores 180 days after treatment with BPCs[121].

Our lab has developed a shape memory polymer (SMP) foam that enhanced both the connective tissue deposition in aneurysm domes and the endothelialization of the necks after implantation in two different animal models[38,39,41,71,92]. We hypothesize that this highly porous, polyurethane foam may stimulate healing through activation of a macrophage phenotype that favors M2-like activity over time.

Here we investigate the polarization of macrophages associated with SMP foam-coated coils (FCCs) compared to bare platinum coil (BPC) controls. We first assess macrophage phenotypes at 30, 90, and 180 days in tissues saved from a previous study in the rabbit elastase aneurysm model[71]. Additionally, we use the THP-1 cell line to investigate *in vitro* polarization of macrophages after exposure to these devices.

Materials and Methods

Devices Tested

The devices tested in this study include SMP FCCs consisting of platinum-tungsten coils with SMP foam cylinders adhered to the outside of the coils. The manufacturing process and device sizes used in the animal study are described in more detail by Boyle, et al. and Herting, et al.[46,71]. Control devices used were BPCs from the Barricade Coil System (Blockade Medical).

Animal Model and Implantation

All tissues used for analysis were obtained from a previous study that utilized the rabbit elastase aneurysm model[71]. Briefly, a segment of the right common carotid artery is isolated, ligated distally, and exposed to elastase enzyme to break down part of the blood vessel wall. After elastase exposure, the access site is closed, and the aneurysm is allowed to grow for at least 3 weeks with exposure to hemodynamic pressure. At this point, the aneurysms were accessed via catheter and treated with either SMP FCCs or BPC controls using angiography.

The animals were sacrificed after 30, 90, or 180 days, and the aneurysms were explanted then fixed in 10% formalin. Aneurysms were embedded in paraffin, then 1 mm thick sections were made using an Isomet Low Speed saw. The metal coil pieces were removed from the 1 mm blocks under a dissection microscope, then these blocks were reembedded in paraffin and sectioned to 4-5 μm. A more detailed description of these procedures can be found in Herting, et al.[71].

Immunofluorescent Staining

Tissue sections were dried overnight at 37°C, then heated to 56°C for 45 minutes immediately before deparaffinization. Paraffin was removed using two changes of Xylene, then sections were washed and rehydrated through descending ethanol concentrations from 100% ethanol to 80% ethanol. Rehydration was completed by immersing the sections in running tap water, then rinsing in 2 changes of deionized (DI) water. Antigen retrieval was performed using a 0.1 M citrate buffer at pH 6.0. Sections were immersed in this buffer and placed in a steamer for 45 minutes at 95°C. After cooling, the sections were washed in tris buffered saline (TBS) then blocked using 4% donkey serum with 0.3% Triton X in TBS for 30 minutes. An additional blocking step was added using 20 μg/mL donkey anti-rabbit IgG F_{ab} fragment (Jackson Immunoresearch) in 0.3% Triton X in TBS for 30 minutes.

Primary antibodies were added to sections in TBS with 0.3% Triton X and 2% donkey serum overnight at 4°C. Primary antibodies used included rabbit anti Iba-1 (Wako, 2 μg/mL), goat anti CD206 (R&D Systems, 8 μg/mL), and mouse anti iNOS (Novus

Biologicals, 10 μg/mL). After primary antibody incubation, sections were washed three times in TBS on a shaker. Secondary antibodies were added to sections in TBS for two hours at room temperature. Secondary antibodies used included donkey anti rabbit Alexa Fluor 488, donkey anti goat Cy3, and donkey anti mouse Cy5 (all Jackson Immunoresearch). Sections were washed again three times in TBS on a shaker after secondary incubation, then DAPI was added in TBS. Slides were washed twice in TBS on a shaker, and finally the slides were mounted with coverslips using Fluoromount-G (Southern Biotech).

Imaging

Fluorescent staining was observed using a Leica DM6B upright microscope. Each slide was scanned to obtain an overview of the whole tissue at a 4X magnification. Then at least 8 regions were captured at a 20X magnification for cell counting. Cells were counted using a macro written in ImageJ that identified overlapping regions of the different stains.

A subset of samples was observed a second time using an IXM Confocal microscope. Images were acquired of 5, randomly selected samples from each group at each timepoint at 40X magnification, including 4 fields of view at the periphery of the aneurysm dome (closer to the aneurysm wall) and 4 fields of view from the innermost area of the aneurysm dome. Cells were counted manually using ImageJ software. These images were used to compare the phenotypes present in the different regions of the aneurysms.

In Vitro Cell Culture

THP-1 monocytes were differentiated to macrophages using 5 ng/mL phorbol 12-myristate 13-acetate (PMA) in complete media at 1 x 10^6 cells per well in low attachment 6-well plates. Complete media was made using RPMI 1640 supplemented with 10% fetal bovine serum (FBS) and 1% penicillin-streptomycin solution (P/S). THP-1 cells were left in differentiation media for 3 days then washed with PBS, and then fresh complete media was added to each well.

Devices were cut to short pieces with 0.25 cm^2 surface area and incubated in FBS for 30 minutes prior to cell seeding. Differentiated macrophages were gently scraped with a cell scraper to lift and collect them from the low attachment well plates. 1 million cells were seeded on each device in 10 µL of complete media in a 6-well plate. Cells were incubated in this small volume for 30 minutes to maximize cell attachment on the devices, and then each well was filled with 3 mL complete media. Controls consisted of cells that remained in the wells where they were differentiated (M0).

RNA Extraction and cDNA Synthesis

Cell lysis was performed either 6 or 24 hours after cell seeding on devices. RNA extraction and purification were performed using an RNeasy Mini Kit (Qiagen). RNA concentration and purity were evaluated on a Nanodrop OneC (ThermoFisher Scientific) and stored at -80°C until ready to use. Reverse transcription was completed using a High Capacity cDNA Reverse Transcription Kit (ThermoFisher Scientific).

qPCR

qPCR was performed on a Quant-iT Studio Series System (Thermofisher Scientific) using the Applied Biosystems PowerSYBR Green PCR Mastermix (Thermofisher Scientific) for detection. Genes investigated included IFNγ, NOS2, HLADR, CD163, CD206, IL1β, IL6, and IL10. The primers used were obtained from Integrated DNA Technologies, and the sequences used for each gene are shown in Table 4.1. The expression of target genes was normalized to the housekeeping gene, GAPDH, and then to the 6 hour M0 control group using the $2^{-\Delta\Delta Ct}$ method.

Table IV-1. Forward and reverse primer sequences to be used for gene expression analysis.

Gene	Forward Sequence	Reverse Sequence
GAPDH	CTGGGCTACACTGAGCACC	AAGTGGTCGTTGAGGGCAATG
IFNγ	TCGGTAACTGACTTGAATGTCCA	TCGCTTCCCTGTTTTAGCTGC
NOS2	TTCAGTATCACAACCTCAGCAAG	TGGACCTGCAAGTTAAAATCCC
HLADR	AGTCCCTGTGCTAGGATTTTTCA	ACATAAACTCGCCTGATTGGTC
CD163	TTTGTCAACTTGAGTCCCTTCAC	TCCCGCTACACTTGTTTTCAC
CD206	CGAGGAAGAGGTTCGGTTCACC	GCAATCCCGGTTCTCATGGC
IL1β	TTCGACACATGGGATAACGAGG	TTTTTGCTGTGAGTCCCGGAG
IL6	CCTGAACCTTCCAAAGATGGC	TTCACCAGGCAAGTCTCCTCA
IL10	GACTTTAAGGGTTACCTGGGTTG	TCACATGCGCCTTGATGTCTG

Statistical Analysis

Data are presented as mean ± SEM. Differences in marker expression from immunostaining and gene expression from qPCR between treatment groups were compared using independent t-tests.

Results

Immunofluorescent Staining of Explanted Tissue Samples

Immunostaining was completed for all animals from the previous study. Slides were stained with DAPI to identify all nuclei, Iba1 to identify all macrophages, CD206 to identify M2 macrophages, and iNOS to identify M1 macrophages.

In the lower magnification images that were analyzed with the ImageJ macro at 30 and 90 days, aneurysms treated with SMP FCCs exhibited significantly higher numbers of $Iba1^{+}$ macrophages and macrophages that were positive for both iNOS and CD206 as shown in Figure 4.2. There were also significantly more cells expressing iNOS and cells expressing CD206 when including cells that stained positively for both markers, but not when considering cells that stained for only the M1 or M2 marker. At 180 days, aneurysms treated with SMP FCCs exhibited significantly higher numbers of cells expressing CD206 (Figure 4.2). When normalized to the number of macrophages counted, there were no significant differences observed between device groups for any phenotype at any timepoint as shown in Figure 4.3. Similarly, there were no differences in M2/M1 ratio observed between device groups at any timepoint as shown in Figure 4.4.

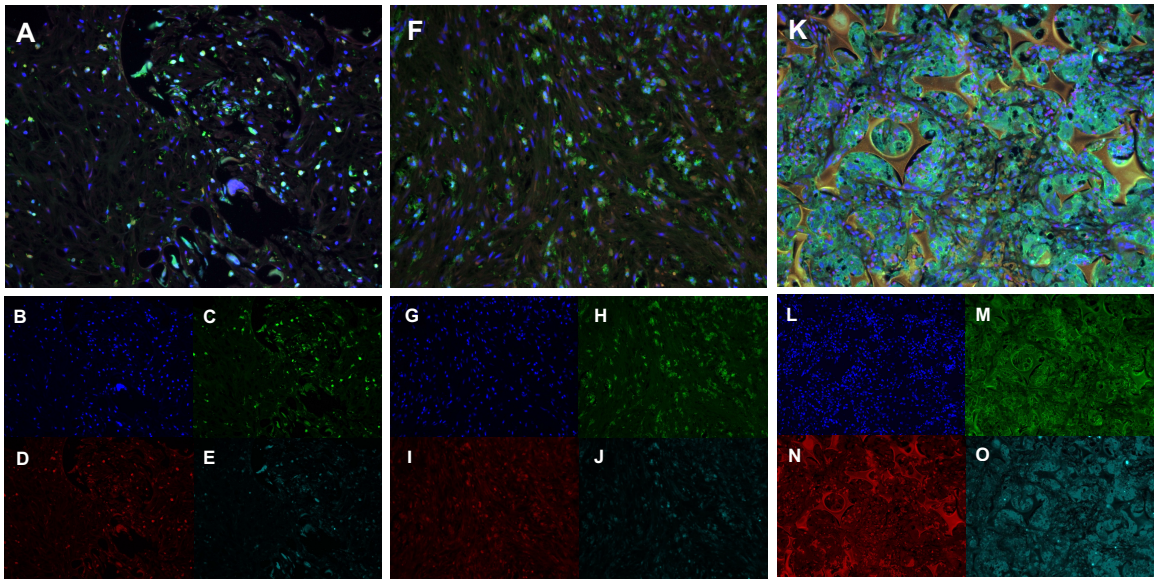

Figure IV-1. Representative 20X images of aneurysms treated with A) bare platinum coils or F,K) foam coated coils. F shows cells present farther from SMP FCC devices and K shows cells present near foam struts, which have some autofluorescence and appear gold in K. All images are from the 30 day treatment group. A, F, and K present the composite of the 4 images below each of them. B, G, and L show DAPI staining; C, H, and M show Iba1$^+$ cells in green; D, I, and N show CD206$^+$ cells in red; and E, J, and O show iNOS$^+$ cells in cyan.

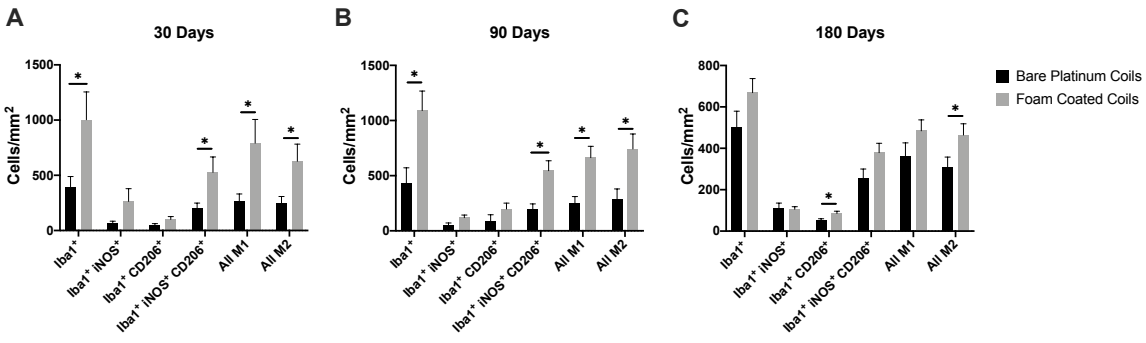

Figure IV-2. Macrophage phenotypes by number of cells per mm^2 at A) 30 days, B) 90 days, and C) 180 days. Error bars shown are standard error of the mean. *indicates $p<0.05$ between device groups.

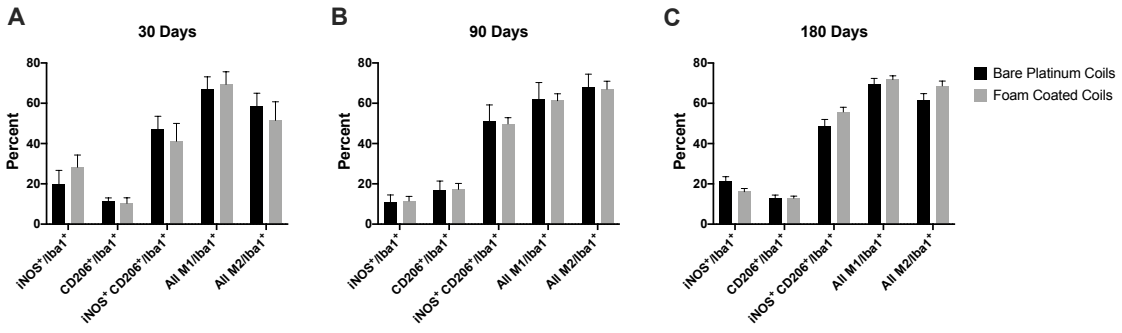

Figure IV-3. Macrophage phenotypes by percentage of macrophages counted at A) 30 days, B) 90 days, and C) 180 days. Error bars shown are standard error of the mean.

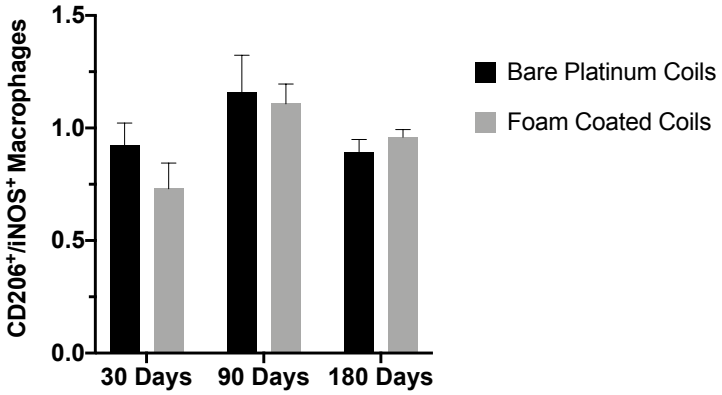

Figure IV-4. Ratio of all M2 marker (CD206) expressing cells to all M1 marker (iNOS) expressing cells at 30 days, 90 days, and 180 days. Error bars shown are standard error of the mean.

When a subset of samples was analyzed with higher magnifications and counted manually, minimal differences were observed in different regions of the aneurysms as demonstrated by Figure 4.5. The only significant difference between regions of any group of aneurysms was found to be in 180 day group of BPC-treated aneurysms. The percentage of all cells that were Iba^+ was significantly greater in the inner region of those aneurysms as shown in Figure 4.6.

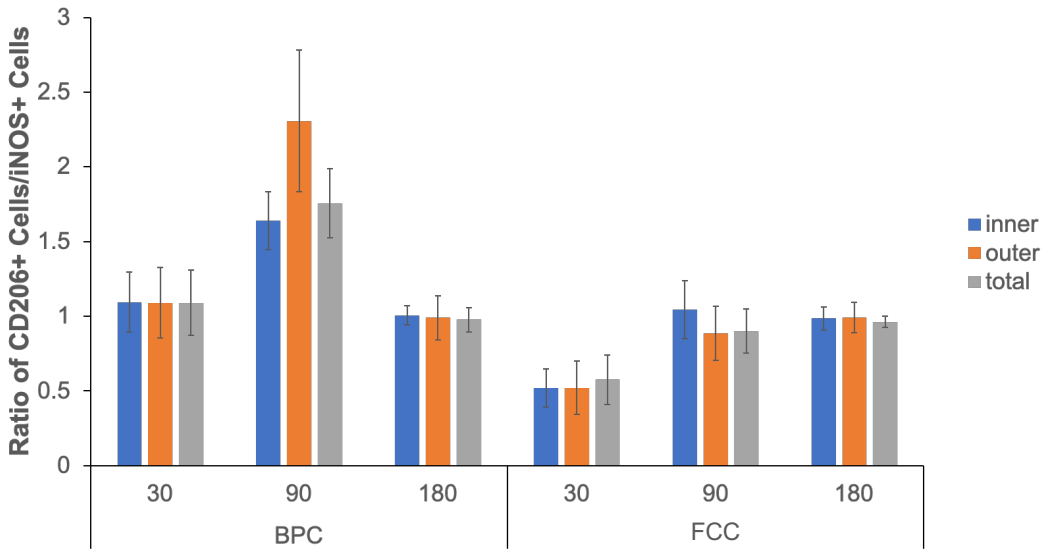

Figure IV-5. Ratio of all M2 marker (CD206) expressing cells to all M1 marker (iNOS) expressing cells at 30 days, 90 days, and 180 days counted manually in the higher magnification images and separated by region of the aneurysm. Error bars shown are standard error of the mean.

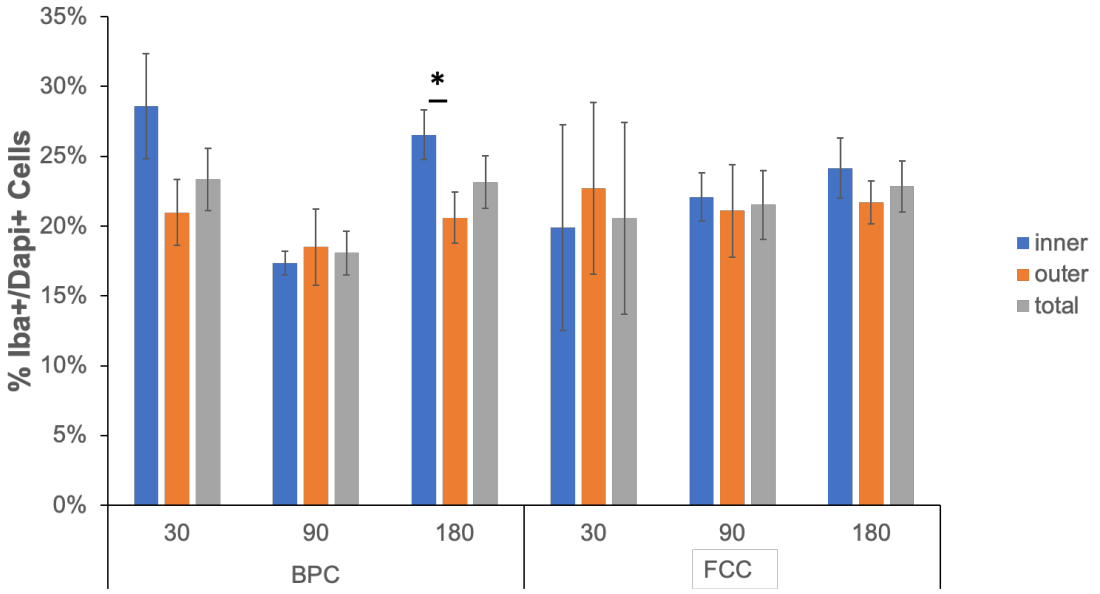

Figure IV-6. Percentage of all DAPI-labeled cells expressing Iba1 at 30 days, 90 days, and 180 days from manual counts in the higher magnification images separated by region of the aneurysm. Error bars shown are standard error of the mean. *indicates $p<0.05$ between inner and outer regions.

The manual counting method used for this subset of samples also made it possible to discriminate multinucleated giant cells (MNGCs) from other Iba1$^+$ macrophages. Using this method and only considering macrophages with a single nucleus, a significantly higher M2/M1 ratio was observed in the BPC-treated group at 90 days as shown in Figure 4.7. At 90 days, significantly higher numbers of Iba1$^+$ macrophages, iNOS$^+$ macrophages, and iNOS$^+$CD206$^+$ macrophages were identified in the FCC-treated group as shown in Figure 4.8. The percentage of Iba1$^+$ cells that were positive for CD206 (with or without iNOS) was greater in the BPC-treated group at 30 days as shown in Figure 4.9. At 90 days, the percentage of Iba1$^+$ cells that were positive for only iNOS was greater in the FCC-

treated group, and the percentage of Iba1$^+$ cells that were positive for only CD206 was greater in the BPC-treated group (Figure 4.9).

When MNGCs were included with single nucleated macrophages, the only significant difference observed in this subset was a greater percentage of Iba1$^+$ cells that were positive for CD206 (with or without iNOS) in the BPC-treated group at 30 days (Figures 4.10 and 4.11).

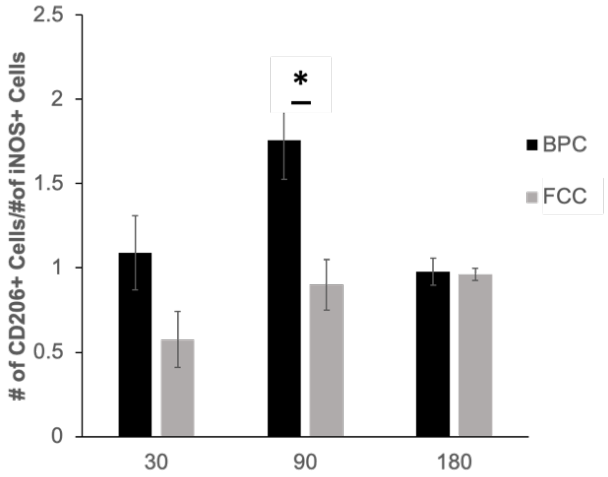

Figure IV-7. Ratio of M2 marker (CD206) expressing, single nucleated cells to M1 marker (iNOS) expressing, single nucleated cells at 30 days, 90 days, and 180 days from manual counts in the higher magnification images. Error bars shown are standard error of the mean. *indicates $p<0.05$ between inner and outer regions.

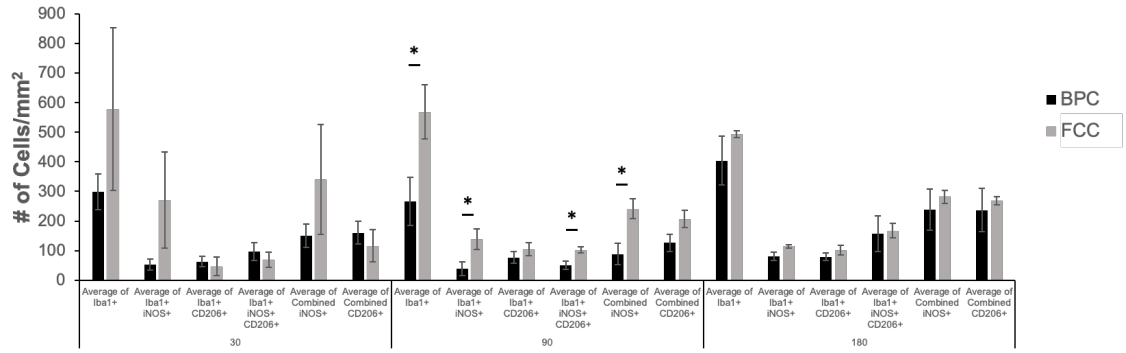

Figure IV-8. Macrophage phenotypes by number of cells per mm^2 at 30 days, 90 days, and 180 days from manual counts in the higher magnification images. Does not include multinucleated giant cells (MNGCs). Error bars shown are standard error of the mean. *indicates p<0.05 between device groups.

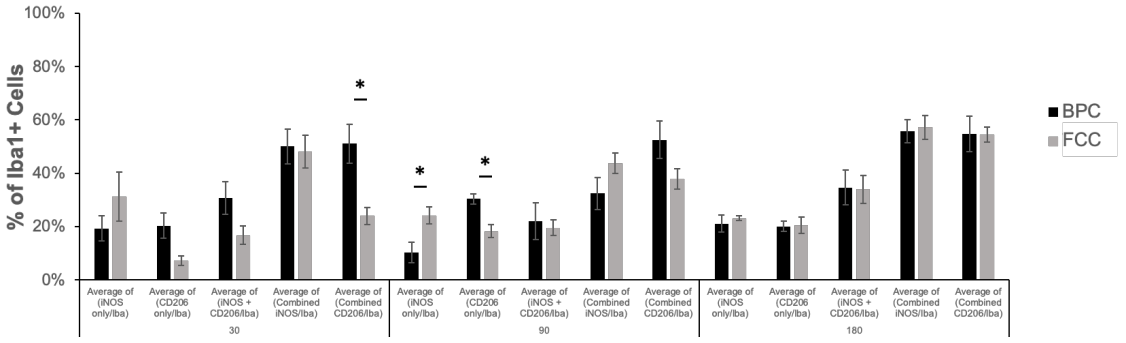

Figure IV-9. Macrophage phenotypes by percentage of macrophages counted at 30 days, 90 days, and 180 days from manual counts in the higher magnification images. Does not include multinucleated giant cells (MNGCs). Error bars shown are standard error of the mean. *indicates p<0.05 between device groups.

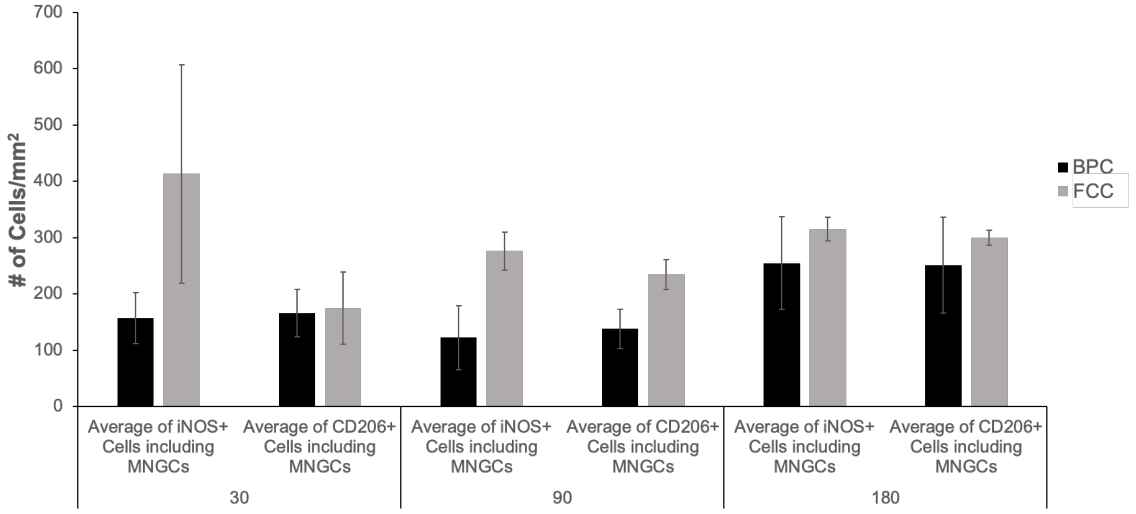

Figure IV-10. Macrophage phenotypes by number of cells per mm^2 at 30 days, 90 days, and 180 days from manual counts in the higher magnification images including multinucleated giant cells (MNGCs). Error bars shown are standard error of the mean.

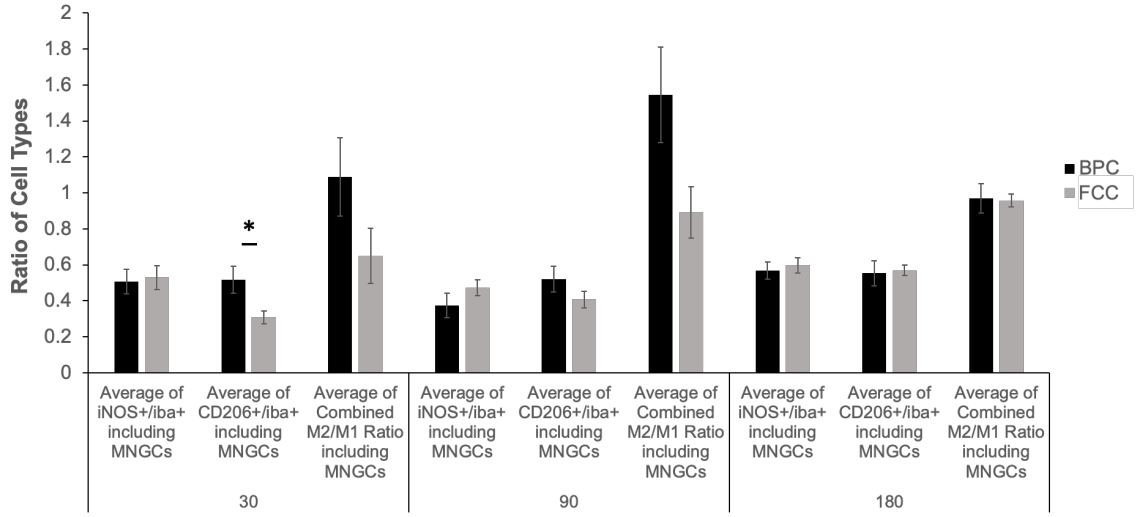

Figure IV-11. Macrophage phenotypes as a ratio of macrophages counted and ratio of all M2 marker (CD206) expressing cells to all M1 marker (iNOS) expressing cells at 30 days, 90 days, and 180 days from manual counts in the higher magnification images including multinucleated giant cells (MNGCs). Error bars shown are standard error of the mean. *indicates $p<0.05$ between device groups.

qPCR

Macrophages were seeded on both types of devices, but in all cases, some of the cells seeded adhered to the plate surrounding the device (i.e. cell adhesion to the devices was not 100%). The extracted RNA concentrations, A260/280, and A260/230 ratios for the samples collected are shown in Table 5.1 (Appendix).

Gene expression data are presented in Figure 4.12. After 6 hours, IFNγ, IL1β, IL6, and IL10 were all upregulated relative to the M0 control in both device groups. HLADR, CD163, and CD206 were downregulated relative to the M0 control in both device groups. NOS2 was slightly downregulated in the BPC group. After 24 hours, IFNγ, NOS2, HLADR, IL1β, IL6, and IL10 were all upregulated relative to the M0 control in both device groups. CD163 and CD206 were downregulated relative to the M0 control in both device groups.

After 6 hours, expression of IFNγ was significantly greater in the FCC group compared to the BPC group. After 24 hours, expression of HLADR and CD206 were significantly greater relative to the 6 hour timepoint in the FCC group.

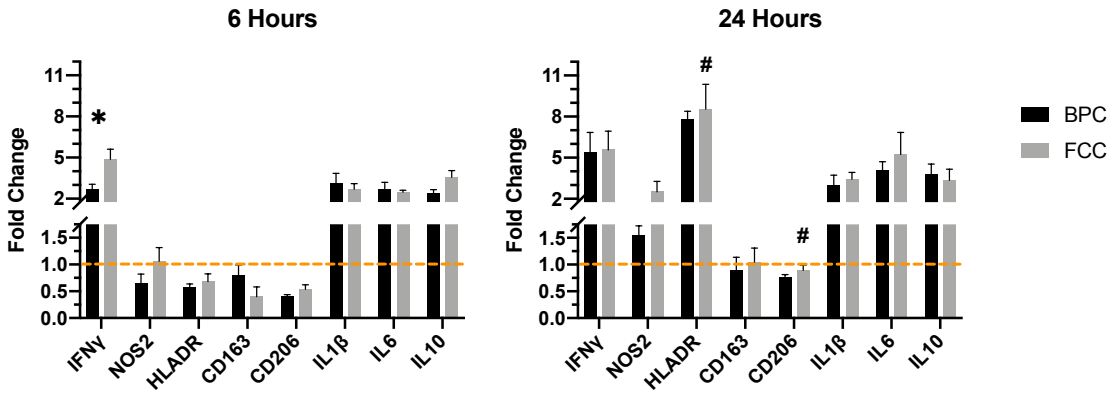

Figure IV-12. Expression of M1- and M2-associated genes by THP-1 derived macrophages seeded on devices for 6 or 24 hours and analyzed by qPCR. Error bars shown are standard error of the mean. *indicates $p<0.05$ between device groups. #indicates $p<0.05$ between timepoints for the FCC group.

Discussion and Conclusions

SMP foam has demonstrated positive healing results in multiple preclinical studies of occlusion applications in different animal models[38–41,71,92,93]. The porous structure is hypothesized to serve as a scaffold that promotes stable clot formation and provides support for the remodeling of this clot to a connective tissue matrix. There is a growing body of evidence that biomaterials and variations of their structure and chemical properties may influence the phenotype of macrophages responding to the implant[44,45,55,56,60,63,119]. Some studies have suggested that the macrophage phenotypes present in the foreign body response may determine the outcome of the implant[59,60].

In this study, we have investigated the macrophage phenotypes present during healing after occlusion of rabbit elastase aneurysms. We utilized tissues from another study that found improved neoendothelialization and enhanced healing in aneurysms

treated with SMP FCCs[71,92]. Results suggest that there are some differences in expression at timepoints evaluated, but there are fewer if MNGCs are included in this analysis. The number of macrophages observed was similar between this evaluation and a previous, published evaluation of the inflammatory cell types present in these aneurysms[92]. These studies identified higher numbers of macrophages at 90 days in aneurysms treated with FCC devices. The presence of more macrophages may be a factor in determining the healing outcomes in these aneurysms. It's possible that more macrophages may be beneficial in some applications as long as the phenotype is not skewed too much toward a pro-inflammatory phenotype.

In the automated analysis, the number of macrophages appears higher at 30 days because of the consideration of MNGCs. In this method, each nucleus identified with DAPI was counted as one cell because of difficulty automating identification of MNGCs with the stains used. This would result in some MNGCs being counted as multiple macrophages and would likely lead to the increased number of macrophages at 30 days. This was corroborated using the manual counting of higher magnification images. The majority of MNGCs evaluated in all groups were positive for both iNOS and CD206. Additionally, the majority of all macrophages evaluated in this study were positive for both iNOS and CD206. Previous studies of other biomaterials have identified macrophages that were positive for both M1 and M2 markers associated with the biomaterial scaffolds[61,122]. These cells may represent an intermediate phenotype between the M1 and M2 extremes.

Manual counts of higher magnification images were also used to investigate the phenotypes of macrophages in different regions of the aneurysms. In the previous pathology evaluations of these tissues, the peripheral regions (closer to the aneurysm walls) of the aneurysms were found to be more completely healed than the innermost regions[92]. However, in this study, there were no differences in the macrophage phenotypes in different aneurysm regions observed. There was a trend toward the presence of more macrophages in the outer regions of aneurysms, but this was not statistically significant.

The M2:M1 ratios for each group were similar and close to 1 when including MNGCs. When MNGCs were excluded, BPC-treated aneurysms had a higher percentage of CD206-expressing cells at 30 and 90 days, with a higher M2:M1 ratio at 90 days. Given the positive healing data in FCC-treated aneurysms, it is possible that early expression of M1-associated markers is important for the progression of the healing response in aneurysms. Other groups have also suggested the importance of both pro-inflammatory and anti-inflammatory phenotypes in the healing process[59,120]. In the automated analysis, which included all samples, FCC-treated aneurysms resulted in higher numbers of macrophages expressing the M2-associated marker at the 180 day timepoint. The early expression of M1-associated markers, followed by a transition to increased presence of M2 marker expressing cells may have factored into the improved healing observed in FCC-treated aneurysms. Additional studies are necessary to investigate this further, and supplemental markers may be helpful in testing these hypotheses. Other commonly-used markers that could be investigated include CD80, CD86, and CCR7 for M1-like macrophages and CD163 for M2-like macrophages[45].

One limitation of this method is the evaluation of only three timepoints that were all one month after implantation or beyond. While we expected differences at these late timepoints because of the healing timecourse for aneurysms, differences in macrophage polarization can be observed at earlier timepoints that contribute to differences in healing at later timepoints[123]. Another limitation is that the tissues were only evaluated by immunostaining because of the methods of fixation and embedding used for the original histologic study. Gene and protein expression studies are important for confirming macrophage phenotypes observed.

In vitro methods are also commonly used to perform more controlled evaluations of macrophage polarization on devices and materials. We utilized a THP-1 monocyte cell line to obtain macrophages that were seeded on devices *in vitro* for gene expression assessment. At 6 hours, we observed significantly greater expression of IFNγ by cells seeded on foam-coated coils compared to those seeded on bare platinum coils. IFNγ is a cytokine associated with M1-like pro-inflammatory macrophage phenotypes. One of the primary functions of IFNγ is in activating macrophages in an immune response, and it is commonly administered with lipopolysaccharide in *in vitro* studies to activate cells toward an M1-like phenotype[57,124]. This agrees with our immunostaining experiments that suggest SMP FCCs result in slightly increased expression of M1-associated markers at early timepoints in the healing process. At 24 hours, we observed significant increases in expression of CD206 and HLADR by cells seeded on foam-coated coils compared to the 6 hour timepoint. CD206 is a cell surface receptor commonly associated with the M2-like, anti-inflammatory macrophage phenotype[125]. Together these differences suggest that

FCCs may lead to a relatively stronger early M1-like response that is followed by a transition toward an M2-like, or more balanced phenotype.

Early M1-like responses have been shown to be associated with angiogenic activity, and are likely essential to a beneficial healing response to implanted devices as mentioned above[59,120]. However, prolonged M1-like responses may lead to necrosis or fibrosis[62]. In most cases, a transition to M2-like responses is expected and desired for effective healing and resolution of the inflammatory response[60].

It is important to note that the genes tested all have complex functions and the gene expression of different macrophage phenotypes is still being clarified. Additionally, gene expression differences may not always correlate perfectly to protein expression and cell function. The use of the THP-1 cell line may also affect the outcome of these studies. While these cells are from a human source, they are a cell line. THP-1 cells have been compared to primary human monocytes for studying macrophage responses to biomaterials, and some differences in the intensity of responses were observed[125].

Other labs have conducted limited evaluations of macrophage phenotypes related to aneurysm occlusion devices. Hoh and collaborators have utilized cytokine-releasing coils and evaluated the bioresponse in a mouse model[114,115,126]. They observed inflammation that stimulated enhanced healing and demonstrated peak M1 and M2 expression at 1 week that decreased with time thereafter[126]. Khashim, et al. suggest that M2 marker expression correlates well with increased histologic healing scores at 180 days in a rabbit elastase model, but only moderately with collagen deposition[121]. In this study, they also reported a higher expression of their M1-associated marker at their earliest

timepoint (30 days) that decreased with time as M2 expression increased and healing progressed. More evaluations of the role of macrophage phenotypes in aneurysm occlusion and healing are needed, particularly in larger animal models at earlier timepoints. These future studies should utilize multiple markers and multiple methods of analysis including immunostaining, qPCR, and ELISA, if possible.

In conclusion, preliminary studies suggest that presence of M1-like macrophage markers early in the healing process, and a transition to a balanced phenotype may be associated with FCC devices. The FCC device, which was observed in previous studies to improve healing in aneurysms, was also associated with higher numbers of macrophages present at 90 days and higher numbers of M2 marker expressing cells at 180 days. The most prominent macrophage phenotype observed at 30, 90, and 180 days associated with both devices expressed both iNOS (M1) and CD206 (M2).

CHAPTER V

SUMMARY, CONCLUSIONS, AND FUTURE DIRECTIONS

Summary

The work in this dissertation evaluated the long term biocompatibility of a SMP FCC device for treating brain aneurysms, developed new methods for evaluating toxicity of degradation products from oxidatively-degradable polymers, tested the cytocompatibility of degradation products from a SMP foam, and finally assessed macrophage phenotypes associated with the use of the SMP FCC device.

Long term implantation studies suggest that the SMP FCC device may enhance the healing response after endovascular occlusion of aneurysms. In particular, the response at the neck of aneurysms yielded robust neoendothelial tissue that is desired to reduce the risk for aneurysm recurrence. Additional evaluation by Jessen, et al. corroborates the suggestion that the intrasaccular healing is enhanced by the treatment with SMP FCC devices[92]. Jessen, et al. also quantified the inflammatory cell types in the surrounding tissue and concluded that the inflammatory response was characteristic of healing after device implantation as opposed to a chronic inflammatory response. Together, these data provide support for the continued evaluation of the SMP FCC devices as a valuable treatment option that may improve outcomes in endovascular occlusion procedures.

Novel methods were described to assess toxicity of degradation products from oxidatively-degradable materials, and these methods were utilized to evaluate the cytocompatibility of degradation products from the SMP foam used in FCC devices

described above. These studies provide researchers with new approaches to complement traditional biocompatibility tests. These new approaches allow for more targeted evaluation of the degradation products from materials with complex, oxidative degradation mechanisms. Additionally, the assessment of degradation products from SMP foam suggested that the degradation of these materials is not likely to cause a cytotoxic reaction *in vivo*, which is consistent with observations from previous studies in multiple animal models. The degradation products from these materials should continue to be evaluated with additional methods and models, but the cytocompatibility results observed here provide important insight to guide future studies.

Preliminary macrophage phenotype assessments *in vitro* and *in vivo* suggest that relative to BPCs, SMP FCCs are associated with higher numbers of macrophages at some timepoints. SMP FCCs may also promote the expression of slightly more M1-like macrophage markers early in the healing process, a transition to a balanced phenotype, and the presence of more M2 marker expressing cells at later timepoints. This process may play a role in the healing outcomes observed for the FCC-treated aneurysms, but additional studies are required to confirm.

Future Directions

Several interesting future directions have been identified related to the studies presented in this dissertation. The degradation rate for the SMP foam used in the FCC devices was faster than expected based on previous *in vitro* and *in vivo* evaluations. This may be related to the rabbit animal model used, the pore size of the material used, or the

stiffness of the devices used. Different animal models have been observed to mount different bioresponses to implanted devices and therapies depending on the species and location of implant[15,127,128]. Biomaterials with different structural properties or surface chemistries have also elicited different responses. Animal studies could be designed to assess each of these factors and their relationship with healing outcomes, oxidative load, degradation rate, and macrophage polarization. Pore size, hydrophilicity, and stiffness can all affect immune responses to biomaterials, and they can be modified for the SMP system used in our lab[36,60,63,70,129]. Devices could also be tested with or without a metal backbone, which could be platinum-tungsten, nitinol, or another material.

The degradation product toxicity approaches established here should be tested for use with additional methods such as mutagenicity, carcinogenicity, systemic toxicity, and reproductive toxicity. The degradation products from materials evaluated here should also be evaluated by these additional test methods. Other cell types should also be tested with the degradation products from these materials, such as macrophages, lymphocytes, fibroblasts, fibrocytes, and endothelial cells. Additional responses that could be evaluated include changes in gene and protein expression, particularly those related to macrophage polarization. It would also be interesting to evaluate changes in macrophage phenotype as these cells are actively degrading materials.

In the future, it may be beneficial for devices to be loaded with cytokines, growth factors, or pharmaceuticals to modulate the bioresponse. Some interesting agents include Interleukin 4 (IL-4) and Interleukin 10 (IL-10), which are cytokines that promote an M2-like response, or dexamethasone, which is an anti-inflammatory drug[45,63]. Extracellular

matrix (ECM) based materials, such as small intestine submucosa (SIS) ECM, are naturally-derived biomaterials that have been observed to induce regenerative macrophage polarization and beneficial healing responses in multiple applications[45,122,130]. These materials may be interesting to incorporate in different forms of SMP devices, such as hydrogel composites which have been previously explored in our lab[131].

REFERENCES

1. Etminan, N. & Rinkel, G. J. Unruptured intracranial aneurysms: development, rupture and preventive management. *Nat. Rev. Neurol.* (2016) doi:10.1038/nrneurol.2016.150.
2. Ajiboye, N., Chalouhi, N., Starke, R. M., Zanaty, M. & Bell, R. Unruptured Cerebral Aneurysms: Evaluation and Management. *Sci. World J.* **2015**, 1–10 (2015).
3. Juvela, S. Prevalence of and risk factors for intracranial aneurysms. *Lancet Neurol.* **10**, 595–597 (2011).
4. Connolly, E. S. *et al.* Guidelines for the management of aneurysmal subarachnoid hemorrhage: A guideline for healthcare professionals from the american heart association/american stroke association. *Stroke* **43**, 1711–1737 (2012).
5. Carod-Artal, F. J. & Egido, J. A. Quality of life after stroke: The importance of a good recovery. *Cerebrovasc. Dis.* **27**, 204–214 (2009).
6. 510(k) Premarket Notification. https://www.accessdata.fda.gov/scripts/cdrh/cfdocs/cfpmn/pmn.cfm?ID=K951256 .
7. Tan, I. Y. L., Agid, R. F. & Willinsky, R. A. Recanalization Rates after Endovascular Coil Embolization in a Cohort of Matched Ruptured and Unruptured Cerebral Aneurysms. *Interv. Neuroradiol.* 27–35 (2011).
8. White, P. M. *et al.* Hydrogel-coated coils versus bare platinum coils for the endovascular treatment of intracranial aneurysms (HELPS): a randomised

controlled trial. *Lancet* **377**, 1655–62 (2011).

9. Murayama, Y. *et al.* Guglielmi Detachable Coil embolization of cerebral aneurysms: 11 years' experience. *J. Neurosurg* **98**, (2003).

10. Crobeddu, E., Lanzino, G., Kallmes, D. F. & Cloft, H. J. Review of 2 decades of aneurysm-recurrence literature, Part 1: Reducing recurrence after endovascular coiling. *Am. J. Neuroradiol.* **34**, 266–270 (2013).

11. Ogilvy, C. S. *et al.* Validation of a System to Predict Recanalization After Endovascular Treatment of Intracranial Aneurysms. *Neurosurgery* **77**, 168–174 (2015).

12. Raymond, J. *et al.* Hydrogel versus bare platinum coils in patients with large or recurrent aneurysms prone to recurrence after endovascular treatment: A randomized controlled trial. *Am. J. Neuroradiol.* **38**, 432–441 (2017).

13. White, J. B., Ken, C. G. M., Cloft, H. J. & Kallmes, D. F. Coils in a nutshell: A review of coil physical properties. *American Journal of Neuroradiology* (2008) doi:10.3174/ajnr.A1067.

14. Brinjikji, W., Kallmes, D. F. & Kadirvel, R. Mechanisms of healing in coiled intracranial aneurysms: A review of the literature. *Am. J. Neuroradiol.* **36**, 1216–1222 (2015).

15. Dai, D. *et al.* Histopathologic and Immunohistochemical Comparison of Human , Rabbit , and Swine Aneurysms Embolized with Platinum Coils. 2560–2568 (2005).

16. Bavinzski, G. *et al.* Gross and microscopic histopathological findings in

aneurysms of the human brain treated with Guglielmi detachable coils. *J. Neurosurg.* **91**, 284–293 (1999).

17. Ding, Y. H. *et al.* Relationship between Aneurysm Volume and Histologic Healing after Coil Embolization in Elastase-Induced Aneurysms: A Retrospective Study. *Am. J. Neuroradiol.* **29**, 98–101 (2008).

18. Leng, B. *et al.* Endovascular treatment of intracranial aneurysms with detachable coils: Correlation between aneurysm volume, packing, and angiographic recurrence. *J. Neurointerv. Surg.* **6**, 595–599 (2014).

19. Slob, M. J., Sluzewski, M. & van Rooij, W. J. The relation between packing and reopening in coiled intracranial aneurysms: A prospective study. *Neuroradiology* **47**, 942–945 (2005).

20. Cloft, H. J. & Viejo, A. HydroCoil for Endovascular Aneurysm Occlusion (HEAL) Study: 3–6 Month Angiographic Follow-Up Results. *Am. J. Neuroradiol.* 152–154 (2007).

21. Killer, M. *et al.* Histological demonstration of healing in experimental aneurysms. *Minim. Invasive Neurosurg.* **52**, 170–175 (2009).

22. Ding, Y. H., Dai, D., Lewis, D. A., Cloft, H. J. & Kallmes, D. F. Angiographic and histologic analysis of experimental aneurysms embolized with platinum coils, Matrix, and HydroCoil. *Am. J. Neuroradiol.* **26**, 1757–1763 (2005).

23. Reinges, M. H. T. *et al.* Bare, bio-active and hydrogel-coated coils for endovascular treatment of experimentally induced aneurysms: Long-term histological and scanning electron microscopy results. *Interv. Neuroradiol.* **16**,

139–150 (2010).

24. Cruise, G. M., Shum, J. C. & Plenk, H. Hydrogel-coated and platinum coils for intracranial aneurysm embolization compared in three experimental models using computerized angiographic and histologic morphometry. *J. Mater. Chem.* **17**, 3965 (2007).

25. Khan, S. N. H., Nichols, C., Depowell, J. J., Abruzzo, T. A. & Ringer, A. J. Comparison of coil types in aneurysm recurrence. *Clin. Neurol. Neurosurg.* **114**, 12–16 (2012).

26. Poncyljusz, W., Zarzycki, A., Zwarzany, Ł. & Burke, T. H. Bare platinum coils vs. HydroCoil in the treatment of unruptured intracranial aneurysms - A single center randomized controlled study. *Eur. J. Radiol.* **84**, 261–265 (2015).

27. Killer, M., Arthur, A. S., Barr, J. D., Richling, B. & Cruise, G. M. Histomorphology of thrombus organization, neointima formation, and foreign body response in retrieved human aneurysms treated with hydrocoil devices. *J. Biomed. Mater. Res. - Part B Appl. Biomater.* **94**, 486–492 (2010).

28. Murayama, Y., Tateshima, S., Gonzalez, N. R. & Vinuela, F. Matrix and bioabsorbable polymeric coils accelerate healing of intracranial aneurysms: Long-term experimental study. *Stroke* **34**, 2031–2037 (2003).

29. Murayama, Y. *et al.* Bioabsorbable polymeric material coils for embolization of intracranial aneurysms: a preliminary experimental study. *J. Neurosurg.* **94**, 454–463 (2001).

30. Murayama, Y. *et al.* Cellular responses of bioabsorbable polymeric material and

Guglielmi detachable coil in experimental aneurysms. *Stroke* **33**, 1120–1128 (2002).

31. Fiorella, D., Albuquerque, F. C. & McDougall, C. G. Durability of aneurysm embolization with matrix detachable coils. *Neurosurgery* **58**, 51–58 (2006).

32. Niimi, Y., Song, J., Madrid, M. & Berenstein, A. Endosaccular treatment of intracranial aneurysms using matrix coils: Early experience and midterm follow-up. *Stroke* **37**, 1028–1032 (2006).

33. Vance, A. & Welch, B. G. The utility of bioactive coils in the embolization of aneurysms. *Neurol. Res.* **36**, 356–362 (2014).

34. Lendlein, A. & Kelch, S. Shape-Memory Polymers. *Angew. Chemie Int. Ed.* **41**, 2034 (2002).

35. Small IV, W., Singhal, P., Wilson, T. S. & Maitland, D. J. Biomedical applications of thermally activated shape memory polymers. *J. Mater. Chem.* **20**, 3356–3366 (2011).

36. Singhal, P. *et al.* Ultra low density and highly crosslinked biocompatible shape memory polyurethane foams. *J. Polym. Sci. Part B Polym. Phys.* **50**, 724–737 (2012).

37. Boyle, A. J. *et al. In vitro* and *in vivo* evaluation of a shape memory polymer foam-over-wire embolization device delivered in saccular aneurysm models. *J. Biomed. Mater. Res. Part B Appl. Biomater.* **104**, 1407–1415 (2016).

38. Rodriguez, J. N. *et al.* Opacification of Shape Memory Polymer Foam Designed for Treatment of Intracranial Aneurysms. *Ann. Biomed. Eng.* **40**, 883–897 (2012).

39. Rodriguez, J. N. *et al.* In vivo response to an implanted shape memory polyurethane foam in a porcine aneurysm model. **102**, 1231–1242 (2013).

40. Landsman, T. L. *et al.* Design and verification of a shape memory polymer peripheral occlusion device. *J. Mech. Behav. Biomed. Mater.* **63**, 195–206 (2016).

41. Horn, J. *et al.* Comparison of shape memory polymer foam versus bare metal coil treatments in an in vivo porcine sidewall aneurysm model. *J. Biomed. Mater. Res. - Part B Appl. Biomater.* **105**, 1892–1905 (2017).

42. Weems, A. C., Wacker, K. T., Carrow, J. K., Boyle, A. J. & Maitland, D. J. Shape memory polyurethanes with oxidation-induced degradation: In vivo and in vitro correlations for endovascular material applications. *Acta Biomater.* **59**, 33–44 (2017).

43. Anderson, J. M., Rodriguez, A. & Chang, D. T. Foreign body reaction to biomaterials. *Semin. Immunol.* **20**, 86–100 (2008).

44. Brown, B. N., Ratner, B. D., Goodman, S. B., Amar, S. & Badylak, S. F. Macrophage polarization: An opportunity for improved outcomes in biomaterials and regenerative medicine. *Biomaterials* **33**, 3792–3802 (2012).

45. Brown, B. N. & Badylak, S. F. Expanded applications, shifting paradigms and an improved understanding of host-biomaterial interactions. *Acta Biomater.* **9**, 4948–4955 (2013).

46. Boyle, A. J. *et al.* In vitro performance of a shape memory polymer foam-coated coil embolization device. *Med. Eng. Phys.* **49**, 56–62 (2017).

47. Scarritt, M. E., Londono, R. & Badylak, S. F. Host response to implanted

materials and devices: An overview. in *The Immune Response to Implanted Materials and Devices: The Impact of the Immune System on the Success of an Implant* (2016). doi:10.1007/978-3-319-45433-7_1.

48. Anderson, J. M. BIOLOGICAL RESPONSES TO MATERIALS. *Annu. Rev. Mater. Res* **31**, 81–110 (2001).

49. Furie, B. & Furie, B. C. Thrombus formation in vivo. *J. Clin. Invest.* **115**, 3355–62 (2005).

50. Wilson, C. J., Clegg, R. E., Leavesley, D. I. & Pearcy, M. J. Mediation of Biomaterial–Cell Interactions by Adsorbed Proteins: A Review. *Tissue Eng.* **11**, 1–18 (2005).

51. Nilsson, B., Ekdahl, K. N., Mollnes, T. E. & Lambris, J. D. The role of complement in biomaterial-induced inflammation. *Mol. Immunol.* **44**, 82–94 (2007).

52. Anderson, J. M. Multinucleated giant cells. *Curr. Opin. Hematol.* **7**, 40–47 (2000).

53. Koh, T. J. & DiPietro, L. A. Inflammation and wound healing: the role of the macrophage. *Expert Rev. Mol. Med.* **13**, 1–12 (2011).

54. Mantovani, A. *et al.* The chemokine system in diverse forms of macrophage activation and polarization. *Trends Immunol.* **25**, 677–686 (2004).

55. Gordon, S., Helming, L. & Martinez Estrada, F. O. Alternative activation of macrophages: Concepts and prospects. in *Macrophages: Biology and Role in the Pathology of Diseases* (2014). doi:10.1007/978-1-4939-1311-4_3.

56. Galdiero, M. R., Biswas, S. K. & Mantovani, A. Polarized activation of macrophages. in *Macrophages: Biology and Role in the Pathology of Diseases* (2014). doi:10.1007/978-1-4939-1311-4_2.

57. Murray, P. J. *et al.* Macrophage activation and polarization: nomenclature and experimental guidelines. *Immunity* **41**, 14–20 (2014).

58. Anderson, J. M. & Jiang, S. Implications of the Acute and Chronic Inflammatory Response and the Foreign Body Reaction to the Immune Response of Implanted Biomaterials. in *The Immune Response to Implanted Materials and Devices* 15–36 (2017). doi:10.1007/978-3-319-45433-7_2.

59. Sussman, E. M., Halpin, M. C., Muster, J., Moon, R. T. & Ratner, B. D. Porous implants modulate healing and induce shifts in local macrophage polarization in the foreign body reaction. *Ann. Biomed. Eng.* **42**, 1508–1516 (2014).

60. Sridharan, R., Cameron, A. R., Kelly, D. J., Kearney, C. J. & O'Brien, F. J. Biomaterial based modulation of macrophage polarization: A review and suggested design principles. *Mater. Today* **18**, 313–325 (2015).

61. Sadtler, K. *et al.* The Scaffold Immune Microenvironment: Biomaterial-Mediated Immune Polarization in Traumatic and Nontraumatic Applications <sup/>. *Tissue Eng. Part A* **23**, 1044–1053 (2017).

62. Scatena, M., Eaton, K. V., Jackson, M. F., Lund, S. A. & Giachelli, C. M. Macrophages: The bad, the ugly, and the good in the inflammatory response to biomaterials. in *The Immune Response to Implanted Materials and Devices: The Impact of the Immune System on the Success of an Implant* (2016).

doi:10.1007/978-3-319-45433-7_3.

63. Davenport Huyer, L. *et al.* Advanced Strategies for Modulation of the Material-Macrophage Interface. (2020) doi:10.1002/adfm.201909331.

64. Chalouhi, N. *et al.* Stent-assisted coiling of intracranial aneurysms: Predictors of complications, recanalization, and outcome in 508 cases. *Stroke* **44**, 1348–1353 (2013).

65. Kallmes, D. F. *et al.* A New Endoluminal , Flow-Disrupting Device for Treatment of Saccular Aneurysms. *Stroke* 2346–2352 (2007) doi:10.1161/STROKEAHA.106.479576.

66. Cekirge, H. S. *et al.* Late angiographic and clinical follow-up results of 100 consecutive aneurysms treated with Onyx reconstruction: Largest single-center experience. *Neuroradiology* **48**, 113–126 (2006).

67. Piotin, M. *et al.* Intracranial aneurysms coiling with matrix: Immediate results in 152 patients and midterm anatomic follow-up from 115 patients. *Stroke* (2009) doi:10.1161/STROKEAHA.108.520866.

68. Knap, D. *et al.* Results of endovascular treatment of aneurysms depending on their size, volume and coil packing density. *Neurol. Neurochir. Pol.* **47**, 467–475 (2013).

69. Kadirvel, R., Ding, Y.-H., Dai, D., Lewis, D. A. & Kallmes, D. F. Differential Gene Expression in Well-healed and Poorly Healed Experimental Aneurysms after Coil Treatment. *Radiology* **257**, 418–426 (2010).

70. Hasan, S. M., Raymond, J. E., Wilson, T. S., Keller, B. K. & Maitland, D. J.

Effects of isophorone diisocyanate on the thermal and mechanical properties of shape-memory polyurethane foams. *Macromol. Chem. Phys.* **215**, 2420–2429 (2014).

71. Herting, S. M. *et al. In vivo* comparison of shape memory polymer foam-coated and bare metal coils for aneurysm occlusion in the rabbit elastase model. *J. Biomed. Mater. Res. Part B Appl. Biomater.* **107**, 2466–2475 (2019).

72. Altes, T. A. *et al.* A Creation of Saccular Aneurysms in the Rabbit: A Model Suitable for Testing Endovascular Devices. *Am. J. Roentgenol.* **174**, (2000).

73. Fujiwara, N. H. *et al.* Serial Angiography in an Elastase-induced Aneurysm Model in Rabbits: Evidence for Progressive Aneurysm Enlargement after Creation. *AJNR Am J Neuroradiol* **22**, 698–703 (2001).

74. Dai, D., Ding, Y. H., Lewis, D. A. & Kallmes, D. F. A proposed ordinal scale for grading histology in elastase-induced, saccular aneurysms. *Am. J. Neuroradiol.* **27**, 132–138 (2006).

75. Schwartz, R. S. *et al.* Restenosis and the proportional neointimal response to coronary artery injury: Results in a porcine model. *J. Am. Coll. Cardiol.* **19**, 267–274 (1992).

76. Rodriguez, J. N. *et al.* Design and biocompatibility of endovascular aneurysm filling devices. *J. Biomed. Mater. Res. - Part A* **103**, 1577–1594 (2015).

77. Sluzewski, M. *et al.* Relation between Aneurysm Volume, Packing, and Compaction in 145 Cerebral Aneurysms Treated with Coils1. *Radiology* (2004) doi:10.1148/radiol.2313030460.

78. Metcalfe, A. *et al.* Cold hibernated elastic memory foams for endovascular interventions. *Biomaterials* **24**, 491–497 (2003).

79. Anderson, J. M., Rodriguez, A. & Chang, D. T. Foreign body reaction to biomaterials. *Semin. Immunol.* **20**, 86–100 (2008).

80. Wang, M. O., Etheridge, J. M., Thompson, J. A., Vorwald, C. E. & Fisher, J. P. Evaluation of the In Vitro Cytotoxicity of Crosslinked Biomaterials. *Biomacromolecules* **14**, 1321–1329 (2014).

81. Standardization, I. O. for. *ISO 10993-5-2009*. (2009).

82. Shi, X. *et al.* In vitro cytotoxicity of single-walled carbon nanotube / biodegradable polymer nanocomposites. *J. Biomed. Mater. Res. - Part A* **86**, 813–823 (2007).

83. Li, R. Y. *et al.* Evaluation of biocompatibility and toxicity of biodegradable poly (DL-lactic acid) films. *Am. J. Transl. Res.* **7**, 1357–1370 (2015).

84. Matsui, M., Ono, L. & Akcelrud, L. Chitin/polyurethane networks and blends: Evaluation of biological application. *Polym. Test.* **31**, 191–196 (2012).

85. Martin, J. R. *et al.* A porous tissue engineering scaffold selectively degraded by cell-generated reactive oxygen species. *Biomaterials* **35**, 3766–3776 (2014).

86. Khetan, S. & Burdick, J. A. Patterning network structure to spatially control cellular remodeling and stem cell fate within 3-dimensional hydrogels. *Biomaterials* **31**, 8228–8234 (2010).

87. West, J. L. & Hubbell, J. A. Polymeric Biomaterials with Degradation Sites for Proteases Involved in Cell Migration. *Macromolecules* **32**, 241–244 (1999).

88. Miller, R. A., Brady, J. M. & Cutright, D. E. Degradation rates of oral resorbable implants (polylactates and polyglycolates): Rate modification with changes in PLA/PGA copolymer ratios. *J. Biomed. Mater. Res.* **11**, 711–719 (1977).

89. Gülden, M., Jess, A., Kammann, J., Maser, E. & Seibert, H. Cytotoxic potency of H 2 O 2 in cell cultures: Impact of cell concentration and exposure time. *Free Radic. Biol. Med.* **49**, 1298–1305 (2010).

90. Metcalfe, A. *et al.* Cold hibernated elastic memory foams for endovascular interventions. *Biomaterials* **24**, 491–497 (2003).

91. Da, L. *et al.* Composite elastomeric polyurethane scaffolds incorporating small intestinal submucosa for soft tissue engineering. *Acta Biomater.* **59**, 45–57 (2017).

92. Jessen, S. L. *et al.* Micro-CT and histopathology methods to assess host response of aneurysms treated with shape memory polymer foam-coated coils versus bare metal coil occlusion devices. *J. Biomed. Mater. Res. - Part B Appl. Biomater.* **108**, 2238–2249 (2020).

93. Jessen, S. L. *et al.* Microscopic Assessment of Healing and Effectiveness of a Foam-Based Peripheral Occlusion Device. *ACS Biomater. Sci. Eng.* **6**, 2588–2599 (2020).

94. Jang, L. K., Fletcher, G. K., Monroe, M. B. B. & Maitland, D. J. Biodegradable shape memory polymer foams with appropriate thermal properties for hemostatic applications. *J. Biomed. Mater. Res. - Part A* **108**, 1281–1294 (2020).

95. Peterson, G. I., Dobrynin, A. V. & Becker, M. L. Biodegradable Shape Memory Polymers in Medicine. *Adv. Healthc. Mater.* **6**, 1–16 (2017).

96. Weems, A. C., Easley, A., Roach, S. R. & Maitland, D. J. Highly Cross-Linked Shape Memory Polymers with Tunable Oxidative and Hydrolytic Degradation Rates and Selected Products Based on Succinic Acid. *ACS Appl Bio Mater* **2**, 454–463 (2019).

97. Williams, J. The Decomposition of Hydrogen Peroxide By Liver Catalase. *J. Gen. Physiol.* **11**, 309–337 (1928).

98. Napoli, A., Valentini, M., Tirelli, N., Müller, M. & Hubbell, J. A. Oxidation-responsive polymeric vesicles. *Nat. Mater.* **3**, 183–189 (2004).

99. Wilson, D. S. *et al.* Orally delivered thioketal nanoparticles loaded with TNF-α–siRNA target inflammation and inhibit gene expression in the intestines. *Nat. Mater.* **9**, 923–928 (2010).

100. Lux, C. D. G. *et al.* Biocompatible Polymeric Nanoparticles Degrade and Release Cargo in Response to Biologically Relevant Levels of Hydrogen Peroxide. *J. Am. Chem. Soc.* **134**, 15758–15764 (2012).

101. Yu, S. S. *et al.* Physiologically Relevant Oxidative Degradation of Oligo(proline) Cross-Linked Polymeric Scaffolds. *Biomacromolecules* **12**, 4357–4366 (2011).

102. Mcgough, M. A. P. *et al.* Poly(Thioketal Urethane) Autograft Extenders in an Intertransverse Process Model of Bone Formation. *Tissue Eng. Part A* **25**, 949–963 (2019).

103. Hafeman, A. E. *et al.* Characterization of the degradation mechanisms of lysine-derived aliphatic poly (ester urethane) scaffolds. (2010) doi:10.1016/j.biomaterials.2010.08.108.

104. Gerges, I. *et al.* Creep-resistant dextran-based polyurethane foam as a candidate scaffold for bone tissue engineering: Synthesis, chemico-physical characterization, and in vitro and in vivo biocompatibility. *Int. J. Polym. Mater. Polym. Biomater.* **65**, 729–740 (2016).

105. Christenson, E. M., Dadsetan, M., Wiggins, M., Anderson, J. M. & Hiltner, A. Poly(carbonate urethane) and poly(ether urethane) biodegradation: In vivo studies. *J. Biomed. Mater. Res. - Part A* **69**, 407–416 (2004).

106. Lynn, A. D., Kyriakides, T. R. & Bryant, S. J. Characterization of the in vitro macrophage response and in vivo host response to poly(ethylene glycol)-based hydrogels. *J. Biomed. Mater. Res. - Part A* **93**, 941–953 (2010).

107. Browning, M. B., Cereceres, S. N., Luong, P. T. & Cosgriff-Hernandez, E. M. Determination of the in vivo degradation mechanism of PEGDA hydrogels. *J. Biomed. Mater. Res. - Part A* **102**, 4244–4251 (2014).

108. Reid, B. *et al.* PEG Hydrogel Degradation and the Role of the Surrounding Tissue Environment. *J. Tissue Eng. Regen. Med.* **9**, 315–318 (2015).

109. Coley, S. *et al.* Cerecyte Coil Trial: Procedural Safety and Clinical Outcomes in Patients with Ruptured and Unruptured Intracranial Aneurysms. *Am. J. Neuroradiol.* **33**, 474–480 (2012).

110. Mcdougall, C. G. *et al.* Bioactive versus Bare Platinum Coils in the Treatment of Intracranial Aneurysms: The MAPS (Matrix and Platinum Science) Trial. *Am. J. Neuroradiol.* **35**, 935–942 (2014).

111. Wilsnack, R. E. Quantitative Cell Culture Biocompatibility Testing of Medical

Devices and Correlation to Animal Tests. *Biomater. Med. Devices. Artif. Organs* **4**, 235–261 (1976).

112. Gad, S. C. & McCord, M. G. Cytotoxicity Testing. in *Safety Evaluation in the Development of Medical Devices and Combination Products* (2008). doi:10.1201/9781439809488.

113. Crobeddu, E., Lanzino, G., Kallmes, D. F. & Cloft, H. J. Review of 2 decades of aneurysm-recurrence literature, Part 2: Managing recurrence after endovascular coiling. *Am. J. Neuroradiol.* **34**, 481–485 (2013).

114. Hoh, B. L. *et al.* Monocyte Chemotactic Protein-1 Promotes Inflammatory Vascular Repair of Murine Carotid Aneurysms via a Macrophage Inflammatory Protein-1 ␣ and Macrophage Inflammatory Protein-2 – Dependent Pathway. 2243–2253 (2011) doi:10.1161/CIRCULATIONAHA.111.036061.

115. Hosaka, K. *et al.* Monocyte Chemotactic Protein-1-Interleukin-6-Osteopontin Pathway of Intra-Aneurysmal Tissue Healing. *Stroke* **48**, 1052–1060 (2017).

116. Rouchaud, A. *et al.* Autologous adipose-derived mesenchymal stem cells improve healing of coiled experimental saccular aneurysms : an angiographic and histopathological study. 1–8 (2017) doi:10.1136/neurintsurg-2016-012867.

117. Ohyama, T. *et al.* Immobilization of basic fibroblast growth factor on a platinum microcoil to enhance tissue organization in intracranial aneurysms. *J Neurosurg* **102**, 109–115 (2005).

118. Chen, J., Yang, L., Chen, Y., Zhang, G. & Fan, Z. Controlled release of osteopontin and interleukin-10 from modified endovascular coil promote cerebral

aneurysm healing. *J. Neurol. Sci.* **360**, 13–17 (2016).

119. Ratner, B. D. A pore way to heal and regenerate: 21st century thinking on biocompatibility. *Regen. Biomater.* (2016) doi:10.1093/rb/rbw006.

120. Spiller, K. L. *et al.* The Role of Macrophage Phenotype in Vascularization of Tissue Engineering Scaffolds. *Biomaterials* **35**, 4477–4488 (2015).

121. Khashim, Z. *et al.* The distribution and role of M1 and M2 macrophages in healing of aneurysms after platinum coil embolization. *Am. J. Neuroradiol.* (2020).

122. Sadtler, K. *et al.* Divergent immune responses to synthetic and biological scaffolds. *Biomaterials* **192**, 405–415 (2019).

123. Brown, B. N. *et al.* Macrophage Phenotype as a Predictor of Constructive Remodeling following the Implantation of Biologically Derived Surgical Mesh Materials. *Acta Biomater* **8**, 978–987 (2012).

124. Fearing, B. V. & Van Dyke, M. E. In vitro response of macrophage polarization to a keratin biomaterial. *Acta Biomater.* **10**, 3136–3144 (2014).

125. Spiller, K. L. *et al.* Differential gene expression in human, murine, and cell line-derived macrophages upon polarization. *Exp. Cell Res.* **347**, 1–13 (2016).

126. Hoh, B. L. *et al.* Temporal cascade of inflammatory cytokines and cell-type populations in monocyte chemotactic protein-1 (MCP-1)-mediated aneurysm healing. doi:10.1136/neurintsurg-2017-013063.

127. Rigdon, R. H. Local Reaction to Polyurethane- A Comparative Study in the Mouse , Rat , and Rabbit *. **7**, 79–93 (1973).

128. Bouzeghrane, F., Naggara, O., Kallmes, D. F., Berenstein, A. & Raymond, J. In vivo experimental intracranial aneurysm models: A systematic review. *Am. J. Neuroradiol.* **31**, 418–423 (2010).

129. Nash, L. D. *et al.* Cold Plasma Reticulation of Shape Memory Embolic Tissue Scaffolds Graphical abstract. doi:10.1002/marc.201600268.

130. Hussey, G. S., Dziki, J. L. & Badylak, S. F. Extracellular matrix-based materials for regenerative medicine. *Nat. Rev. Mater.* **3**, 159–173 (2018).

131. Landsman, T. L. *et al.* A Shape Memory Foam Composite with Enhanced Fluid Uptake and Bactericidal Properties as a Hemostatic Agent Graphical abstract HHS Public Access. doi:10.1016/j.actbio.2016.10.008.

APPENDIX A

SUPPLEMENTAL FIGURES

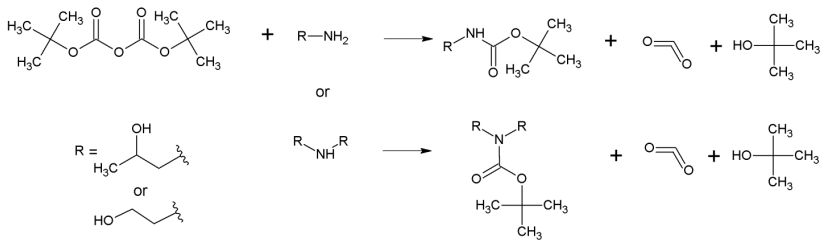

Scheme 1. Boc-protection of primary (upper route) and secondary (lower route) amines in preparation for urethane synthesis.

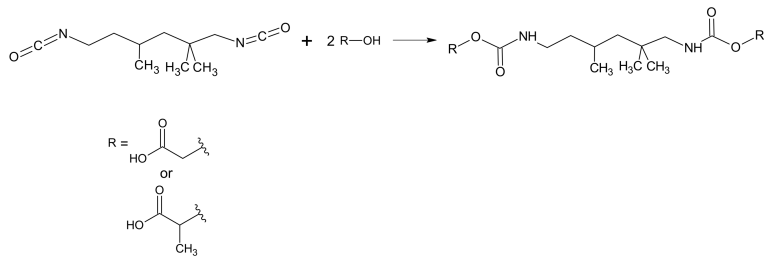

Scheme 2. Synthesis route for TMHDI-Gly (upper R group) and TMHDI-Lac (lower R group).

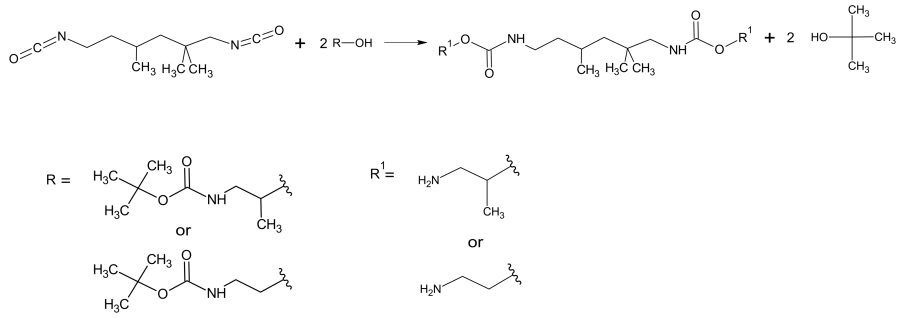

Scheme 3. Synthesis route for TMHDI-Amino (upper R groups) and TMHDI-EA (lower R groups).

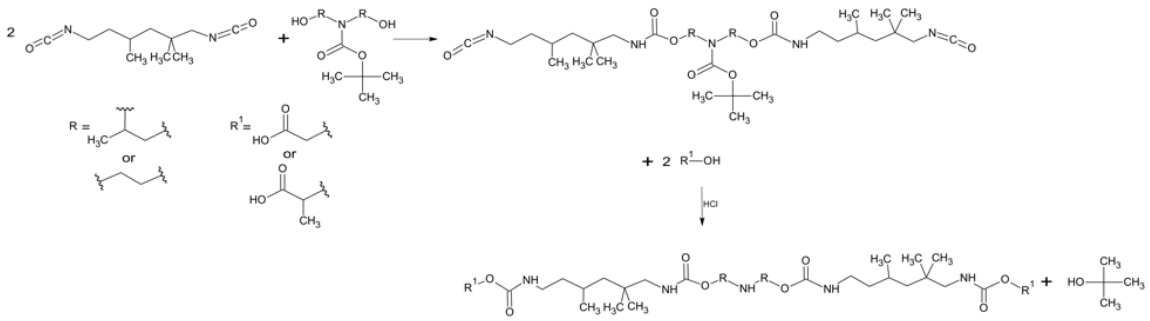

Scheme 4. Synthesis route for carboxylic acid-terminated byproducts: TMHDI-Bis-Gly (upper R group and upper R^1 group), TMHDI-Bis-Lac (upper R group and lower R^1 group), TMHDI-DEA-Gly (lower R group and upper R^1 group), and TMHDI-DEA-Lac (lower R group and lower R^1 group).

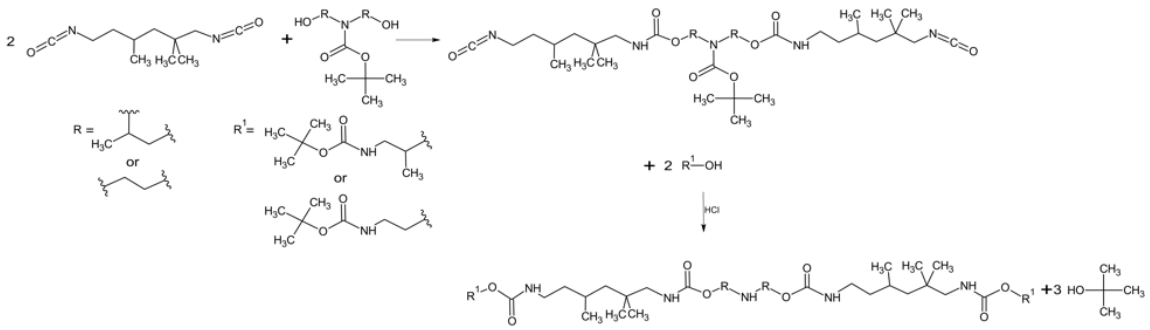

Scheme 5. Synthesis route for amine-terminated byproducts: TMHDI-Bis-Amino (upper R group and upper R^1 group), TMHDI-Bis-EA (upper R group and lower R^1 group), TMHDI-DEA-Amino (lower R group and upper R^1 group), and TMHDI-DEA-EA (lower R group and lower R^1 group).

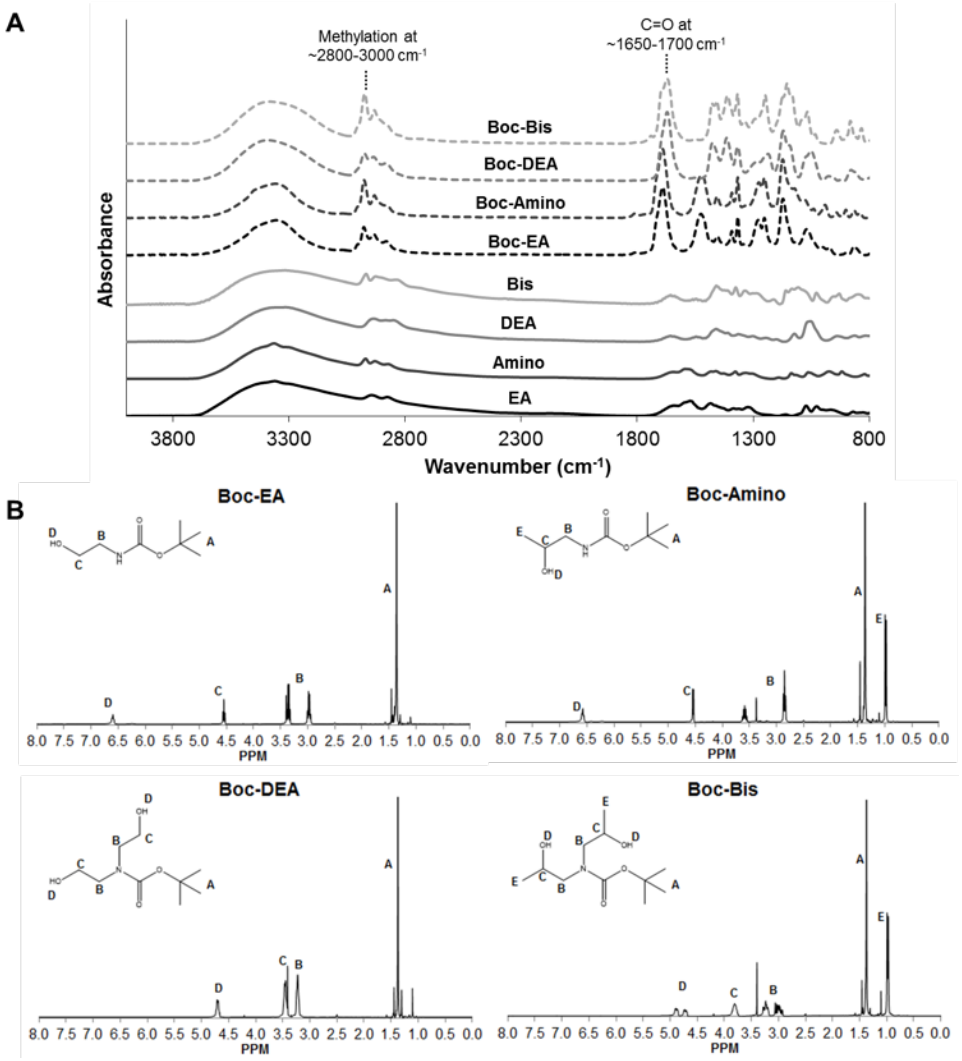

Figure V-1. Spectroscopic confirmation of boc-protection of amine groups in starting materials for byproduct synthesis. (A) Fourier transform infrared and (B) nuclear magnetic resonance spectra of boc-protected ethanolamine (Boc-EA), 1-amino-2-propanol (Boc-Amino), diethanolamine (Boc-DEA), and bis(2-hydroxypropyl) amine (Boc-Bis).

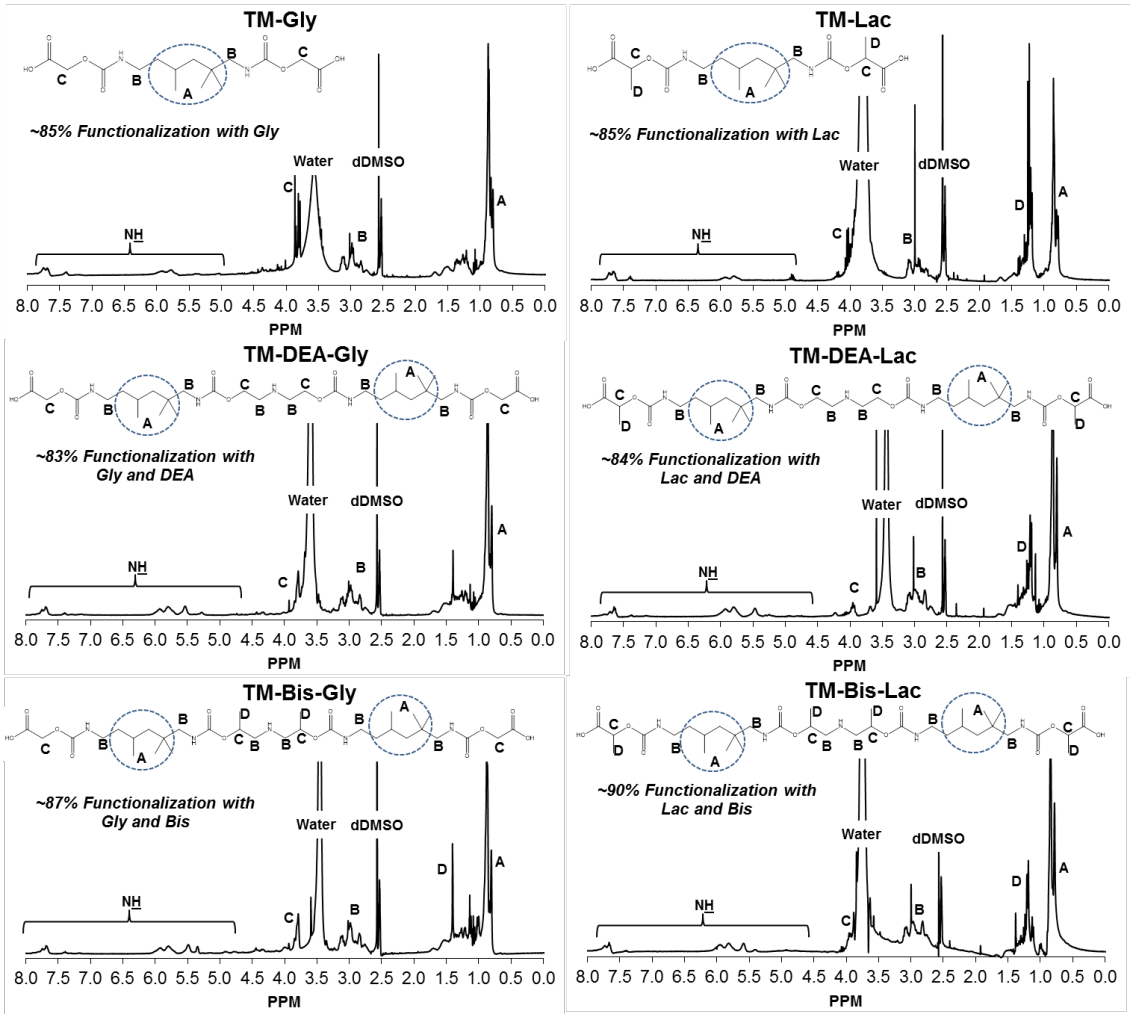

Figure V-2. Nuclear magnetic resonance spectra of carboxylic acid-terminated degradation byproducts. Percent functionalizations were calculated based on the areas under the integral curves of groups B and C for each product.

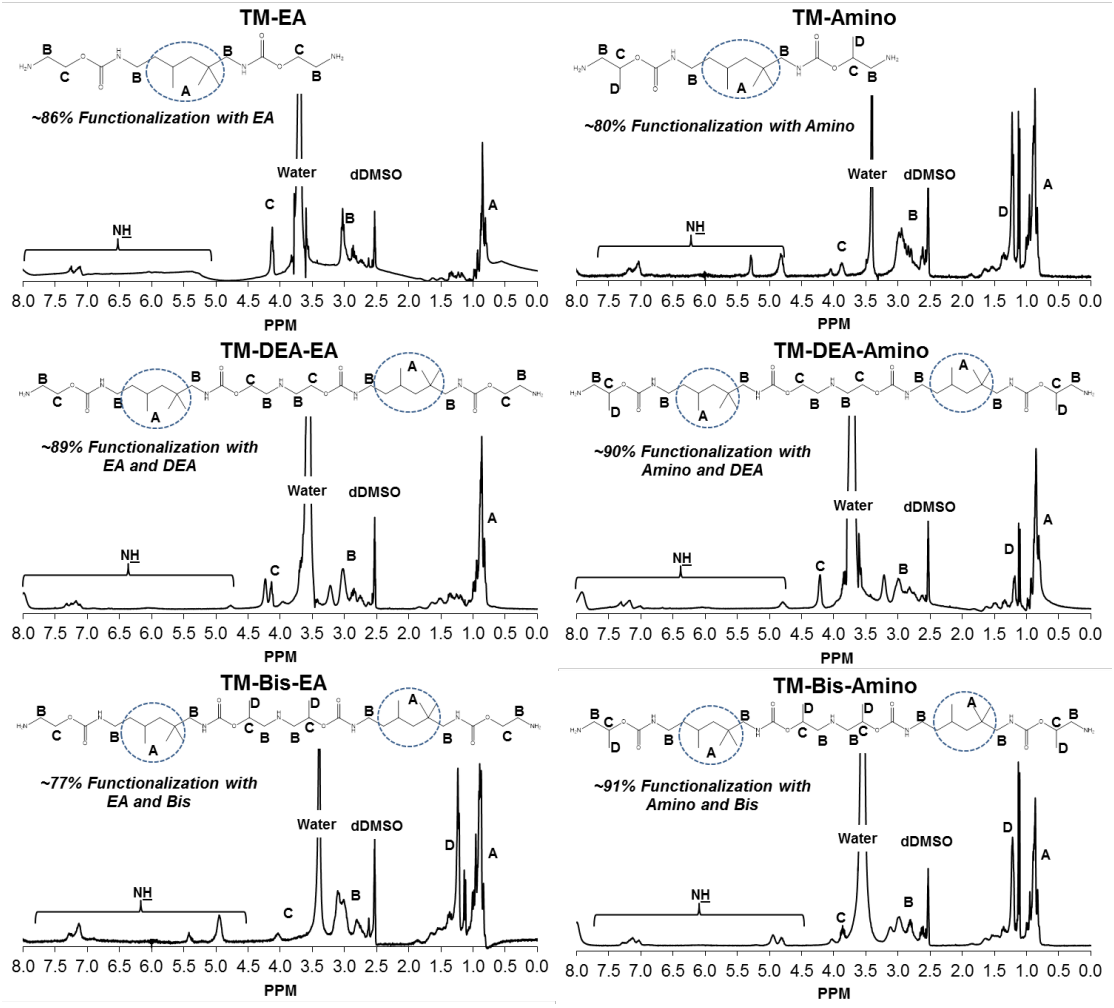

Figure V-3. Nuclear magnetic resonance spectra of amine-terminated degradation byproducts. Percent functionalizations were calculated based on the areas under the integral curves of groups B and C for each product.

Table V-1. Concentration and purity of RNA extracted from THP-1 derived macrophages *in vitro.*

Timepoint	Group	Concentration (ng/µL)	A260/280	A260/230
6 hours	M0	216.625	2.063	2.093
		436.764	2.113	2.198
		225.219	2.051	1.862
	BPC	146.505	2.042	2.003
		204.372	2.052	2.082
		316.656	2.081	2.164
	SMP FCC	100.1	2.01	1.85
		171.404	2.049	2.001
		253.916	2.057	1.524
24 hours	M0	234.862	2.055	1.639
		506.667	2.115	2.069
		512.377	2.096	2.218
	BPC	131.74	1.996	1.96
		133.863	2.027	2.047
		248.84	2.065	1.952
	SMP FCC	185.023	2.058	1.711
		159.947	2.047	2.11
		145.686	2.024	1.891